

# **Structural Elucidation, Modification and Anticancer Properties of a Lead Compound Nicotinamide *N*-Methyltransferase Inhibitor**

**by Hai Phuong Ha**

Thesis submitted in fulfilment of the requirements for  
the degree of

**Master of Science by Research**

under the supervision of Dr Tristan Rawling  
and the co-supervision of Associate Professor Andrew McDonagh

University of Technology Sydney  
Faculty of Science

June 2021





## Certificate of authorship and originality

I, Hai Phuong Ha, certify that the work in this thesis has not previously been submitted for a degree nor has it been submitted as part of the requirements for a degree except as fully acknowledge within the text.

I also certify that this thesis is written by me and all the data contained therein has been collected, collated by myself. All assistance in the writing of this thesis, including sources of information, literature used, consultation and academic supervision has been acknowledged and indicated in the thesis.

This research is supported by the Australian Government Research Training Program.

Hai Phuong Ha

Production Note:

Signature removed prior to publication.

June 2021





## Acknowledgements

First and foremost, I would like to thank my former supervisor, Associate Professor Alison Ung for helping me in the beginning of my Master with project directions and guidance in synthetic chemistries in a research laboratory. Secondly, I would like to thank my supervisors, Dr Tristan Rawling and Associate Professor Andrew McDonagh for helping me through this project from where I left off to finish. Tristan, your support this year has been indispensable. Thank you for your guidance and wisdom, your unrivalled knowledge of synthetic chemistries and biological works, and your solace, understanding and encouragement through all the failed experiments. Your significant contribution of personal time has not gone unnoticed and will never be! Without you my Masters would not have been possible.

Thank you everyone from Tristan's group, as well as my fellow HDR students across 511-531 labs. To Matt, thank you so much for giving me a lot of advice in the chemistry aspects and always help me to look for chemicals even when I did not check the OCID. To Ariane, thank you for showing me how to use the plate reader and share your thoughts about what might be wrong with the bioassay that I was trying to develop. Ritik, my drug candidates' analogues would not be completed without you lending me some of your boronic acids. To Edward, for all the help in tissue culture, seeding the plates, preparing all the reagents and equipment needed for the MTS assay. Without your enormous support, I don't think I would be able to finish the cell works within such a short timeframe. And of course, to "Cow"-milla, thanks for always be there and support me through the hardest time of my project, listening to all my garbage and putting up with all the funny-not-so-funny Tiktok videos I sent you in the middle of the night (I will keep bothering you as long as I'm still at UTS). And to Tom, Gina, Ana, Jake, Anjar, Bishwa, Sergio and all honours people who passed through over the years, for the hours of garbage we would talk about during break (or even in the middle of our work), without you guys I don't think I would have made it through the last two years. There are many more that could be mentioned but will not be forgotten.

To my uni fam, who made the days bearable and brought life and laughter into what was undoubtedly two stressful years for all of us. Sorry guys (Brooke, Eda,

Nikki and Miss Rafeek) for dealing with a less-than present friend this year and for always keeping me grounded. Now it is my turn to repay the support, care and unrivalled friendship you all provided. To Eda, thank you for always be there to support me, thank you for being there on the day that I felt most horrible and gave me a lift home (and you too, Koray!). To Oksana, my former student also a new friend but all the more valuable for it. Thank you for helping me with the freeze-drying and listening to my anxiety-talk whenever I fail doing the reactions. Thank you all for the countless gossip sessions, for the much-needed tea breaks, drinks every Friday (and randomly pop-up drinks sessions after lunch) and for all the teaching company; org chem, phys chem, chem 1 and chem 2 has never had more competent demonstrators. Dhiyana, you are one of my best friends in our uni fam group; thank you for all the coffee dates, brunch dates and groceries shopping dates in the weekends, the dinners and the drinks, and for being a lifelong friend that I always know I can rely on. And Brooke, thank you for your endless supports, for always helping me proof-read my work to find grammatical errors, despite how tedious it must be to read pages and pages of work not in your expertise (Tbh, no one could ever be more English than you are!!!).

The following people also required a special mention; again my principal supervisor Tristan for teaching me how to perform cell work and his constant support and advice in regards to the many things I would ask him, especially when they were often not related to this project, Associate Professor Andrew McDonagh and Professor Michael Cortie for their support, advice and for helping me with my internal assessments and transitions, Dr Dayanne Bordin Mozaner for technical support for the GC-MS and QTOF instruments, Dr Ronald Shimmon for his training provided, synthetic chemistry advices and endless technical support with the NMR, Mercedes Ballesteros, Sarah Osvath and Dr. Luke Bebe for PC2 lab inductions, tissue culture and plate reader inductions and technical support in those labs, Anthea Harris, Nishath Geekiyanage, Dr Jason Ashmore and Mahmoud El Safadi for their endless alternative ideas and approaches when I was stuck for ideas and for lending me glasswares, share me some chemicals and let me use instruments in teaching labs; Dr Brian Reedy for helping me with the UV-Vis (even though the spectrums look soooo crap) and endless hours of chat about so much random things!!!

To my family, to whom this must seem a never-ending journey – I do promise I will leave uni one day! To mum and dad, thanks for your constant love and support. Even though we live 7000 km away from each other, every day goes by I still can clearly feel your endless care and encouragement. Thank you so much for providing me with not only emotional support but also financial support during the hardest time of my study, I can never thank you enough. To my younger brother, thank you for dealing with such a crazy sibling like me, thank you for always trying to relieve the stresses of time by taking care of all household tasks without ever asking for help for all the time. And finally, to “Timtam”. No one person should ever have to deal with so much crazy and I am grateful to you every day for sticking by me. Your love has kept me going through even the worst of time. Here’s to many more (less awful) years.

## Abstract

Nicotinamide *N*-methyltransferase (NNMT) is an enzyme that together with the methyl donor *S*-adenosyl methionine (SAM) catalyses the methylation of nicotinamide and related compounds. NNMT has been involved in a range of diseases including cancers and metabolic disorders. The development of NNMT inhibitors (NNMTIs) may lead to new therapeutic drugs for these disorders. Research into the development of NNMTIs has occurred over the past decade, however the inhibitors that have come out of these programs lack potency and specificity. Therefore the development of NNMTIs with therapeutic potential remains an unmet need.

Recently a library of mono-*N*-alkylated tetrahydroisoquinoline (THIQ) compounds were synthesised in a different research, and one analogue (compound **23**, see page 24) was shown to inhibit NNMT from a screening service offered by Eli Lilly. The original aim of this project was to optimise the NNMT inhibitory activity of **23** by synthesising and testing of a range of analogues.

A key step in the synthesis of **23** and its analogues was mono-alkylation of the amine group in THIQ with propargyl bromide. The reaction had been reported to give exclusively the mono-alkylated product when performed with 2 equivalences of propargyl bromide, however when the reaction was conducted the <sup>1</sup>H NMR of the product indicated that dialkylation had occurred. Therefore this project began with an investigation to confirm that compound **23** was indeed a di-alkylated product. Two series of THIQ analogues- one mono-alkylated series and one di-alkylated series were synthesised. In total, eight compounds were synthesised. The information obtained from these reaction outcomes, was used to further understand each reaction mechanism.

The NNMT inhibitory activity of the THIQ analogues was next assessed using an NNMT inhibition assay reported in the literature. The assay involved the NNMT mediated formation of a fluorescent quinolinium product whose formation could be followed and quantified using a plate reader. After several attempts at assay optimisation, it was discovered that the assay was not sufficiently sensitive to follow the reaction kinetics. Decreased sensitivity was attributed to quenching of the

quinolinium fluorescence by the assay buffer system. Unfortunately, time constraints prevented assay optimisation.

The anticancer activity of THIQ libraries was assessed against the MDA-MB-231 breast cancer cell line. These assays showed that four of eight compounds reduced cell viability at concentrations below 50  $\mu$ M. Further testing is now required to establish if the observed anticancer activity is mediated by inhibition of NNMT or by actions at other cellular targets.

## Contents

<b>Certificate of authorship and originality.....</b>	<b>iv</b>
<b>Acknowledgements .....</b>	<b>vi</b>
<b>Abstract .....</b>	<b>ix</b>
<b>Contents.....</b>	<b>xi</b>
<b>List of Figures .....</b>	<b>xv</b>
<b>List of Schemes .....</b>	<b>xvii</b>
<b>List of Tables.....</b>	<b>xix</b>
<b>List of Abbreviations .....</b>	<b>xx</b>
<b>Chapter 1 Introduction .....</b>	<b>1</b>
1.1. Introduction .....	1
1.2. NNMT and its activity .....	1
1.3. NNMT in non-diseases states .....	3
1.3.1. Detoxification and metabolism .....	3
1.3.2. NNMT as a regulator of the actions of NAM and NAD <sup>+</sup> .....	3
1.4. Implication of NNMT in disease states.....	4
1.4.1. NNMT upregulation in cancer .....	4
1.4.2. NNMT in association with type-2 diabetes (T2D) .....	5
1.4.3. NNMT in neurological disorders .....	7
1.5. The structure of NNMT .....	7
1.6. NNMT Inhibitor development.....	10
1.6.1. NAM derivatives as NNMTIs.....	10

1.6.2. NAM-Adenosine and NAM-Amino Acid conjugates as NNMTIs.....	11
1.6.3. MNA analogues NNMTIs .....	14
1.6.4. Quinoline and Isoquinoline derivatives as NNMTIs.....	14
1.6.5. A covalent NNMTI targeting Cys 165 unique to NNMT .....	16
1.6.6. Bi-substrate inhibitors.....	16
1.6.7. Suicide Inhibitors – a new introduced target.....	21
1.7. Preliminary work: Identification of a new NNMTI Lead compound.....	24
1.8. Project aims and objectives.....	26
<b>Chapter 2 Structural Elucidation of THIQ analogues and synthesis of mono- and di-alkylated THIQ analogue libraries .....</b>	<b>28</b>
2.1. Introduction .....	28
2.2. Results and Discussion.....	28
2.2.1. Identification of products from the alkylation of THIQ .....	28
2.2.2. Develop an exclusively mono- <i>N</i> -alkylated synthetic protocol .....	33
2.2.3. Develop an exclusively di- <i>N</i> , <i>N</i> -alkylated synthetic protocol.....	36
2.2.4. Synthesis of aromatic azides .....	41
2.2.4.1. Synthesis aryl azides from aryl halides .....	42
2.2.4.2. Aryl boronic acids to aryl azides conversion.....	44
2.2.5. Copper-Catalysed Azide-Alkyne Cycloaddition reaction .....	46
2.2.6. Chelating – a useful step to a better Click reaction workup .....	48
2.2.7. Synthesis of an <i>N</i> -alkylated click analogue (FHMxx).....	49
2.2.8. Synthesis of an <i>N</i> , <i>N</i> -alkylated click analogue (FHDxx) .....	53
2.3 Experimental .....	60
2.3.1. General experimental .....	60
2.3.1.1. Proton ( <sup>1</sup> H) NMR Spectroscopy.....	60
2.3.1.2. Carbon ( <sup>13</sup> C) NMR Spectroscopy.....	60



2.3.1.3. High-Resolution Mass Spectroscopy (HRMS) .....	60
2.3.1.4. Column Chromatography.....	61
2.3.1.5. Thin Layer Chromatography (TLC) .....	61
2.3.1.6. Melting Points .....	61
2.3.1.7. High Vacuum .....	61
2.3.1.8. Reagents and Solvents.....	61
2.3.2. Chemical Reaction Procedures.....	62
2.3.2.1. Synthesis of the THIQ core structure.....	62
2.3.2.2. General synthesis of aryl azides from aryl boronic acids ...	64
2.3.2.3. Standard Copper-Catalysed Azide-Alkyne Cycloaddition...	65
2.3.2.4. Isolation procedure of an alkylated crude.....	70
<b>Chapter 3 In vitro assessment of NNMT inhibitory activity.....</b>	<b>72</b>
3.1. Introduction .....	72
3.2. Screening methods to determine the inhibitory activity of NNMTIs .....	72
3.2.1. HPLC-MS based NNMT assay .....	72
3.2.2. Fluorescent-based assay .....	73
3.2.2.1. NAM-coupled fluorescent assay .....	73
3.2.2.2. SAH-coupled fluorescent-based assay.....	74
3.2.2.3. Non-coupled fluorescent-based assay.....	75
3.2.3. Assessment of NNMT assay sensitivity and limit of detection .....	81
3.2.3.1. Synthesis of 1-MQ.....	81
3.2.3.2. Plate reader detection of 1-MQ in various solvent systems.	82
<b>Chapter 4 In vivo biological assay to assess Anticancer Properties of NNMTIs .....</b>	<b>86</b>
4.1. General Introduction to Assessment of Cytotoxicity.....	86
4.2. MTS Assay .....	86

4.3. Screening for Cytotoxicity.....	87
4.4. Discussion of Cytotoxic Activity Results Against MDA-MB-231 .....	89
4.5. Experimental procedure.....	91
4.5.1. General reagents for cell culture .....	91
4.5.2. Cell culture .....	91
4.5.3. Cell Viability.....	91
<b>Chapter 5   General Conclusions and Future Directions.....</b>	<b>93</b>
5.1. General discussion and conclusions.....	93
5.2. Future directions .....	94
<b>References .....</b>	<b>96</b>

## List of Figures

<b>Figure 1</b>	Methylation of NAM by SAM catalysed by NNMT enzyme ...	<b>2</b>
<b>Figure 2</b>	NNMT links NAD <sup>+</sup> and methinone metabolism ...	<b>4</b>
<b>Figure 3</b>	Effects of NNMTIs on intracellular levels of NAD <sup>+</sup> salvage ...	<b>7</b>
<b>Figure 4</b>	Ribbon cartoon of 3-Dimensional (3D) NNMT structure ...	<b>9</b>
<b>Figure 5</b>	Structures of reference compounds SAH, Sinefungin, MNA ...	<b>10</b>
<b>Figure 6</b>	Core structure of NAM-like inhibitors developed ...	<b>11</b>
<b>Figure 7</b>	Schematic overview of first generation NNMTIs ...	<b>12</b>
<b>Figure 8</b>	Schematic overview of second generation NNMTIs ...	<b>13</b>
<b>Figure 9</b>	Schematic overview of alkylated NAM analogue as NNMTIs	<b>14</b>
<b>Figure 10</b>	Schematic overview of <i>N</i> -methylated Quinoline ...	<b>15</b>
<b>Figure 11</b>	Structure of covalent NNMTI <b>10</b> targeted Cys 165 receptor	<b>16</b>
<b>Figure 12</b>	Schematic overview of the interaction between ...	<b>17</b>
<b>Figure 13</b>	3D structure derived from the molecular docking software ...	<b>18</b>
<b>Figure 14</b>	Schematic overview of design strategy of the third ...	<b>19</b>
<b>Figure 15</b>	Schematic overview of designing new NNMTIs ...	<b>20</b>
<b>Figure 16</b>	High-affinity alkynyl bisubstrate inhibitor of NNMT	<b>21</b>
<b>Figure 17</b>	Structure of compound <b>17</b> as covalently modify ...	<b>22</b>
<b>Figure 18</b>	Inactivation of NNMT targeting Cys 195 by <i>N</i> -methylated ...	<b>23</b>
<b>Figure 19</b>	Schematic overview of compound <b>23</b> synthetic route	<b>24</b>
<b>Figure 20</b>	<sup>1</sup> H NMR spectrum of the THIQ alkylation reaction crude product ...	<b>25</b>
<b>Figure 21</b>	The S <sub>N</sub> 2 alkylation of THIQ, yielding unknown compounds ...	<b>26</b>
<b>Figure 22</b>	The formation of the Iminium ion through the elimination ...	<b>29</b>

<b>Figure 23</b>	<sup>1</sup> H NMR spectrum of THIQ product ...	<b>30</b>
<b>Figure 24</b>	<sup>1</sup> H NMR spectrum of the <i>N</i> -alkylated product ...	<b>31</b>
<b>Figure 25</b>	HRMS spectrum of compound <b>26</b>	<b>32</b>
<b>Figure 26</b>	<sup>1</sup> H NMR of the di- <i>N</i> , <i>N</i> -alkylated isolate from the crude mixture ...	<b>33</b>
<b>Figure 27</b>	HRMS spectrum of compound <b>27</b>	<b>33</b>
<b>Figure 28</b>	<sup>1</sup> H NMR spectrum of the first attempt crude in re-developing ...	<b>34</b>
<b>Figure 29</b>	<sup>1</sup> H NMR spectrum of the second attempt crude in re-developing ...	<b>35</b>
<b>Figure 30</b>	<sup>1</sup> H NMR spectrum of the crude from the second synthesis ...	<b>37</b>
<b>Figure 31</b>	<sup>1</sup> H NMR spectrum of the crude from the third synthesis attempt	<b>37</b>
<b>Figure 32</b>	Proposed mechanism for Polymerisation of <b>27</b> .	<b>39</b>
<b>Figure 33</b>	Possible catalytic cycle for the amino acid-promoted coupling ...	<b>43</b>
<b>Figure 34</b>	Proposed mechanism of CuAAC reaction ...	<b>47</b>
<b>Figure 35</b>	Chelation Mechanism of EDTA with Copper	<b>48</b>
<b>Figure 36</b>	<sup>1</sup> H NMR spectrum of <b>23</b> ...	<b>49</b>
<b>Figure 37</b>	<sup>1</sup> H NMR spectrum of <b>FHM02</b> ...	<b>50</b>
<b>Figure 38</b>	<sup>1</sup> H NMR spectrum of <b>FHM03</b> and <b>FHM04</b>	<b>51</b>
<b>Figure 39</b>	<sup>1</sup> H NMR spectrum of <b>FHM05</b>	<b>52</b>
<b>Figure 40</b>	<sup>1</sup> H NMR spectrum of <b>24</b> ...	<b>54</b>
<b>Figure 41</b>	<sup>1</sup> H NMR spectrum of <b>FHD02</b>	<b>55</b>
<b>Figure 42</b>	Structures of proposed compounds <b>FHD03</b> and <b>FHD04</b>	<b>56</b>
<b>Figure 43</b>	<sup>1</sup> H NMR spectrum of <b>FHD05</b>	<b>58</b>
<b>Figure 44</b>	The reaction of NAM in the presence of NNMT and SAM-forming ...	<b>73</b>
<b>Figure 45</b>	The schematic reaction of Ellman's Assay	<b>74</b>
<b>Figure 46</b>	The reaction of SAH with DTNB and DMSO ...	<b>75</b>

<b>Figure 47</b>	Non-coupled fluorescent assay reaction	<b>76</b>
<b>Figure 48</b>	Fluorescent intensity measured over 15 minutes	<b>78</b>
<b>Figure 49</b>	Fluorescent intensity measured over time ...	<b>80</b>
<b>Figure 50</b>	<sup>1</sup> H NMR spectrum of synthesised product 1-MQ	<b>82</b>
<b>Figure 51</b>	Detection of various concentrations of 1-MQ prepared ...	<b>83</b>
<b>Figure 52</b>	Detection of various concentrations of 1-MQ prepared ...	<b>84</b>
<b>Figure 53</b>	Mitochondrial cleavage of MTS to formazan	<b>87</b>
<b>Figure 54</b>	All compounds % viability at three tested concentrations	<b>88</b>
<b>Figure 55</b>	The structure of tested compounds against MDA-MB-231	<b>89</b>

## List of Schemes

<b>Scheme 2.2.1</b>	The Pictet-Spengler cyclisation reaction ...	<b>28</b>
<b>Scheme 2.2.1.1</b>	Original protocol of the THIQ alkylation reaction	<b>30</b>
<b>Scheme 2.2.1.2</b>	The new S <sub>N</sub> 2 alkylation of THIQ with propargyl bromide ...	<b>36</b>
<b>Scheme 2.2.1.3</b>	An exhaustive alkylation reaction for the synthesis ...	<b>41</b>
<b>Scheme 2.2.4.1</b>	Aryl halide to aryl azide proposed synthetic route	<b>42</b>
<b>Scheme 2.2.4.1a</b>	The S <sub>N</sub> 2 alkylation of a bromomethylbenzene ...	<b>42</b>
<b>Scheme 2.2.4.1b</b>	The Ullman-type coupling reaction between ...	<b>43</b>
<b>Scheme 2.2.4.2</b>	The conversion of aryl boronic acids to aryl azides ...	<b>44</b>
<b>Scheme 2.2.4.2.1</b>	The S <sub>N</sub> 2 reaction of ethyl-4-bromobutanoate ...	<b>46</b>
<b>Scheme 2.2.5</b>	The general synthetic scheme for the 1,4-click ...	<b>48</b>
<b>Scheme 3.3.1.2</b>	Synthesis of 1-MQ product	<b>81</b>

## List of Tables

<b>Table 1</b>	IC <sub>50</sub> concentrations of NNMTIs	<b>23</b>
<b>Table 2</b>	Four azides with different substituents at para-position ...	<b>45</b>
<b>Table 3</b>	Chemical structures of the <b>FHMxx</b> analogue series	<b>53</b>
<b>Table 4</b>	Reaction conditions for the synthesis of <b>FHD03</b> and <b>FHD04</b>	<b>57</b>
<b>Table 5</b>	Chemical structures of the <b>FHDxx</b> analogue series	<b>59</b>
<b>Table 6A</b>	Concentrations of all components that need to be prepared ...	<b>77</b>
<b>Table 6B</b>	Outline of the assay	<b>77</b>
<b>Table 7</b>	Changes in procedure of the enzyme activity assay	<b>79</b>
<b>Table 8</b>	Changes in concentrations of NNMT, SAM and Quinoline	<b>79</b>
<b>Table 9</b>	MDA-MB-231 MTS screening results as % viability ...	<b>89</b>

## List of Abbreviations

<i>ATP</i>	Adenosine triphosphate
<i>Aox</i>	Aldehyde oxidase
<i>AChE</i>	Acetylcholinesterase
<i>ACP</i>	Acetophenone
<i>BHMT</i>	Betaine-homocysteine S-methyltransferase
<i>BSA</i>	Bovine Serum Albumin
<i>Bu<sub>3</sub>N</i>	Tributylamine
<i>CuAAC</i>	Copper-catalysed azide-alkyne cycloaddition
<i>CHCl<sub>3</sub></i>	Chloroform
<i>CuSO<sub>4</sub></i>	Copper (II) sulfate
<i>CuI</i>	Copper (I) iodide
<i>COSY</i>	Correlated Spectroscopy
<i><sup>13</sup>C NMR</i>	Carbon-13 Nuclear Magnetic Resonance
<i>DNA</i>	Deoxyribonucleic acid
<i>DDAH</i>	Dimethylarginin Dimethylaminohydrolase
<i>DTT</i>	Dithiothreitol
<i>DTNB</i>	5,5-dithio-bis-(2-nitrobenzoic acid)
<i>DCM</i>	Dichloromethane
<i>DEPT</i>	Distortionless enhancement by polarisation transfer
<i>DMSO</i>	Dimethyl Sulfoxide
<i>ESI</i>	Electrospray Ionisation
<i>EtOH</i>	Ethanol



<i>EtOAc</i>	Ethyl Acetate
<i>EDTA</i>	Ethylenediaminetetraacetic acid
<i>FtSz</i>	Filamenting temperature-sensitive mutant Z
<i>GNMT</i>	Glycine N-methyltransferase
<i>GAMT</i>	Guanidinoacetate N-methyltransferase
<i>HFD</i>	High Fat Diet
<i>HTS</i>	High Throughput Screening
<i>HMBC</i>	Heteronuclear Multiple Bond Correlation
<i>HSQC</i>	Heteronuclear Single Quantum Coherence Spectroscopy
$^1\text{H}$ NMR	Hydrogen-1 Nuclear Magnetic Resonance
<i>HILIC</i>	Hydrophilic Interaction Chromatography
<i>HCHO</i>	Formaldehyde
<i>HCOOH</i>	Formic Acid
<i>HRMS</i>	High Resolution Mass Spectroscopy
<i>h-NNMT</i>	Human Nicotinamide N-methyltransferase
<i>h-INMT</i>	Human Indole(ethyl)amine N-methyltransferase
<i>h-PNMT</i>	Human Phenylethanolamine N-methyltransferase
<i>IC<sub>50</sub></i>	Inhibitory Concentrations
<i>i-PrOH</i>	Iso-propanol
<i>KOH</i>	Potassium Hydroxide
<i>K<sub>2</sub>CO<sub>3</sub></i>	Potassium Carbonate
<i>LuxS</i>	S-ribosylhomocysteine Lyase
$[M+H]^+$	Molecular Ion (M) protonated with additional Hydrogen atom

<i>MNA</i>	1-Methylnicotinamide
<i>mRNA</i>	Messenger Ribonucleic Acid
<i>M.W.</i>	Molecular Weight
<i>MTs</i>	Methyltransferase Proteins
<i>MeOH</i>	Methanol
<i>MeCN</i>	Acetonitrile
<i>MgSO<sub>4</sub></i>	Magnesium Sulfate
<i>m/z</i>	Mass-to-charge ratio
<i>NAD<sup>+</sup></i>	Nicotinamide Adenine Dinucleotide
<i>NAM</i>	Nicotinamide
<i>NNMTI(s)</i>	Nicotinamide N-methyltransferase Inhibitor(s)
<i>NA</i>	Nicotinic Acid
<i>NaOH</i>	Sodium Hydroxide
<i>Na<sub>2</sub>CO<sub>3</sub></i>	Sodium Carbonate
<i>NMR</i>	Nuclear Magnetic Resonance
<i>OATs</i>	Organic Anion Transporters
<i>PEMT</i>	Phosphatidylethanolamine N-methyltransferase
<i>PCC</i>	Polyamine Catabolic Cycle
<i>PSR</i>	Pictet-Spengler Reaction
<i>pK<sub>a</sub></i>	Acid Dissociation Constant
<i>QTOF</i>	Quadrupole time-of-flight
<i>RT</i>	Retention Time
<i>SAM</i>	S-adenosyl methionine

<i>S<sub>N</sub>2</i>	Nucleophilic Substitution, Bimolecular
<i>Sirt1</i>	Sirtuin 1
<i>STAT1</i>	Signal Transducer and Activator of Transcription 1
<i>STAT3</i>	Signal Transducer and Activator of Transcription 3
<i>SAR</i>	Structure-Activity Relationship
<i>SAH</i>	S-adenosyl-L-homocysteine
<i>SIBLing</i>	Suicide-inhibitor-based protein labelling
<i>T2D</i>	Type-2 Diabetes
<i>TGF-β<sub>1</sub></i>	Transforming Growth Factor β <sub>1</sub>
<i>THIQ</i>	6,7-dimethoxy-1,2,3,4-tetrahydroisoquinoline
<i>TNB</i>	2-nitro-5-thiobenzoate
<i>TLC</i>	Thin Layer Chromatography
<i>UHP</i>	Ultra-High Performance
<i>WAT</i>	White Adipose Tissue
<i>1-MQ</i>	1-Methylquinolinium
<i>2py</i>	<i>N</i> 1-methyl-2-pyridone-5-carboxamide
<i>3D</i>	3-Dimensional
<i>4py</i>	<i>N</i> 1-methyl-4-pyridone-3-carboxamide
<i>8HQ</i>	8-hydroxyquinoline







# Chapter 1 Introduction

## 1.1. Introduction

Nicotinamide *N*-methyltransferase (NNMT) is an enzyme that transfers methyl groups to nitrogen atoms on a range of substrates. NNMT is a histone methylation modulator that regulates energy metabolism. It is predominantly expressed in the liver. Simultaneously, a lower expression has been detected in the kidney, lung, skeletal muscle, placenta, heart and brain. NNMT has been involved in various diseases and physiological processes including Parkinson's disease, cancers and metabolic disorders, such as obesity and obesity-related metabolic conditions, for instance, type-2 diabetes (T2D). However, whether NNMT plays a role in these conditions remains in its infancy. Thus, NNMT has been suggested as an attractive therapeutic target for drug discovery in the treatment of certain metabolic and chronic diseases. Hence, most research to date has been focussing on the development of small molecular inhibitors of NNMT before investigating the correlation between diseases and the enzyme itself.

This chapter summarises the structure and function of NNMT, its potential role of human NNMT in non-disease and disease states and highlights the therapeutic potential of NNMT as a drug target. The design and development of NNMT inhibitors (NNMTIs) are discussed, including work carried out at UTS that led to the current project.

## 1.2. NNMT and its activity

NNMT is a cytosolic enzyme that catalyses the methylation of nicotinamide (NAM) and other pyridines to form pyridinium ions<sup>1</sup>. A general reaction scheme for NNMT-mediated methylation is shown in **Figure 1**. In this reaction, NAM interacts with S-adenosyl-L-methionine (SAM) – a methyl donor to yield *N'*-methylnicotinamide (MNA), catalysed by NNMT. This methylation reaction also produces S-adenosyl-L-homocysteine (SAH), eventually hydrolysed to adenosine and homocysteine under physiological conditions (**Figure 1**)<sup>2</sup>. MNA is further oxidised by Aldehyde oxidase (Aox) to form *N1*-methyl-2-pyridone-5-carboxamide

(2py) and *N*1-methyl-4-pyridone-3-carboxamide (4py), which can be found in excreted urine<sup>3,4</sup>. *N*-methylation has been proposed as a metabolic pathway for NAM excretion, and NNMT is the only enzyme in the human body known to convert NAM to MNA. Therefore, NNMT could participate in regulating intracellular nicotinamide levels and modulating its excretion following the *N*-methylation process.

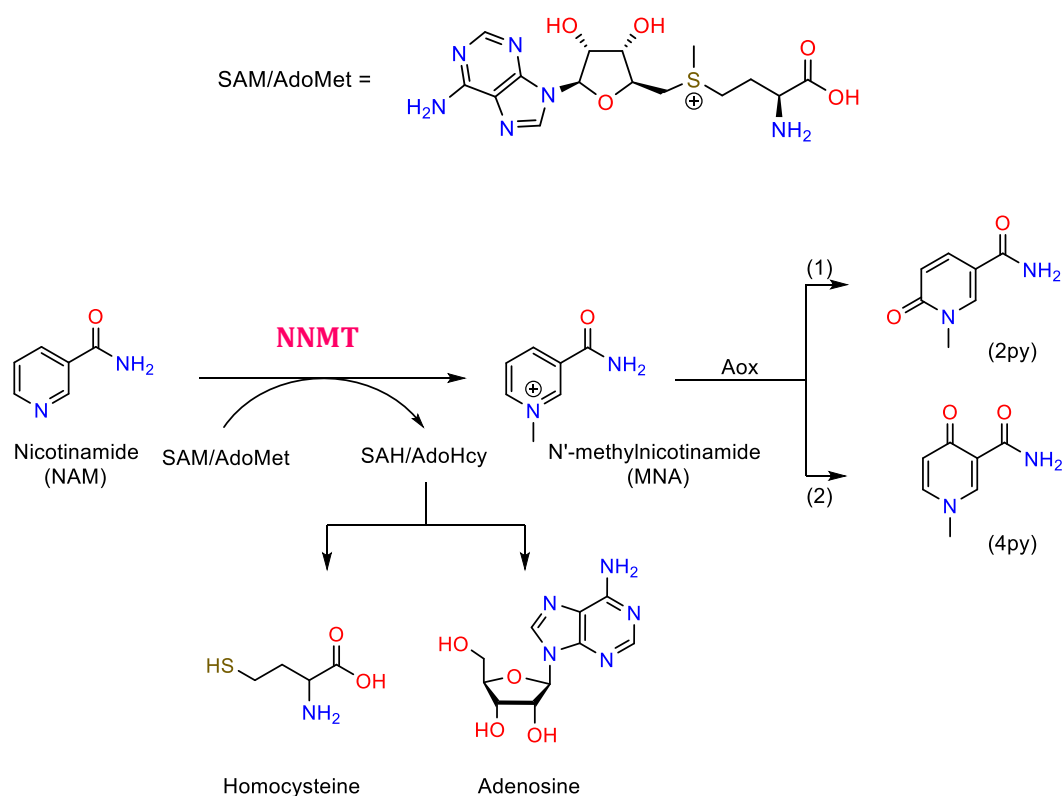


**Figure 1.** Methylation of NAM by SAM catalysed by NNMT enzyme, forming MNA and SAH. MNA product is further oxidised to give the products 2py and 4py. By-substrate SAH is broken down to Homocysteine and Adenosine.



### 1.3. NNMT in non-diseases states

#### 1.3.1. Detoxification and metabolism

Thirty years ago, the role of NNMT in the human body was thought to be exclusive in detoxification and metabolism. It plays a crucial role in the biotransformation and detoxification of many xenobiotic compounds by catalysing NAM, pyridines and other structural analogues to yield MNA pyridiniums<sup>3,5</sup>. The metabolism of drugs, toxic chemicals, hormones, and micronutrients is a crucial topic in pharmacology and endocrinology. It is often implicated in many diseases and pathophysiological processes, such as cancer and resistance to chemotherapy<sup>6</sup>. *N*-methylation is one method by which the liver metabolises drugs and other xenobiotic compounds.

#### 1.3.2. NNMT as a regulator of the actions of NAM and NAD<sup>+</sup>

Apart from the unique ability to utilise NAM as a methyl acceptor substrate, NNMT is also believed to be involved in the regulation of Nicotinamide Adenine Dinucleotide (NAD<sup>+</sup>) biosynthesis by metabolising NAM, a precursor for NAD<sup>+</sup> (**Figure 2**)<sup>7</sup>. NAD<sup>+</sup> is a central co-enzyme for fuel oxidations and the interconversion of different metabolites classes, including the conversion of carbohydrates to lipids<sup>8</sup>. NAD<sup>+</sup> also serves as a cosubstrate for the sirtuins, which constitute a family of NAD<sup>+</sup>-dependent sirtuin deacetylases<sup>9</sup>. By taking NAM away from the NAD<sup>+</sup> metabolism pathway, NNMT activation drives the depletion of NAD<sup>+</sup>, ameliorate fatty liver diseases and liver fibrosis.<sup>10,11,12,13</sup>. Also, the involvement of NNMT in the NAD<sup>+</sup> metabolic process may influence the activity of sirtuin. In addition, activation of NNMT impacts the methylation capacity in tissues; the index ratio between SAM and SAH decreases, followed by a reduction in gene methylation that is believed to be the cause of tumorigenesis<sup>14</sup>. Hence, NNMT has emerged as a modulator of cell metabolism by connecting metabolic and epigenetic pathways.

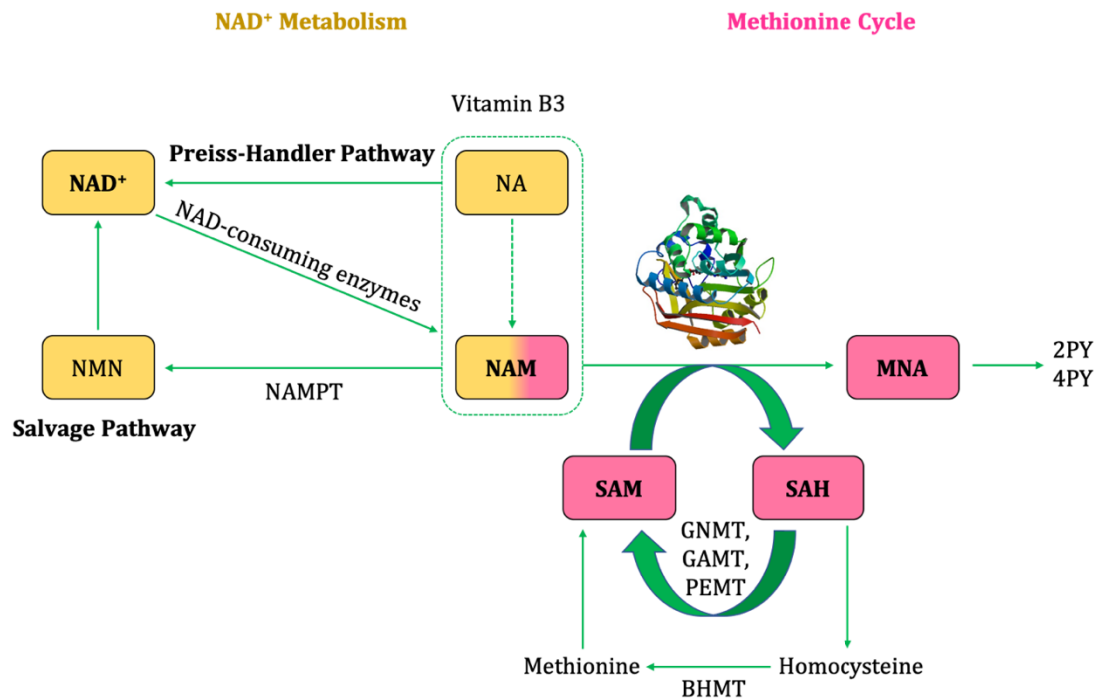


**Figure 2.** NNMT links NAD<sup>+</sup> and methionine metabolism. Nicotinic acid (NA) is metabolised to NAM via the amidation pathway. NA and NAM are the common forms of Vitamin B<sub>3</sub>, NA is from plant-derived food while NAM is from animal-derived food. NA and NAM are converted to NAD<sup>+</sup> through the Preiss-Handler and Salvage pathways respectively. NAD<sup>+</sup> is metabolised to NAM by the enzymatic activities of NAD<sup>+</sup>-consuming enzymes such as Surtuins and PARPs. NNMT methylates NAM using SAM as a methyl donor, yielding MNA and SAH as explained in **Figure 1**. GNMT, GAMT, PEMT are the main methyltransferases mediating SAM catabolism in the liver. BHMT is the enzyme responsible for the re-methylation of homocysteine to generate methionine.

#### 1.4. Implication of NNMT in disease states

NNMT was initially thought to be primarily involved in the metabolism and clearance of xenobiotics. However, recent research suggests NNMT plays a far more complex role in several important disease states.

##### 1.4.1. NNMT upregulation in cancer

With advancements in microarray and proteomic techniques, it becomes apparent that NNMT expression is increased in a wide variety of cancers, such as bladder cancer<sup>14</sup>, lung cancer<sup>15</sup>, colorectal cancer<sup>16,17</sup>, gastric cancer<sup>18,19</sup> and hepatocellular cancer<sup>17,6</sup>. Prior research has revealed the association between

highly expressed NNMT and poor prognosis in solid tumors. NNMT could be involved in cell proliferation, viability, metastatic potential as well as tumor cell sensitivity to chemotherapeutic treatment<sup>20</sup>. In breast cancer, NNMT protects cells from oxidative damage and enhances chemoresistance through stabilising sirt1 protein<sup>21</sup>. Other studies have shown that NNMT knockdown decreased the proliferative, migratory and invasive of various cancers; these findings support the notion that NNMT overexpression enhances the aggressiveness of various cancers<sup>22</sup>. The factors driving the upregulation of NNMT in cancers is unknown, leading to the proximal mechanism of NNMT action has yet to be elucidated. A plausible pathway came up in one study proposed that NNMT acts as a methyl donor sink, in which enhanced NNMT expression decreased the SAM:SAH ratio, leading to the DNA hypomethylation, which results in cancers<sup>23</sup>. While the precise cellular mechanism of NNMT overexpression that promote tumour development and progression remains unclear, it has been recently shown that NNMT acts as a master metabolic regulator of cancer-associated fibroblasts<sup>24</sup>. Thus, NNMT inhibitors (NNMTIs) may serve as useful therapeutics to help further investigate the complex activities of NNMT in cancers.

#### 1.4.2. NNMT in association with type-2 diabetes (T2D)

A recent study has shown that the expression of NNMT in adipose tissue results in an increased occurrence of T2D and NNMT levels positively correlate with insulin resistance<sup>13</sup>. High supplementation of NAM could induce severe adverse effects such as liver injury, insulin resistance and glucose tolerance. All of which are significant hallmarks for the pathogenesis of obesity and T2D<sup>25</sup>. For instance, prolonged feeding of high NAM was reported to reduce insulin sensitivity in glucose-tolerant patients because MNA could increase blood glucose, hence mediating insulin concentration<sup>13</sup>. In another aspect, NNMT has a significant impact on the metabolic pathways of amino acids tryptophan, tyrosine and arginine<sup>26</sup>. These amino acids are responsible for the synthesis of biological products which have significant regulatory effects on energy metabolism, protecting pancreatic cells, promoting insulin secretion and increasing the body's tolerance to glucose<sup>27,28,29,30</sup>.

Up to date, there has been no evidence that abnormal activity, upregulation or downregulation of NNMT have a direct and significant impact on T2D. However, it is increasingly evident that high NNMT expression and activity in the white adipose tissue, as observed in obesity, trigger adiposity-induced insulin resistance and related metabolic syndromes, particularly T2D<sup>25,27</sup>. Increasing white adipose tissues leads to increased insulin resistance across the entire body, decreased glucose uptake, increased circulating glucose (hyperglycaemia) and can result in T2D. With the upregulation of NNMT, NAM would not be salvageable, and as such, the NAD<sup>+</sup>-dependent processes would be hindered<sup>31</sup>. This may limit fuel oxidation and promote fat storage since decreasing NAD<sup>+</sup> could reduce energy metabolism. The loss of SAM could result in the SAM-mediated polyamine flux pathway losing its ability to regulate energy expenditure in the adipose tissues, which leads to increased white adipose tissue (WAT) mass (**Figure 3**). These unique features provide a better indication of how NNMT might indirectly contribute to the cause of T2D through obesity, rendering NNMT an attractive target for treating T2D.

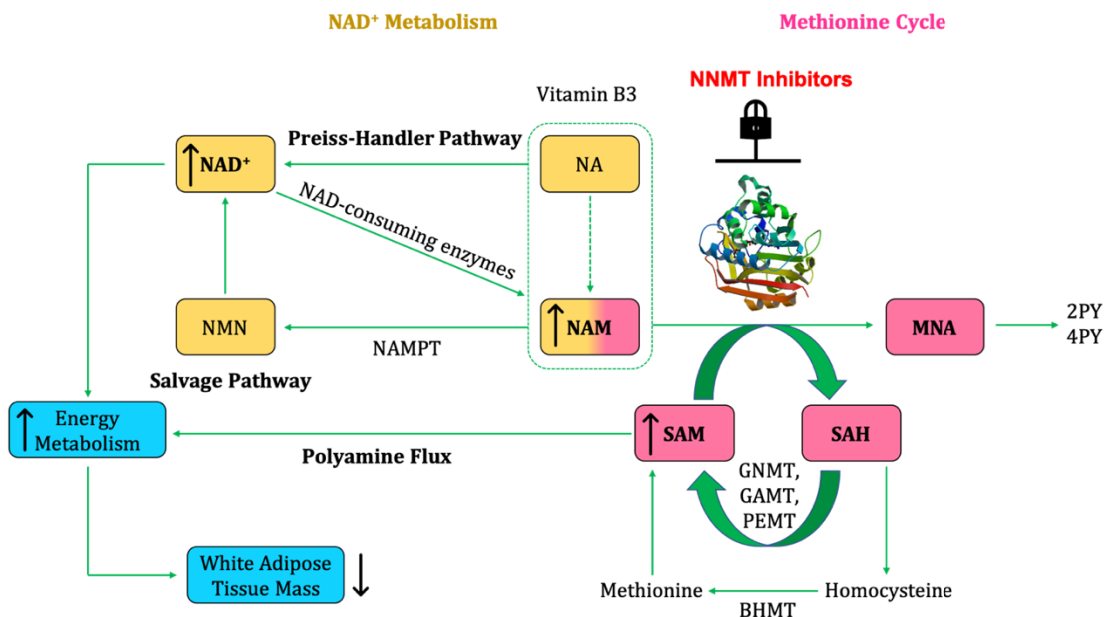


**Figure 3.** Effects of NNMT Inhibitors on intracellular levels of NAD<sup>+</sup> salvage pathways and methionine cycle. Inhibiting NNMT enzyme increases NAM concentration and leading to less-to-none competition between NAD<sup>+</sup> and NNMT. Hence more NAD<sup>+</sup> is formed that increases energy metabolism and reduces the amount of fat stored in body. In addition, increasing SAM – since the methionine cycle is blocked – allows the polyamine flux to easily occur, contributing to energy metabolism and thus reducing WAT mass.

### 1.4.3. NNMT in neurological disorders

NNMT also involves in neurological disorders. One such example is the link between NNMT over-expression in brain cells and Parkinson's disease<sup>32,33,34</sup>. Upregulation of NNMT lowers the amount of NAM available for NAD<sup>+</sup> synthesis and also increases the production of neurotoxic *N*-methylpyridinium compounds that poison Complex I, leading to diminished ATP production<sup>34</sup>. When NNMT is over-expressed in the human body, it increases homocysteine level through the chemical process shown above (**Figure 1**). This has been shown to result in schizophrenia<sup>32,35</sup>. Moreover, NNMT is extremely polymorphic in humans<sup>36</sup>; this may play a role in damaging transcription regulation, which is a known genetic indicator for bipolar disorders<sup>32</sup>.

### 1.5. The structure of NNMT

Human *h*-NNMT was first identified and isolated by cDNA cloning from the liver and was confirmed to be present in the cytosol<sup>37,38,39</sup>. The NNMT gene was also found to have a significant expression level in kidney, lung, musculoskeletal placental, cardiac and adipose tissue. It was found to contain 264 amino acids with a molecular weight (M.W.) of 29574.02 (g·mol<sup>-1</sup>), 16.5 kb in length, 3 exons and 2 introns<sup>3,13</sup>.

The 3-dimensional (3D) structure of NNMT contains nine  $\alpha$ -helices and nine  $\beta$ -strands connected by numerous coils and turns. Located close to the *N*-terminus and  $\beta$ -hairpin is a feature described as a 'cap', which is the SAM cofactor entrance formed by two  $\alpha$ -helices (**Figure 4A**). The NNMT protein structure is divided into three binding pockets, which together are classified as the active sites. These are categorised as the adenosine group (A), amino acid moiety (B) and nicotinamide pocket (C) (**Figure 4B**)<sup>40</sup>. In the study by Peng *et al.*, using NAM and SAH – the immediate product following a donation of the methyl group of SAM – as ligands for the substrate and cofactor-binding sites, respectively, the residues involved in binding of the substrate and cofactor were identified. The interactions between NAM and SAH with the protein receptors were generated into the 2D diagram via

BioVia Discovery Studio 4.5 using the crystal structure NNMT (Protein Data Bank code: 6B1A) (**Figure 4C**). NAM structure fits onto the receptors and interacts with Asp 197, Ser 213 while SAH occupies two adjacent binding sites, adenosine pocket (Tyr 20, Thr 163) and amino acid pocket (Val 143, Asp 142). In addition, tyrosine residues constitute a significant proportion of each of the binding sites. This structural information has been utilised in the design of first general NNMTIs.

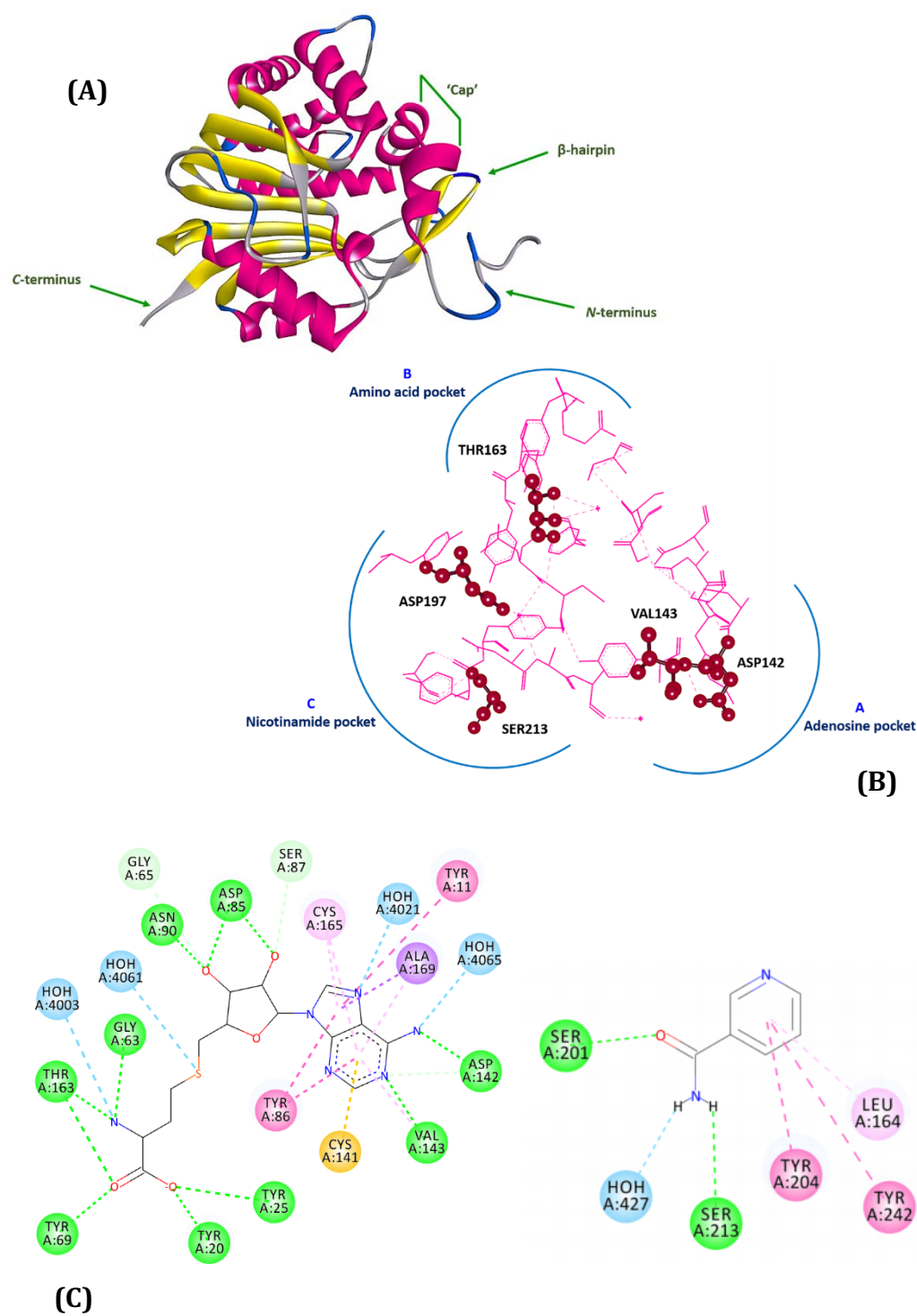


**Figure 4.** **(A)** Ribbon cartoon of 3-Dimensional (3D) Nicotinamide *N*-methyltransferase (NNMT) structure. Pink denotes  $\alpha$ -helix; yellow,  $\beta$ -strand; grey, coil; and blue, turn. **(B)** Protein structure of NNMT showing the active site divided into three binding pockets: A, adenosine pocket; B, amino acid pocket; C, nicotinamide pocket. **(C)** Schematic overview of the SAH structure (left) and NAM structure (Right) interact with the defined active sites of *h*NNMT through water hydrogen bond (Blue),

conventional hydrogen bond (Green), carbon hydrogen bond (Light Green), pi-sigma bond (Purple), pi-sulfur bond (Yellow), pi-pi stacked (Pink) and pi-alkyl (Light Pink).

## 1.6. NNMT Inhibitor development

Since NNMT is associated with various diseases, small molecule inhibitors of NNMT (NNMTIs) have been developed as potential therapeutics. The majority of NNMTIs were derived from the substrates and products of the NNMT enzymatic reaction, also known as reference compounds (**Figure 5**), as these compounds are known to fit within the NNMT active site. In the following section NNMTIs are discussed based on the reference compound from which they were designed.

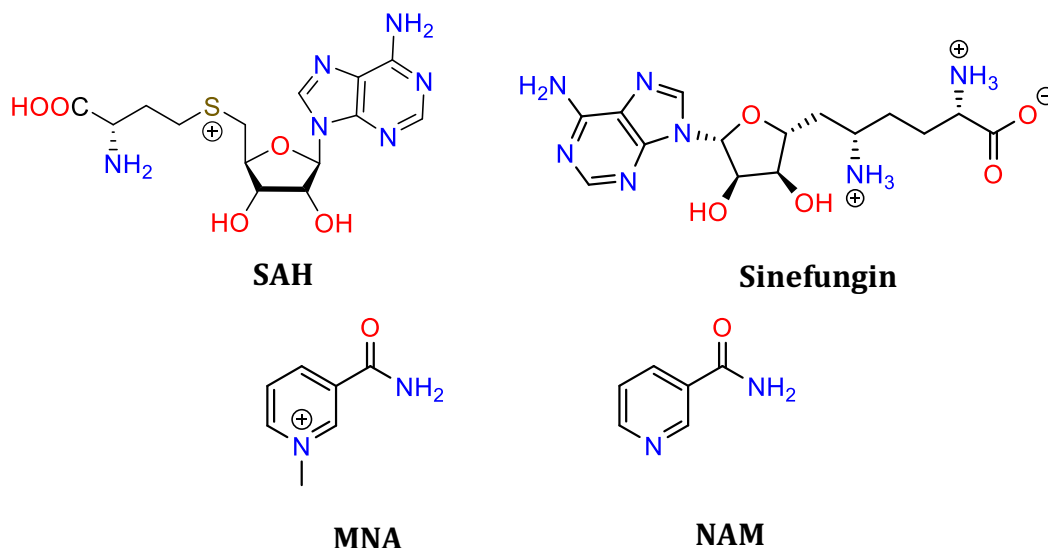


**Figure 5.** Structures of reference compounds SAH, Sinefungin, MNA as reported to be NNMTIs

### 1.6.1. NAM derivatives as NNMTIs

As reported, NNMT catalyses the transfer of a methyl group from the cofactor SAM to NAM to yield the *N*-methylated product MNA. It was found that MNA inhibits NNMT both *in vivo* and *in vitro*<sup>5,40–42</sup> and therefore development of NNMTIs derived from NAM was the direction taken in two studies.



Ruf *et al.* commenced from methoxy-substituted NAM derivative **0** (Figure 6)<sup>43</sup>, which was discovered in high throughput screening campaign of an in-house library of compounds and inhibited human NNMT with an  $IC_{50}$  of  $2445 \pm 79$  nM. A further 22 derivatives synthesised and from this compound library, two compounds stood out as having significant inhibitory activity. Compound **1**, which employed an extra methyl group relative to compound **0**, possessed an  $IC_{50} = 837 \pm 71$  nM, a 3-fold increase compared to **0**. Replacing the methoxy moiety in **0** with an *N*-methyl amine moiety yielded compound **2**, which inhibited NNMT with a 4-fold increase in activity compared to **0** ( $IC_{50} = 588 \pm 75$  nM). For further investigation of inhibitory activity, these compounds were evaluated in an *in vitro* biochemical as well as the cell-based assay and resulted in a decrease in MNA levels for over 2 hours post-dosing. This clearly suggests that compounds **1** and **2** can engage the NNMT target to achieve enzymatic inhibition resulting in MNA reduction.

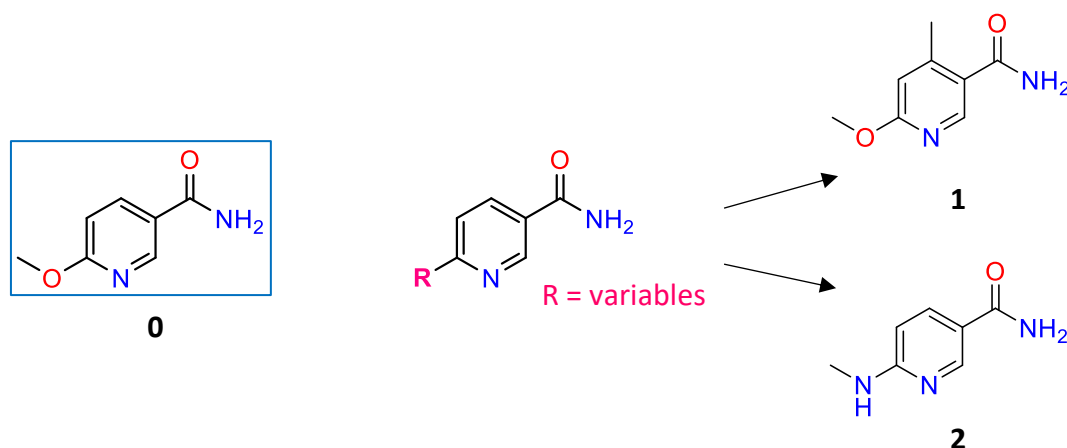


**Figure 6.** Core structure of NAM-like inhibitors developed by Ruf *et al.*. Compound **0** is the reference compound. Compound **1** and **2** was found to be the most potential NNMT inhibitors.

### 1.6.2. NAM-Adenosine and NAM-Amino Acid conjugates as NNMTIs

In the study of Van Haren *et al.*, the NAM mimicking moiety – benzamide was used to design a series of novel NNMTIs aimed at specifically exploiting both the adenosine binding domain and nicotinamide pockets. This design strategy was envisioned to impart selective binding towards NNMT relative to other SAM-dependent methyltransferases. Specifically, it was expected that important interactions with key residues conserved in the NNMT active site, such as Val 143 and Asp 142, would be maintained. Of note in the structure of proposed inhibitors

is the omission of the amino acid moiety that is present in the SAM cofactor (**Figure 7**). This omission was made based upon the designing plan as they wanted to introduce the NAM-Amino Acid conjugates NNMTIs to study whether NAM-adenosine NNMTIs has any influences on NAM-Amino Acid. NAM-adenosine analogues showed very little NNMT inhibition at a concentration of 250  $\mu$ M or more. This lack of inhibition may be explained by both the omission of the pyridine nitrogen as well as the absence of interactions with the amino acid binding pocket with Tyr 20. This explanation is supported by the significantly reduced enzymatic activity that previously reported for the Y20A mutant of NNMT<sup>44</sup>.

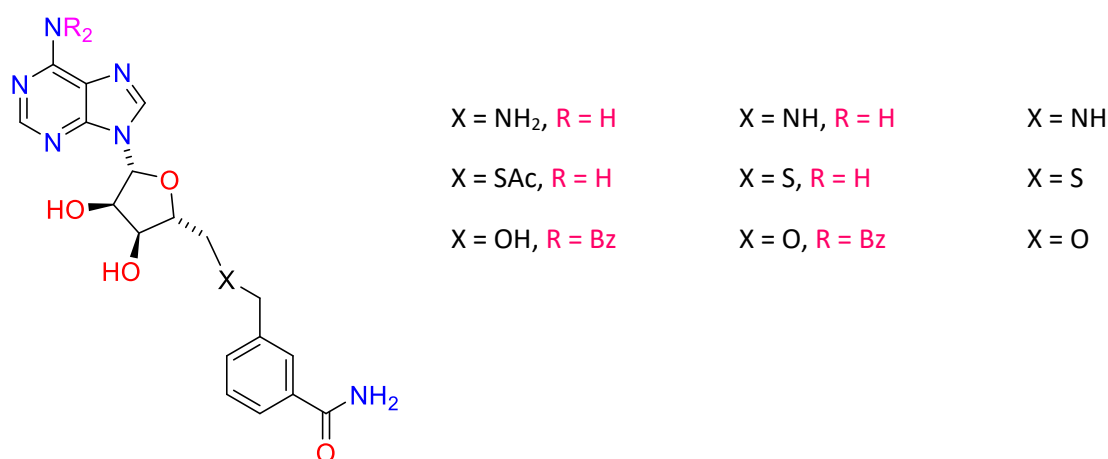


**Figure 7.** Schematic overview of first generation NNMTIs where the adenosine moiety was introduced and the NAM core structure was replaced with a mimicking group. Adenosine moiety and NAM-like rings were connected via different linkers.

To separately assess the role of the SAM amino acid group, another series of NNMTIs comprised of a NAM mimic linked to a carboxylic acid or amide moiety were introduced. To examine the binding requirements for interaction with the NNMT amino acid pocket, compounds bearing a terminal carboxylic acid, a primary amide or an amino acid moiety were prepared. Of 8 synthesised compounds, 3 showed improved inhibitory function with IC<sub>50</sub> ranging from 30 to 60  $\mu$ M (**Figure 8**). The most active compounds in this series were the 6- and 7-carbon spaced compounds **3** and **5** containing a terminal carboxylic acid (**Table 1**). The exception is compound **4**, which contains a terminal amide. This indicates that the most active compounds

were those containing either a terminal carboxylic acid or a terminal amide. In addition, linking the benzamide unit to a simple carboxylate gave much better inhibition and provided key insights into the preferred spacing and rigidity of the linker used to connect the respective bi-substrate mimicking functionalities.

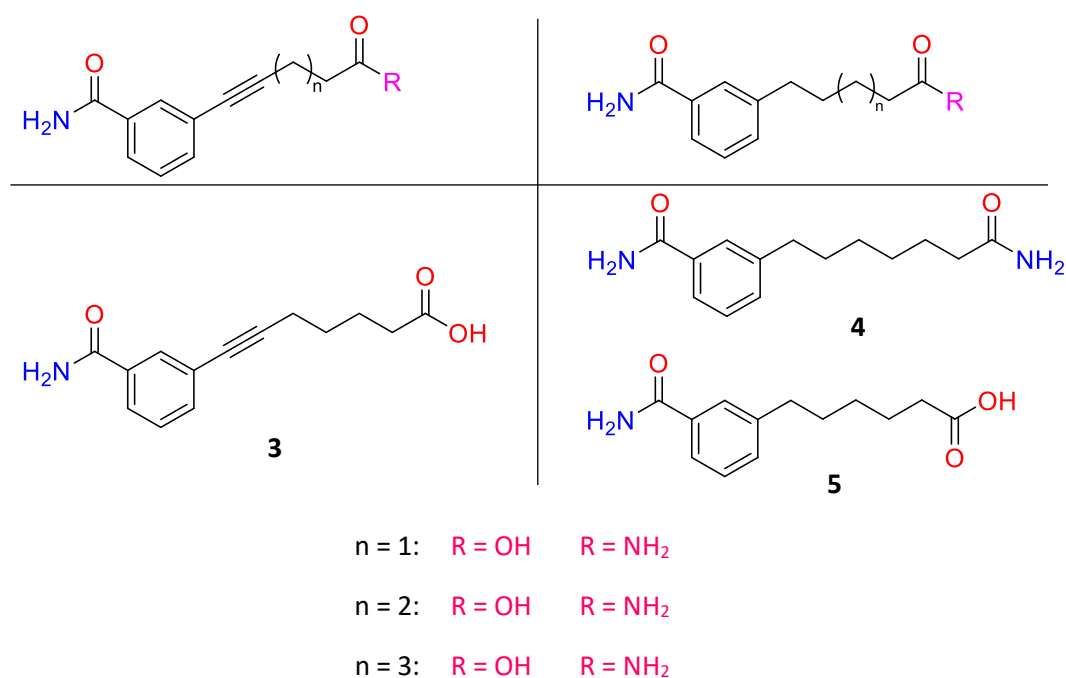


**Figure 8.** Schematic overview of second generation NNMTIs comprised of NAM-mimicking ring linked to carboxylic, amide or amino acid moiety with different linkage length. Compound **3,4** and **5** exhibit competitive inhibition.

### 1.6.3. MNA analogues NNMTIs

Van Haren *et al.* utilised MNA as the lead compound for NNMTIs development. MNA inhibited NNMT with an IC<sub>50</sub> concentration of 24.6 ± 3.2 µM<sup>40</sup>. Having such a promising IC<sub>50</sub>, they attempted to modify the structure of MNA by introducing different substituents to the pyridyl nitrogen of MNA (**Figure 9**). However, the results showed that addition of groups larger than a methyl group – as present in MNA – reduced inhibitory activity.

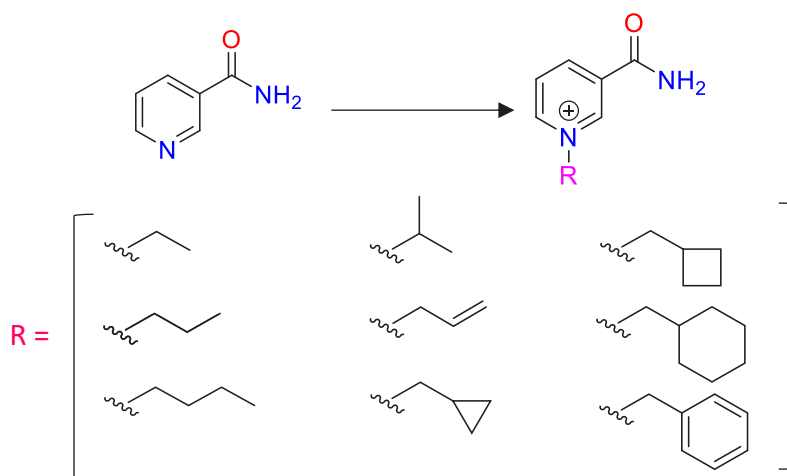


**Figure 9.** Schematic overview of alkylated NAM analogue as NNMTIs

#### 1.6.4. Quinoline and Isoquinoline derivatives as NNMTIs

A recent study conducted by Neelakanta *et al.* aimed to explore the NNMT inhibitory activity of *N*-methylated heterocycles containing several different aromatic scaffolds, including quinoline and isoquinoline<sup>41</sup>. In this study, *N1*-methylated quinolinium and *N2*-methylated quinolinium were studied (**Figure 10A**). Neelakanta *et al.* attempted to synthesise 1-methylquinolinium (1-MQ) with different substituents on each carbon in the scaffold. This approach provided incredibly positive outcomes in inhibiting the enzyme, with the IC<sub>50</sub> concentration of one compound reaching as low as 1.2  $\mu$ M and most other inhibitors falling in the range of 1.2 to 21  $\mu$ M. In a further investigation, the -CH<sub>3</sub> group was replaced with different steric and electronic properties to test if the replacement would affect the inhibitory capacity (**Figure 10B**). The results revealed that the activity of *N1*-

substituted quinolinium was inversely correlated with the size of the substituent, with  $IC_{50}$  concentration reaching over 1000  $\mu M$ . An analogue of *N*2-methylated isoquinolinium was also studied briefly, only compound **9** exhibits the lowest  $IC_{50}$  of 6.3  $\mu M$ . The quinolinium analogue series demonstrated significant NNMT inhibition, exhibited very low micromolar potency ( $IC_{50} \sim 1 \mu M$ ) and presented a promising scaffold to selectively bind to NNMT as a potent inhibitor (**Figure 10C**).

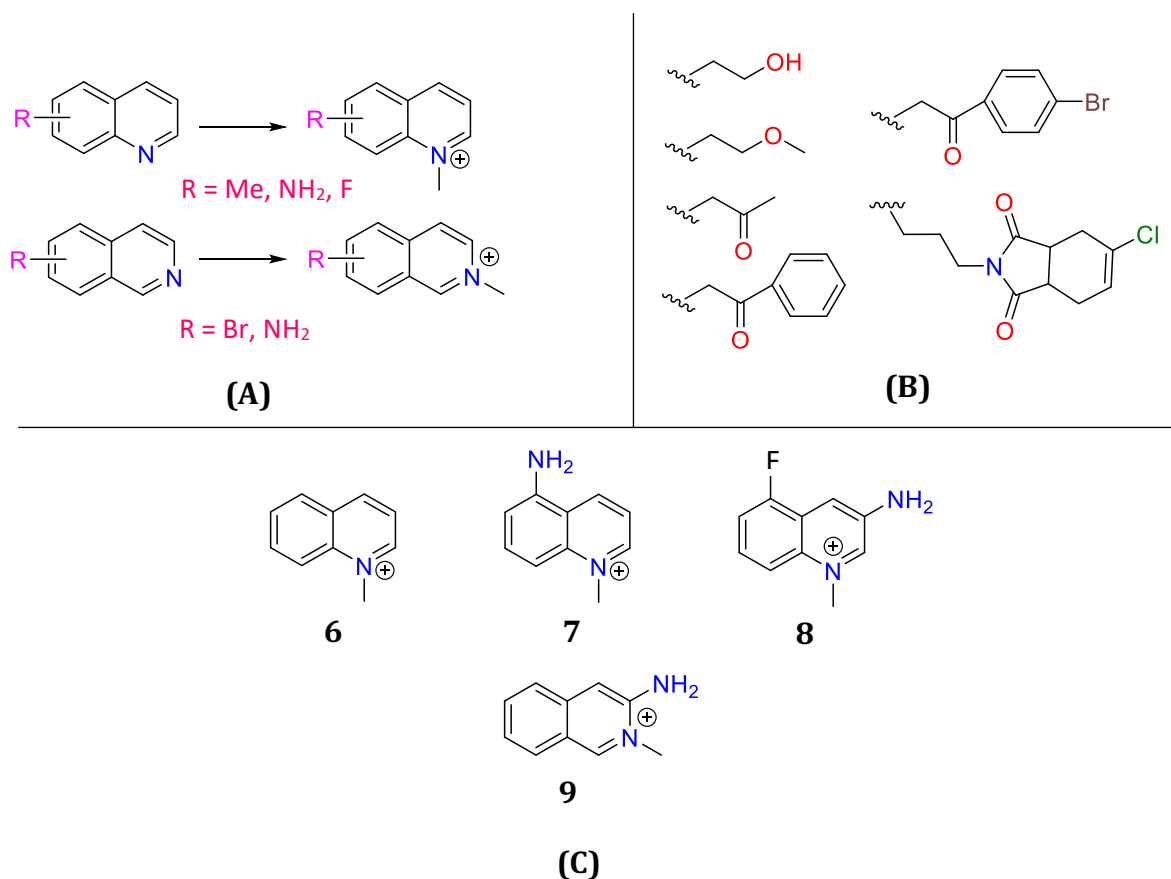


**Figure 10.** (A) Schematic overview of *N*-methylated Quinoline and Isoquinoline with different substituents on the adjacent aromatic ring as proposed NNMTIs. (B) Structure of moieties that replaced with the methyl group on *N*-methylated position. (C) Potential NNMTIs exhibited exceptional inhibitory activities.

### 1.6.5. A covalent NNMTI targeting Cys 165 unique to NNMT

In a different approach, a covalent ligand **10** targeting non-catalytic Cysteine 165 (Cys 165) has been developed to inhibit NNMT (**Figure 11**)<sup>2</sup>. Compound **10** acts as a suitable inhibitor through strong reactivity with Cys 165 ( $IC_{50} = 10 \mu M$ ). The reason behind this approach was that Cys 165 could only be found in NNMT and not in other methyltransferase proteins (MTs)<sup>44</sup>. With **10** being the only compound that is able to interact with Cys 165 in the receptor, it is still unclear whether binding to Cys 165 could switch off the activity of the enzyme. Nonetheless, Cys 165 residue will be taken into consideration when designing the potential NNMT inhibitors in this project.

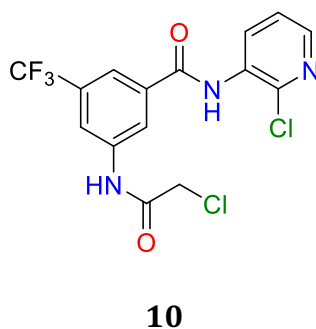


**Figure 11.** Structure of covalent NNMT inhibitor **10** targeted Cys 165 receptor

### 1.6.6. Bi-substrate inhibitors

The first ternary NNMTI was designed with the aim of interacting with all the defined receptors at the NNMT active site simultaneously. Compound **11** showed strong inhibition of NNMT with an  $IC_{50}$  of  $29.2 \pm 4.0 \mu M$ , similar to the inhibitory activity of SAH and MNA (**Table 1**). Following this approach, there have been some attempts to modify compound **11**, leading to the introduction of a new type of NNMTI – bi-substrate inhibitors.

Up to date, a lot of researches have been conducted on bisubstrate inhibitors, targeting both the substrate and cofactor binding sites of the enzyme. In support, the interaction between NAM and substrate SAM with three active sites has been revealed. Most ligand-protein interactions (**Figure 12**) in this binding pocket are conserved, which suggests that NNMT enzymatic products, such as SAH (**Figure 5**),

could also act as inhibitors. IC<sub>50</sub> concentrations of these NNMTIs were reported and are compiled in **Table 1**. Based on these findings, trivalent inhibitor compound **11** was designed to bind to all three pockets A, B and C of NNMT, proving that **11** could act as an inhibitor by occupying all active sites<sup>40</sup>.

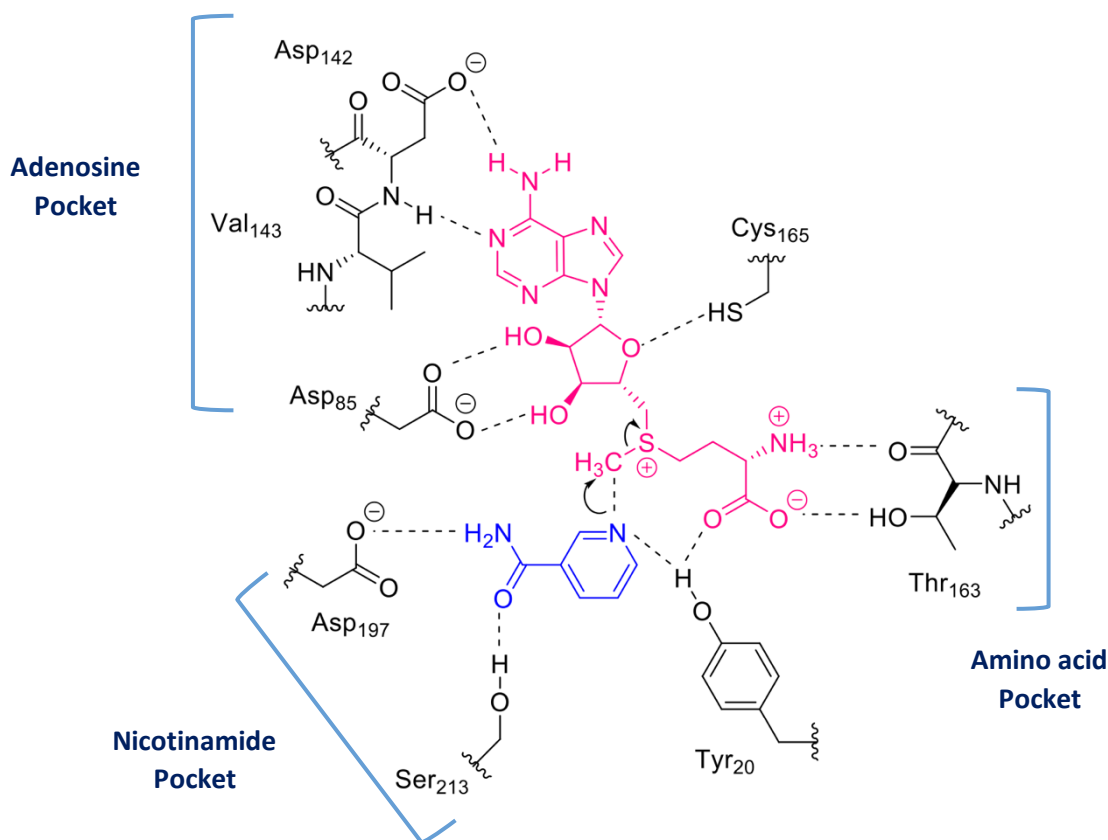


**Figure 12.** Schematic overview of the interaction between methylation product and three active sites of NNMT. The carboxylate oxygen atom in the homocysteine moiety creates a hydrogen bond with two hydroxyl (-OH) groups from the side chain Tyr 20 and Thr 163. Ribose OH groups interact with Asp 85. The N1 nitrogen forms H-bonds with the main chain amide nitrogen of Val 143 and there are conserved H-bonds of this moiety to Asp 142. The nicotinamide moiety binds to Asp 197, Ser 213 as well as Tyr 20. The nicotinamide pocket binds to NAM (in blue) and substrate SAM resides within the amino acid pocket and adenosine pocket.

Further research on bisubstrate inhibitors showed that the linkage between the substrate mimic and cofactor mimic from compound **11**, with an increase in the linker length, led to **12** and **13**, which were examined for their inhibitory activity (**Figure 13B**)<sup>45</sup>. Based on the structure of **11**, **12** and **13**, a suggestion can be made

that binding of at least the NAM and amino acid pockets is necessary for significant NNMT inhibition.

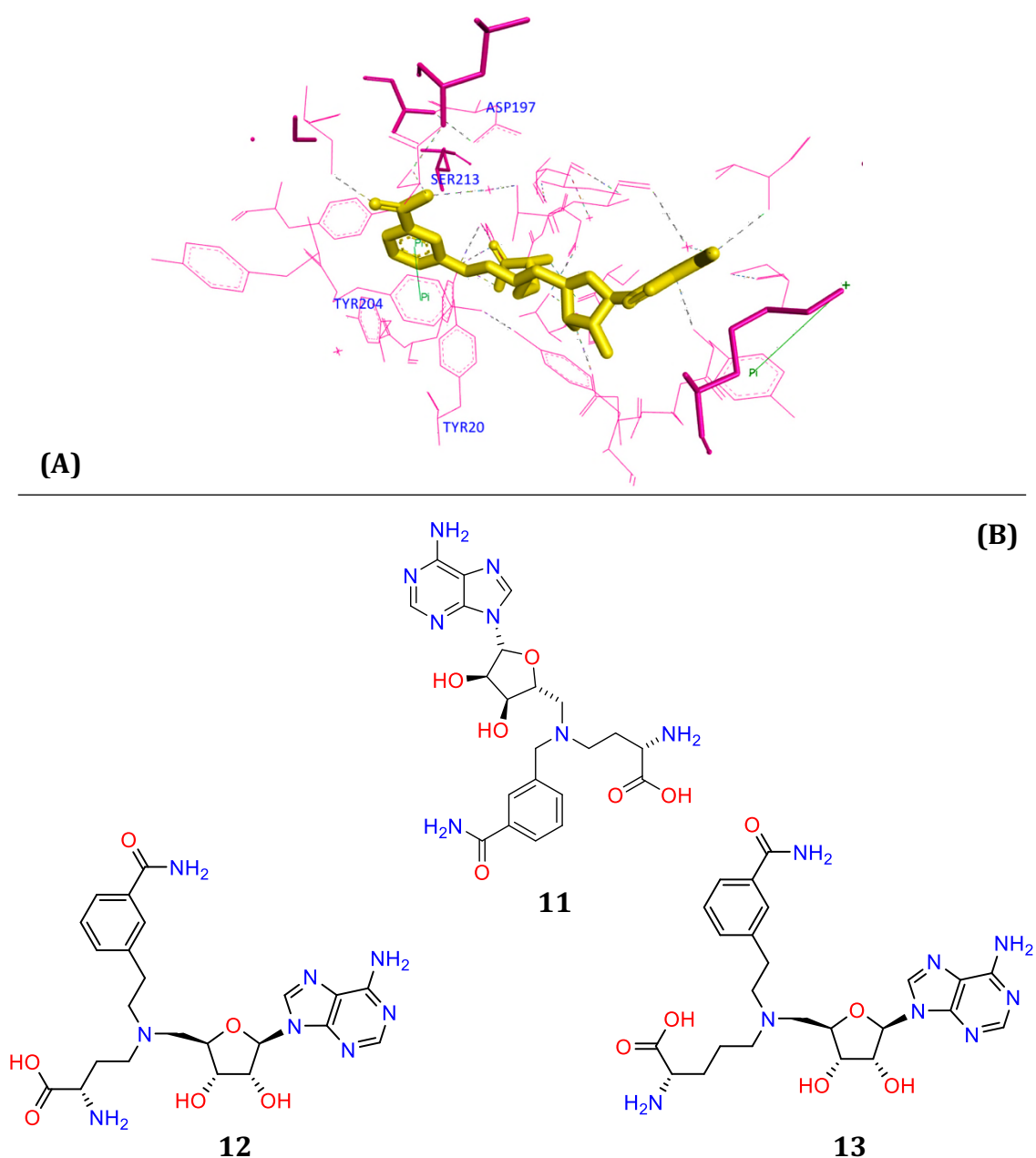


**Figure 13.** (A) 3D structure derived from the molecular docking software showing the binding of inhibitor **11** within the NNMT enzyme. NAM pyridine ring was replaced by 3-amido phenyl structure. This structure nests nicely within Ser 213 and Asp 197. No interaction can be seen between Tyr 20 and the structure itself due to the loss of N1 nitrogen. The  $\pi$ - $\pi$  stacking with Tyr 204 remains unchanged, which leads to the sufficiency in compensating for the loss of N1-nitrogen in pyridine ring of NAM. (B) The first synthesised bisubstrate NNMTIs **11** and its developed compounds **12**, **13**.



The lead NNMT inhibitor **11** was modified through changes to the nicotinamide moiety, replacement with other aromatic substituents and variation in the length of the linker connecting the amino acid moiety<sup>46</sup>. Based on the high conservation of the residues in the adenosine binding pocket, no changes were made to the adenosine group (**Figure 14**). The investigation revealed that incorporation of a naphthalene moiety while maintaining the linker length to the amino acid resulted in much better inhibitory activity, with an  $IC_{50}$  of 1.4  $\mu$ M (**Compound 14**). Replacing the naphthalene moiety reintroduced the hydrophobic nicotinamide binding pocket via  $\pi$ - $\pi$  stacking interactions, proving the importance of  $\pi$ - $\pi$  bonding with Tyr 204 as a key interaction to improve inhibitory activity.

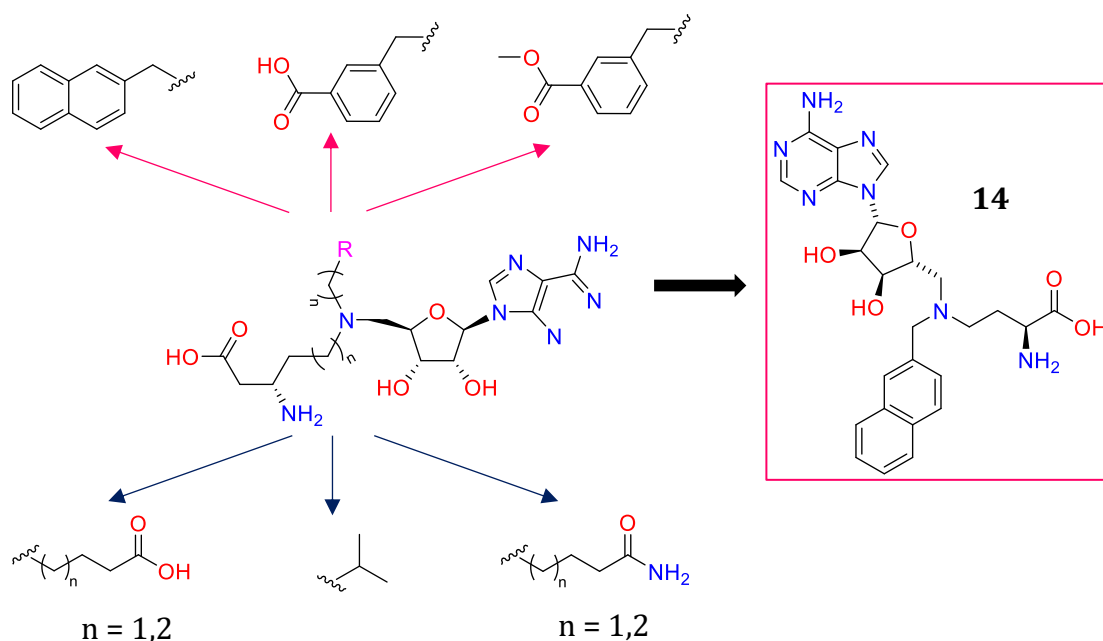


**Figure 14.** Schematic overview of the design strategy of the third generation NNMTIs based on trivalent bisubstrate NNMTI **11**. Compound **14** exhibited enhanced activity

A more recent study attempted to design NNMT bi-substrate inhibitors by changing the linker length and type from the sinefungin moiety to an aromatic system mimicking NAM<sup>47</sup>. Of the many novel synthesised compounds, compound **15** showed very competitive inhibitory activity, with an established  $K_i$  of  $1.6 \pm 0.3 \mu\text{M}$  and a claim to be the most potent inhibitor to date. The difference between this inhibitor and other known bi-substrate inhibitors is the adoption of the propargyl linker to conjugate SAM and a substrate analogue. In total, the propargyl linker of **15** may provide insights into the orientation of the methyl transfer of NNMT.

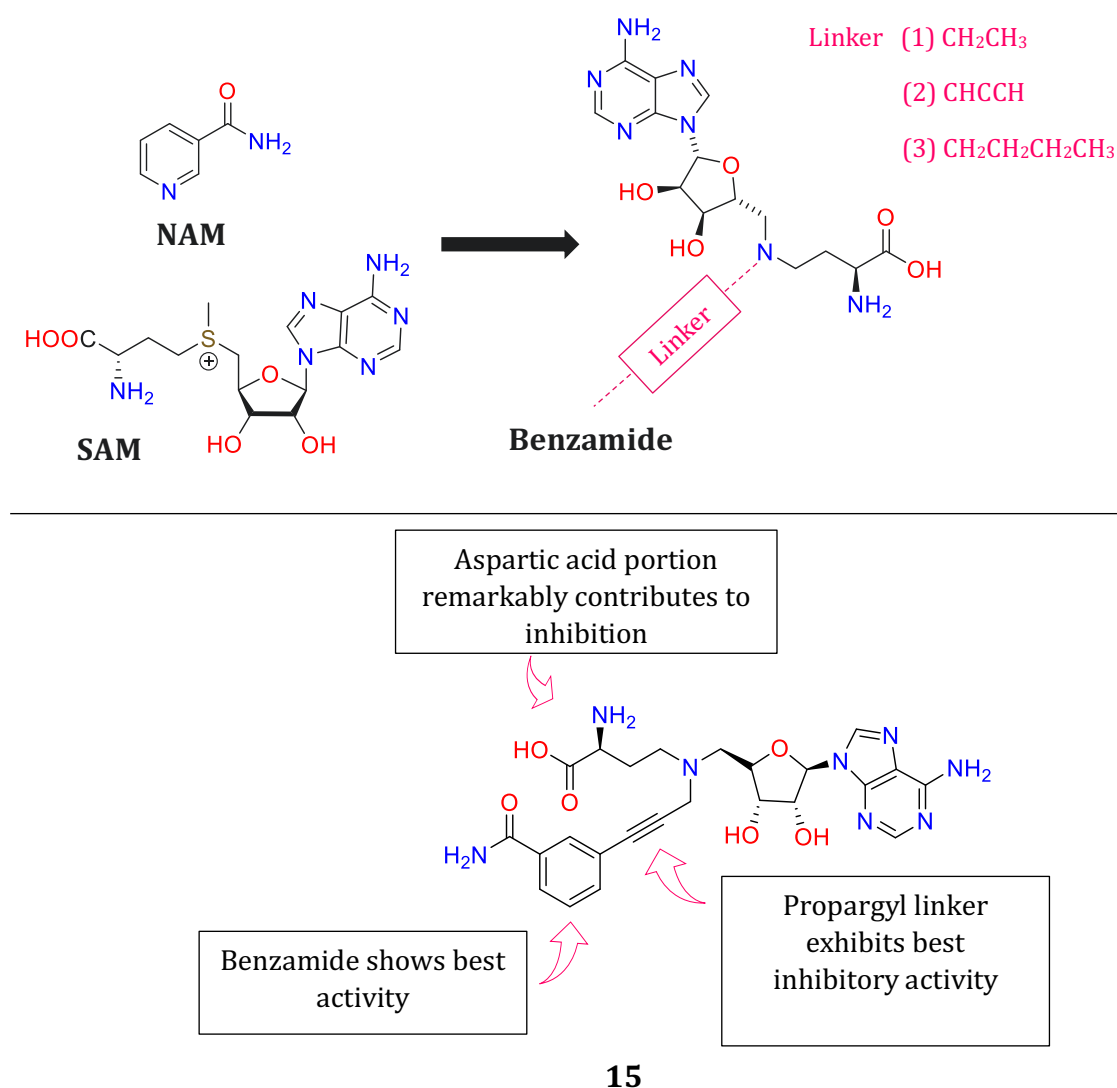


**Figure 15.** Schematic overview of designing new NNMTIs with the newly introduced alkyne linker. Compound **15** with propargyl linker exhibits best inhibition

At the same time this work was introduced, another study was published with the similar approach of designing high affinity alkynyl bi-substrate NNMTIs<sup>48</sup>. In this work, they synthesised compound **16** through a different synthetic scheme. Changing the linker from a NAM-like ring and sinefungin moiety to a C-C type (rather than C-N and C-S) revealed **16** to be a highly potent, subnanomolar (500 pM) NNMTI. The use of a propargyl linker in designing bi-substrate inhibitors has shown to improve NNMT inhibitory activity. Alkynes provide unique rigidity, geometry and spatial occupancy that cannot be captured by other common linkers and could be a new approach to better design and synthesise NNMT bi-substrate inhibitors.

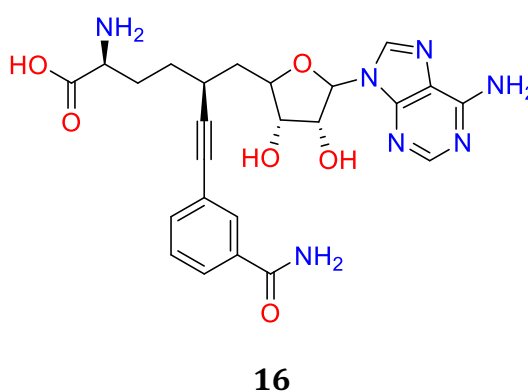


**Figure 16.** High-affinity alkynyl bisubstrate inhibitor of NNMT

#### 1.6.7. Suicide Inhibitors – a new introduced target

Research was recently undertaken to explore a different type of NNMTI – suicide inhibitors, the first NNMT-directed activity-based probes<sup>49</sup>. This new direction took full advantage of the ability to transfer a methyl group from SAM to various reported substrates. By designing a suitable substrate to exploit the broad substrate scope of NNMT, the *N*-methylated product could act as a potent NNMTI and directly neutralise the enzyme activity. Compound **17** was proposed to covalently modify the active site Cys 159 in dimethylarginine dimethylaminohydrolase enzyme (DDAH) and therefore was thought to be a potent precursor to generate suicide inhibitors<sup>50,51,52,53</sup>. The same study also revealed that in neutral form, **17** was unreactive; however, protonation of the nitrogen on the pyridine ring by enzymatic activity enhanced the electrophilicity of the 4-chloro position; the process of NNMT *N*-methylation mimicked this effect. Applying this

theory, six compounds were developed in order to test the ability to receive a methyl group from SAM during NNMT enzymatic activity (**Figure 17**).

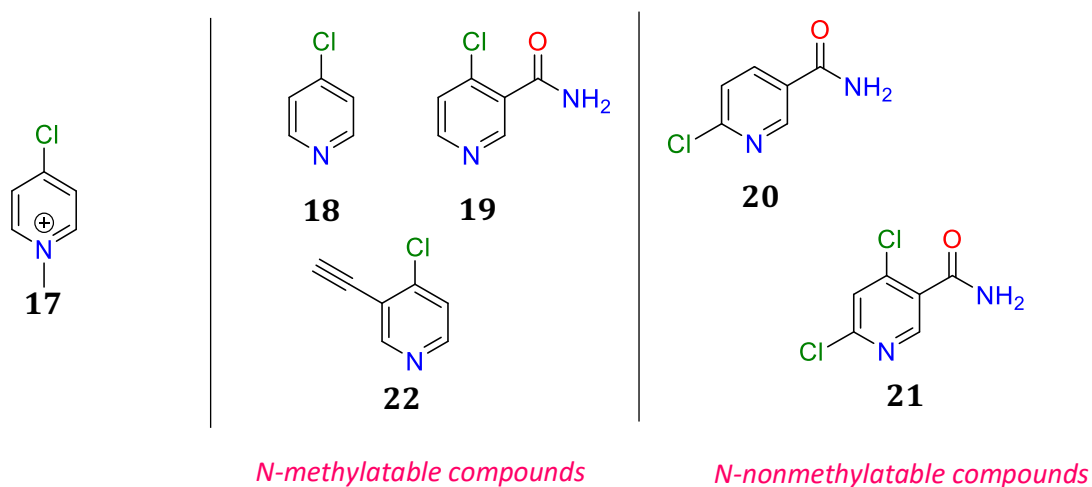


**Figure 17.** Structure of compound **17** as covalently modify active site Cys 159. Proposed compounds **18-22** as suicide NNMT inhibitors. **18, 19, 22** undergoes N-methylated in the enzymatic reaction while **20** and **21** does not.

Three compounds, **18, 19** and **22**, were found to be suicide inhibitors reliant on NNMT catalysis to generate the reactive species. Testing on a cellular level confirmed that compounds **18, 19** and **22** inhibited NNMT activity with  $EC_{50}$  in the double-digit micromolar range. In conclusion, three compounds **18, 19** and **22** were successfully utilised as NNMT substrates to generate the corresponding N-methylated products. The research also confirmed that the proposed theory of covalently modifying Cys 159 was correct and worked on NNMT (**Figure 18**). Because these compounds rely on enzyme catalysis to generate the reactive species, they are considered mechanism-based inactivators. Despite showing modest potency in inhibiting NNMT, suicide inhibitors could reduce off-target toxicity because NNMT would be generating its own inhibitor. Designing suicide-inhibitors could be a new approach in improving the potency and selectivity of NNMTIs.

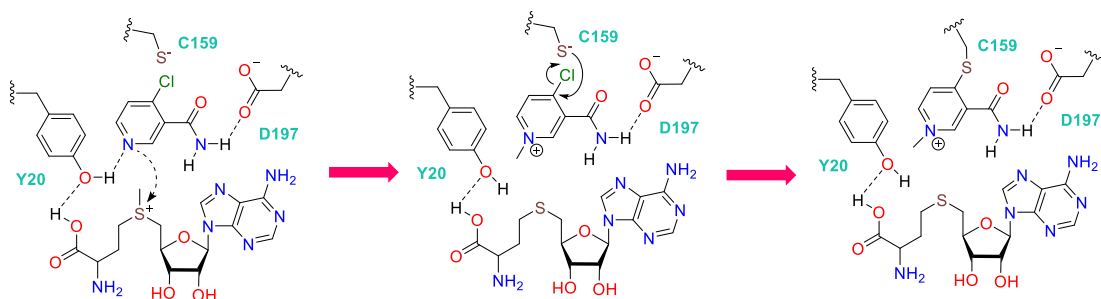


**Figure 18.** Inactivation of NNMT targeting Cys 159 by *N*-methylated product on compound **19**. In solution, **19** is found to be less reactive neutral form and so remains quiescent towards biological nucleophiles. The active site residues bind with **19** and the *N*-methylation process starts to occur. Cys 159 deprotonation, possibly facilitated by its neighbour residues, leads to attack on C<sub>4</sub> of the inactivator. The pyridinium form of the inactivator allows stabilisation of the subsequent tetrahedral sigma-complex, followed by the elimination of Chlorine atom. Finally, deprotonation of the covalent adduct and Cys159 move away, switch-off NNMT activity.

**Table 1.** IC<sub>50</sub> concentrations of NNMTIs<sup>a</sup>

Compound	IC <sub>50</sub> in $\mu\text{M}$	Compound	IC <sub>50</sub> in $\mu\text{M}$
SAH	26.3 $\pm$ 4.4	<b>6</b>	12.1 $\pm$ 3.9
Sinefungin	3.9 $\pm$ 0.3	<b>7<sup>b</sup></b>	1.2 $\pm$ 0.1
MNA <sup>b</sup>	24.6 $\pm$ 3.2	<b>8<sup>b</sup></b>	1.2 $\pm$ 0.2
<b>0</b>	2.445 $\pm$ 0.079	<b>9</b>	6.3 $\pm$ 2.7
<b>1</b>	0.84 $\pm$ 0.071	<b>10</b>	10
<b>2</b>	0.58 $\pm$ 0.075	<b>11<sup>b</sup></b>	29.2 $\pm$ 4.0
<b>3</b>	57.8 $\pm$ 4.2	<b>12</b>	14.0 $\pm$ 1.5
<b>4</b>	69.0 $\pm$ 14.8	<b>13</b>	160 $\pm$ 1.0
<b>5</b>	30.8 $\pm$ 3.6	<b>14</b>	1.41 $\pm$ 0.16

<sup>a</sup> Values are given as means  $\pm$  standard error were reported based on triplicate performance.

<sup>b</sup> IC<sub>50</sub> value reported with no selectivity profiling data were provided.

### 1.7. Preliminary work: Identification of a new NNMTI Lead compound

Despite the progress in NNMTIs development reported in section 1.6, all currently identified NNMTIs suffer from low potency or poor physiochemical properties that limit their therapeutic potential. Thus, the need for new NNMTIs continues. Compound **23** (**Figure 19**) was synthesised as part of an antibacterial drug discovery. Compound **23** was submitted to the Lilly Open Innovation Drug Discovery program and found to inhibit *h*NNMT with an  $IC_{50}$  1  $\mu$ M, and thus shows promise as a new and structurally novel NNMTI lead compound.

The synthesis of **23** is shown in **Figure 19**. Starting with commercially available 3,4-dimethoxyphenethylamine, a ring formation reaction with formic acid produces the THIQ core, which is then *N*-alkylated with propargyl bromide to yield an alkyne intermediate. In parallel, an organic aryl boronic acid was converted to an aryl azide, which was then coupled to the alkyne intermediate “Click chemistry” in a Copper-catalysed azide-alkyne cycloaddition (CuAAC) reaction, yielding **23** (**Figure 19**).

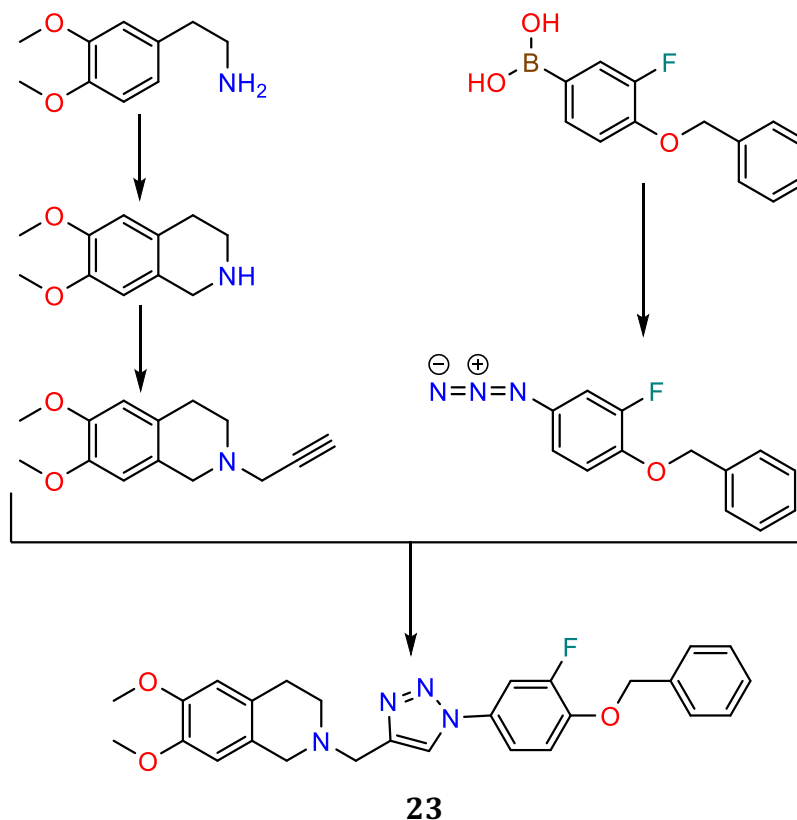


**Figure 19.** Schematic overview of compound **23** synthetic route

The original plan for my Masters research was to synthesise an analogue library of **23** with the aim of optimising its NNMT inhibitory potency. Therefore, attempts to synthesise a large quantity of the key alkyne intermediate were carried out (**Figure 19**) by *N*-alkylation of the THIQ core with 2.5 equivalents of propargyl bromide following the previously developed synthetic procedure. The product formed following the originally established protocol produced a  $^1\text{H}$  NMR spectrum (**Figure 20A**) that contained an excess number of proton signals that did not correlate with the expected structure. The original researchers attributed this anomaly to the amine inversion, where both wedge and ladder structure of a  $\text{sp}^3$  hybridised amine exist in the equilibrium (**Figure 20B**); as well as the technological limitations of the NMR. Upon revising the synthetic scheme, it was noticed that 2.5 molar equivalents of propargyl bromide was used and this could lead to over-alkylation of THIQ. It was suspected that the product could be a mixture of the mono- and di-substituted compounds (compounds **A** and **B**, respectively, **Figure 21**). Thus, the new goal of this research project is to resolve the conundrum and use the outcomes to generate new NNMTIs.

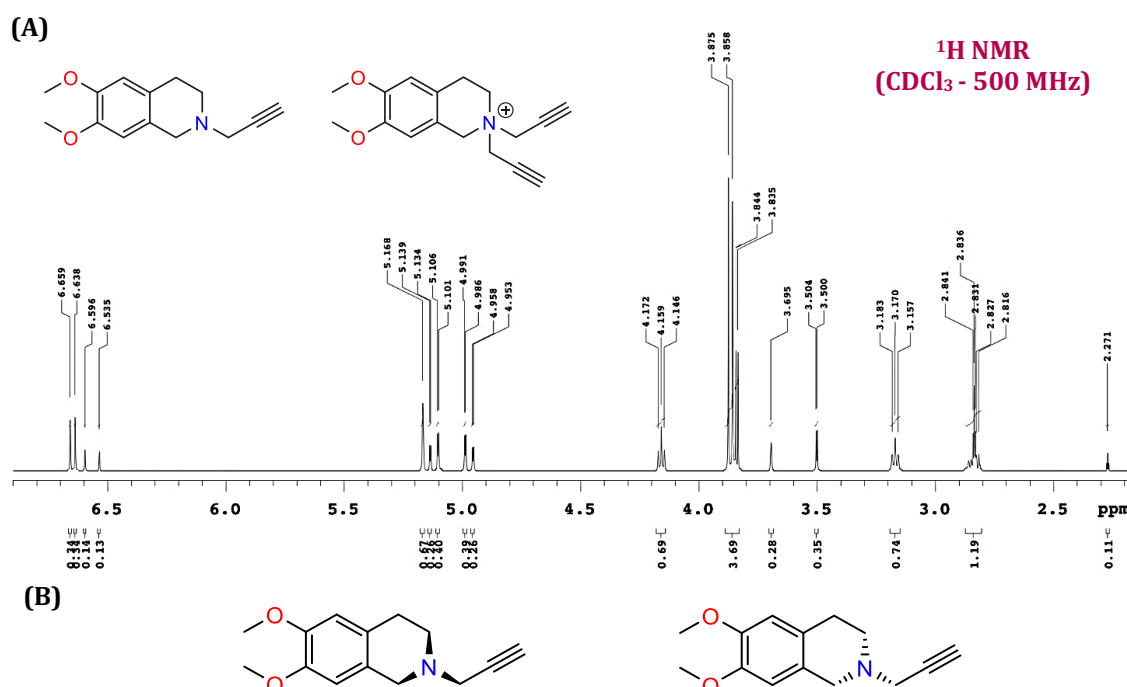


**Figure 20.** (A).  $^1\text{H}$  NMR spectrum of the THIQ alkylation reaction crude product. (B). The two possible versions of the alkylation product based on the amine conversion theory.

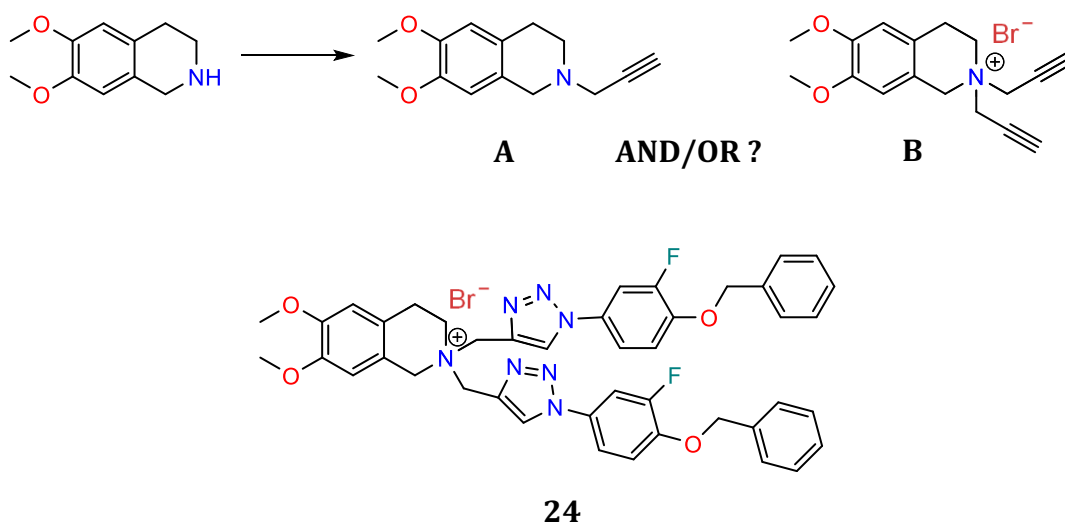


**Figure 21.** The  $S_N2$  alkylation of THIQ, yielding unknown compounds that were predicted to be **A** and/or **B**, remain to be further elucidated. If the hypothesis is correct that **B** was the only product formed, **24** might be the final compound that has ever been made

### 1.8. Project aims and objectives

NNMT is a potential drug target for a range of diseases, and research at UTS identified a new NNMTI lead compound **23**. Questions remain about the true structural identity of **23** because a key reaction intermediate in the synthesis of **23**, the THQI-alkyne, maybe with a mono- or di-alkylated product. Thus, the aims and objectives of my project are:

- To determine the chemical structure of **23** by NMR and MS
- To develop synthetic protocols to prepare exclusively either the mono-*N*-alkylated or di-*N*, *N*-alkylated product
- To carry out the synthesis of two NNMTIs libraries based on the structure of compound **23** and **24**
- To determine the inhibitory activity of synthesised drug candidates
- To assess anti-cancer properties of the synthesised compounds





## Chapter 2      Structural Elucidation of THIQ analogues and synthesis of mono- and di-alkylated THIQ analogue libraries

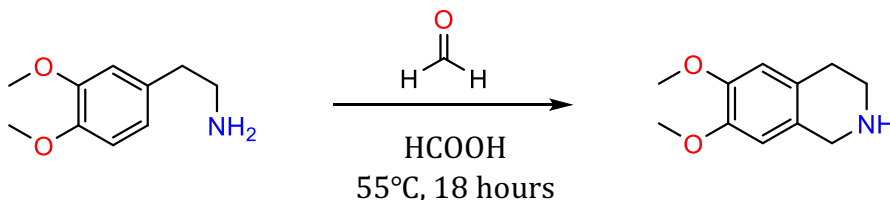
### 2.1. Introduction

Compound **23** was identified as a promising NNMTI, however its optimisation cannot occur until its true structure is confirmed. Critical to confirming the structural identity of **23** is understanding the product(s) that are produced by *N*-alkylation of the THIQ core with propargyl bromide. Thus, the synthetic chemistry component of this project first involved repeating the THIQ *N*-alkylation reaction and fully characterising the reaction product.

### 2.2. Results and Discussion

#### 2.2.1. Identification of the reaction product(s) from the reaction of THIQ with propargyl bromide.

The first step was to prepare 6,7-dimethoxy-1,2,3,4-tetrahydroisoquinoline (THIQ) using the Pictet-Spengler Reaction (PSR) (**Scheme 2.2.1**). In this reaction, a  $\beta$ -aryl ethylamine undergoes an acid-mediated condensation followed by the ring closure. The PSR reaction readily occurs under mild conditions with nucleophilic aromatic rings such as indole or pyrrole, giving products in high yields<sup>54</sup>. In this work, the reaction involved a phenyl ring and required harsher reaction conditions. Thus, the reaction was done under reflux for a longer time.



**Scheme 2.2.1.** The Pictet-Spengler cyclisation reaction (PSR) with 3,4-dimethoxyphenethylamine reacts with paraformaldehyde under acidic conditions.

In the first stage, the reaction begins with a lone pair on the nitrogen atom of 3,4-dimethoxyphenethylamine attacks to an aldehyde's centre carbon. In acidic conditions, the carbonyl oxygen protonation occurs, subsequently giving an iminium ion (Schiff base) after water is removed. The methoxy group at the third position on an aromatic ring, acting as an electron-donating group, activating the ring system at a para position, then adding across as an electrophile, leads to an intramolecular cyclisation reaction. This reaction is an electrophilic substitution at the iminium carbon, which results in the formation of the expected product (**Figure 22**).

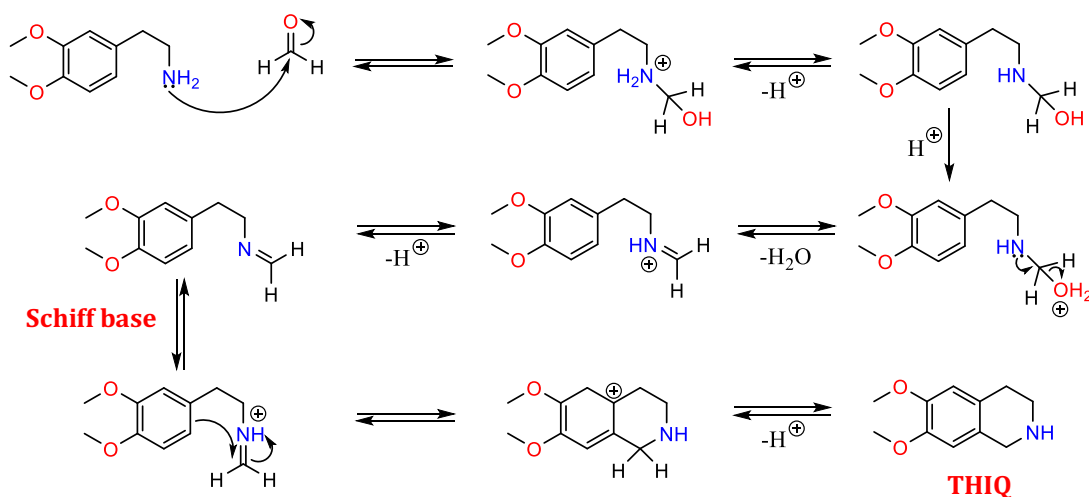


**Figure 22.** The formation of the Iminium ion through the elimination of water followed by the *para*-activation on an aromatic ring to the intramolecular cyclisation, resulting in the final THIQ product.

After 18 hours of refluxing at 55°C, the reaction mixture was basified and extracted with DCM, resulting in dark yellow residue, which left under high vacuum overnight to afford a pure product as a light-yellow solid. <sup>1</sup>H NMR was run to confirm the formation of the product (**Figure 23**). Two singlet peaks at 6.58 ppm and 6.51 ppm correspond to two protons on an aromatic ring, indicate the success of the reaction. A singlet peak at 3.96 ppm, with the integration of two protons, can be attributed to the newly formed bond at C1. Additionally, 15 protons from the integration of <sup>1</sup>H NMR, nine peaks observed in <sup>13</sup>C NMR equivalent to 9 different carbon environments revealed the presence of the product. The mass was confirmed by HRMS (ESI) to be 194.2423 [M+H]<sup>+</sup>, calculated for C<sub>11</sub>H<sub>15</sub>NO<sub>2</sub> [M+H]<sup>+</sup> 194.2427.

The  $^1\text{H}$  NMR spectrum and the melting point of the product was in good agreement with previously reported data.<sup>55</sup>

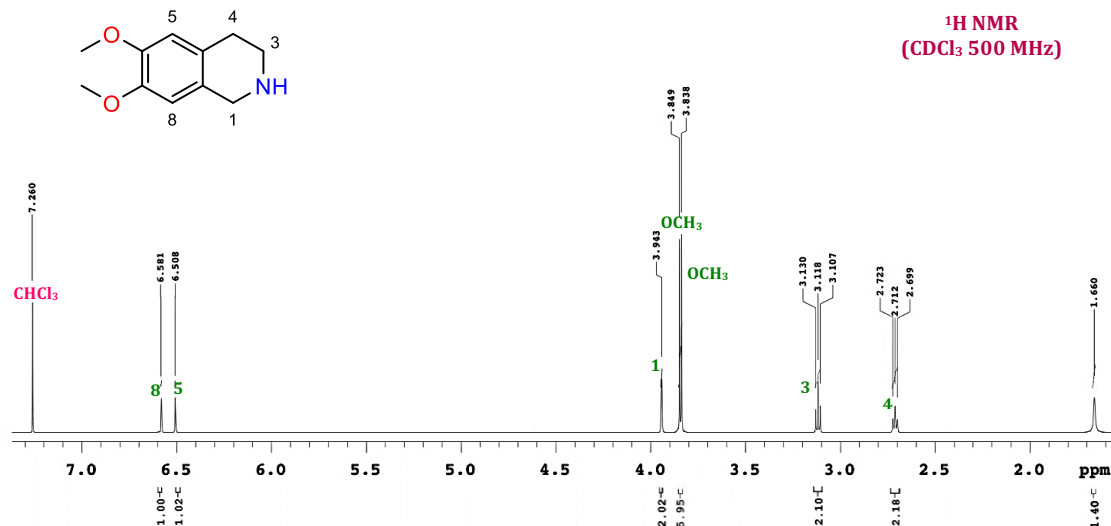
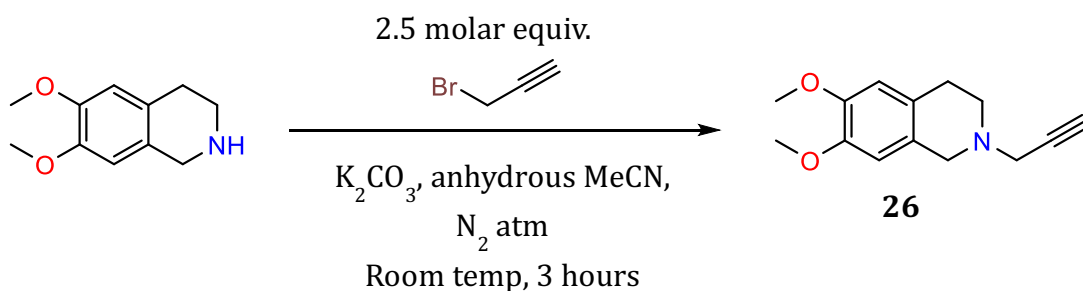


**Figure 23.**  $^1\text{H}$  NMR spectrum of the THIQ product. The resonance of H-1 at 3.94 ppm arises from the  $\text{CH}_2$  group between the phenyl ring and the nitrogen atom, indicates that ring formation has occurred to give the desired product.

The second step was to prepare the THIQ-alkyne precursor by reacting the synthesised THIQ with propargyl bromide. As outlined in the preliminary result section in **Chapter 1**, the obtained crude was thought to be a mixture of the mono-*N*-alkylated and the di-*N*, *N*-alkylated compounds. The reaction was reperformed according to the synthetic scheme outlined below where THIQ was reacted with propargyl bromide (2.5 molar equivalent) for 3 hours at room temperature (**Scheme 2.2.1.1**). As expected, the obtained crude NMR for this attempt was identical to the one seen in **Figure 20** (see page 25).



**Scheme 2.2.1.1** Original protocol of the THIQ alkylation reaction

To enable the structural elucidation of two compounds in the crude, finding a way to isolate it from the crude product was necessary. Since the di-*N*, *N*-alkylated product was suspected to be present in the crude, such high polarity allows it to be more soluble in water than the mono-*N*-alkylated compound. Following this fact, the isolation was performed by dissolving the crude in deionised (DI) water. After 10 minutes of sonicating, the undissolved solid was collected by filtration, which yielded the  $^1\text{H}$  NMR as seen in **Figure 24**, which confirmed to be the mono-*N*-alkylated compound **26** after analysing.

The mono-*N*-alkylated product **26** was characterised by the presence of a triplet at 2.27 ppm ( $J = 2.5$  Hz) with the integration of 1 proton, indicating the hydrogen signal at the terminal alkyne due to anisotropy. The triplet arising from the terminal hydrogen can be explained by the long-range coupling, where the  $-\text{CH}_2$  adjacent to the sp carbon splits the terminal hydrogen with a coupling constant of 2.5 Hz. The most important observation is the ratio of signal integrations arising from protons on the propargyl arm to those on the THIQ group. As seen in the NMR spectrum, proton at H-8 and H-5 compared to H-3' is 1:1 ratio, which indicates one arm of the propargyl linkage to one group of THIQ.

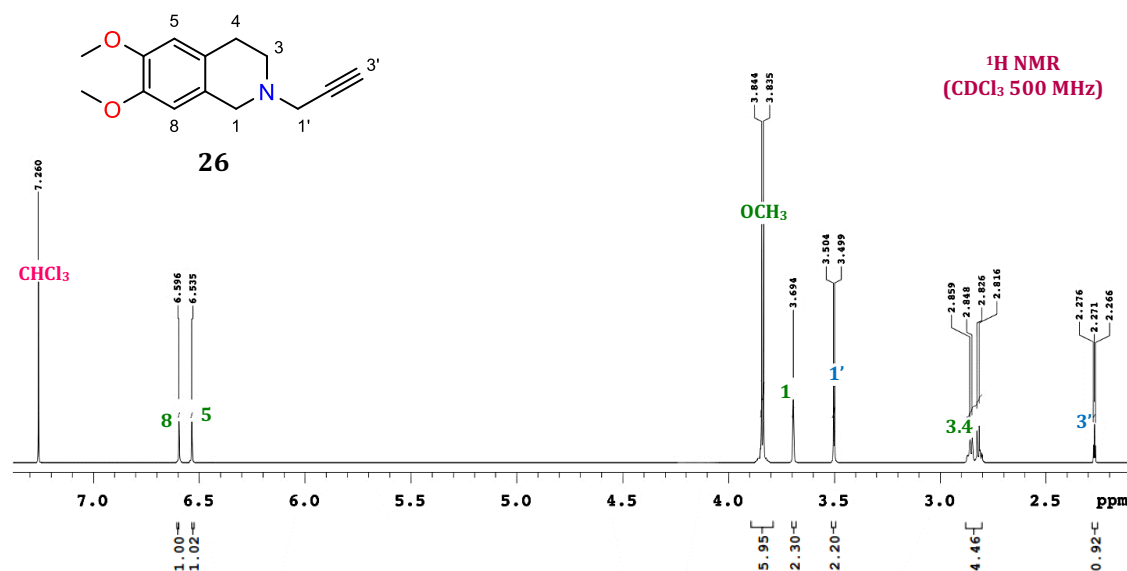


**Figure 24.**  $^1\text{H}$  NMR spectrum of the *N*-alkylated product. The triplet at 2.27 ppm arises from the proton on the terminal alkyne. The doublet at 3.50 ppm correlates to the two protons on the carbon adjacent to the terminal alkyne. These features confirm the formation of an *N*-alkylated product.

The reaction converted the secondary amine to the tertiary amine results in higher electron density on nitrogen to a greater extent. This causes any protons on the THIQ ring to appear further upfield in the spectrum; H-1 is seen at 3.50 ppm instead of 3.96 ppm. It also explains the overlapping in protons signal H-3 and H-4 seen in the spectrum at 2.84 ppm because the effect of the external magnetic field has the most impact on H-3 (**Figure 24**). The final confirmation test on the  $^{13}\text{C}$  NMR shows 14 carbon peaks, and the mass was confirmed by HRMS (ESI) to be 232.1333  $[\text{M}+\text{H}]^+$ , calculated for  $\text{C}_{14}\text{H}_{17}\text{NO}_2$   $[\text{M}+\text{H}]^+$  232.1332 (**Figure 25**). Hence, an **unknown A** was confidently claimed to be compound **26**.

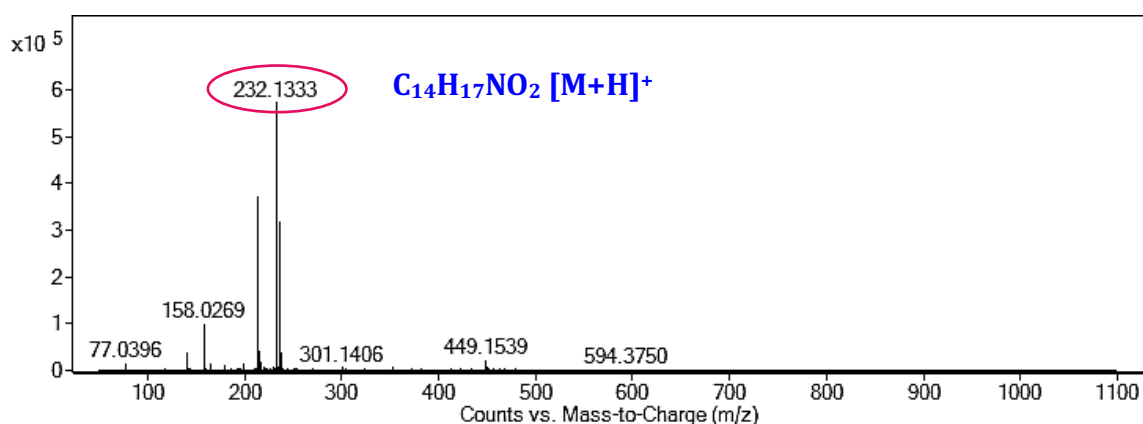


**Figure 25.** HRMS Spectrum of compound **26**.

Since a small amount of the mono-*N*-alkylated product is soluble in water, the collected filtrate was washed with Dichloromethane (DCM) to extract the monoalkylated compound. The aqueous layer was freeze dried to yield a *N,N*-dialkylated product **27** with the  $^1\text{H}$  NMR as seen in **Figure 26**. It can be seen from the  $^1\text{H}$  NMR spectrum that the splitting patterns of each proton have changed significantly. Proton H-5 and H-8 are shifted slightly downfield compared to compound **26**. Protons at H-4 and H-3 are observed as two triplets. The H-3 resonance appears to be drastically downfield. Again, it can be seen that the terminal alkyne triplet appears further upfield but the ratio is now 2:1 with the protons at H-8 and H-5, which indicates two side arms of propargyl to one part THIQ. A Mass spectrum was also obtained for this compound (**Figure 27**). The *N,N*-dialkylated product is a quaternised molecule so an  $[\text{M}]^+$  fragment was detected instead of an

[M+H]<sup>+</sup> fragment as seen in the MS of compound **26**. This MS is fully consistent with the structure of the dialkylated product **27**.

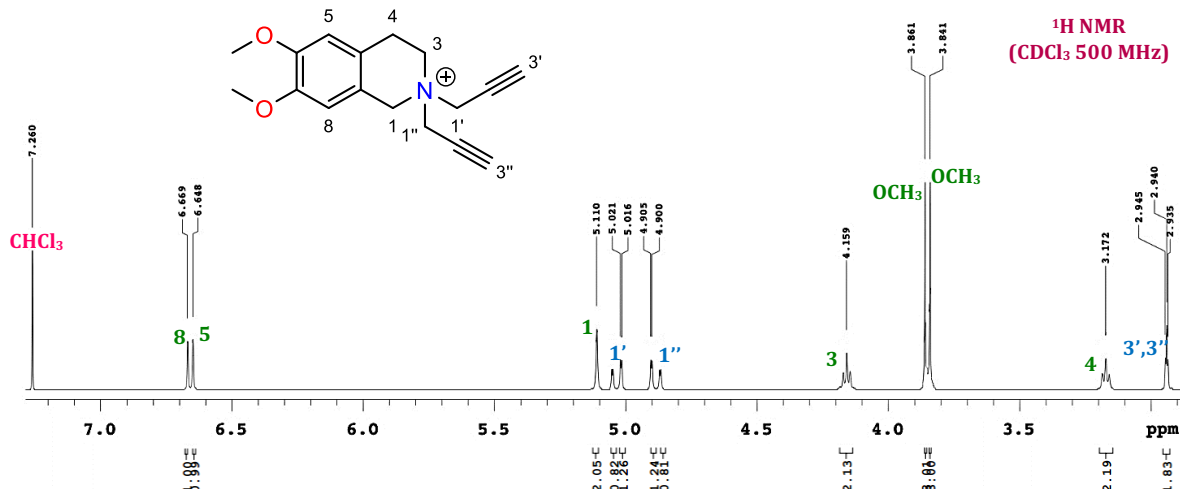


**Figure 26.** <sup>1</sup>H NMR of the di-*N*, *N*-alkylated compound isolated from the crude mixture. Analysis of the full set of NMRs confirmed that this is compound **27**.

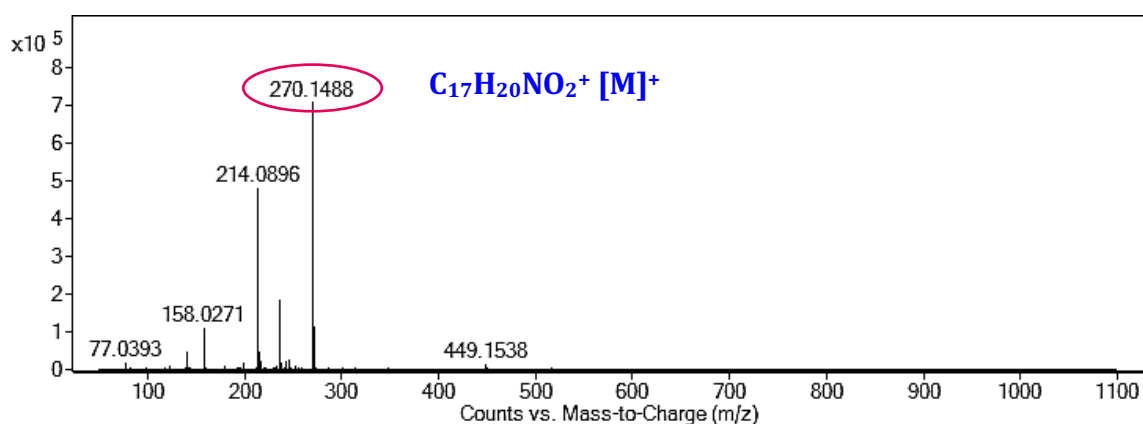


**Figure 27.** HRMS Spectrum of compound **27**.

### 2.2.2. Develop an exclusively mono-*N*-alkylated synthetic protocol

The development was first begun by revising the original synthetic protocol. It was noticed that the amount of propargyl bromide used in the current method was 2.5 molar equivalent to THIQ so it could form a mixture of **26** and **27**. Thus, reducing the amount of propargyl bromide used was thought to prevent this effect. In the first attempt, propargyl bromide used was reduced to 1.5 molar equivalent, using a similar method described in **Scheme 2.2.1.1** (page 30). The crude product

was extracted with  $\text{CHCl}_3$ . Removal of solvent yielded a crude product with the  $^1\text{H}$  NMR spectrum, as seen in **Figure 28**. The  $^1\text{H}$  NMR contains both compound **26** and **27**, however the amount of **26** is greater than **27**.

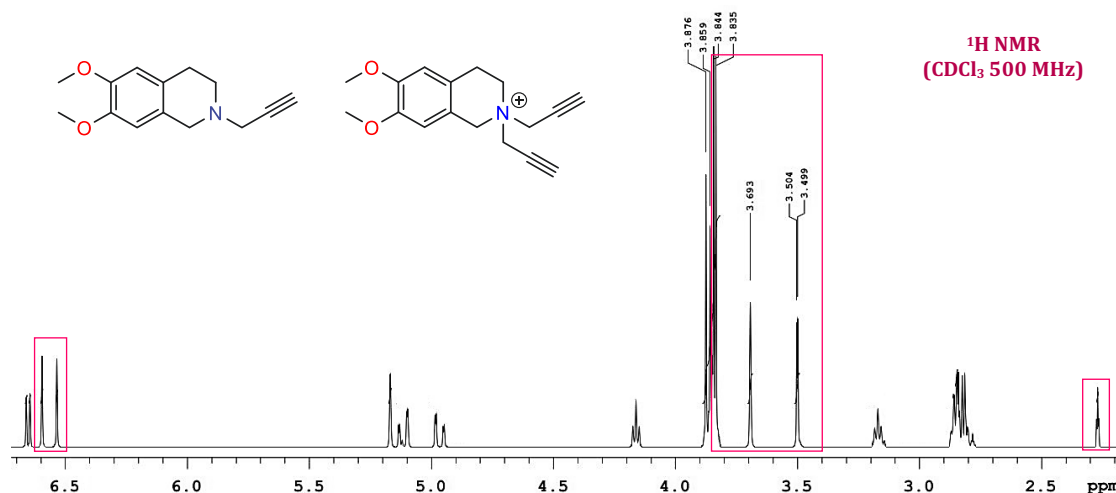


**Figure 28.**  $^1\text{H}$  NMR spectrum of the first attempt crude in re-developing a synthetic scheme.

With such a promising result, the second synthesis attempt was carried out with the 1.0 molar equivalent of propargyl bromide. The crude  $^1\text{H}$  NMR spectrum obtained from this attempt can be seen in **Figure 29**. Only **26**'s signals can be seen with a trace of unreacted THIQ. A third synthesis was performed using a similar procedure, as described in the second attempt. The reaction time increased to 5 hours instead of 3 hours and slightly increased propargyl bromide used to 1.1 molar equivalent. By prolonging the reaction time and a somewhat larger amount of propargyl bromide, it was thought to allow THIQ to fully convert to **26**. However, there was no change in the final crude as THIQ can still be detected.



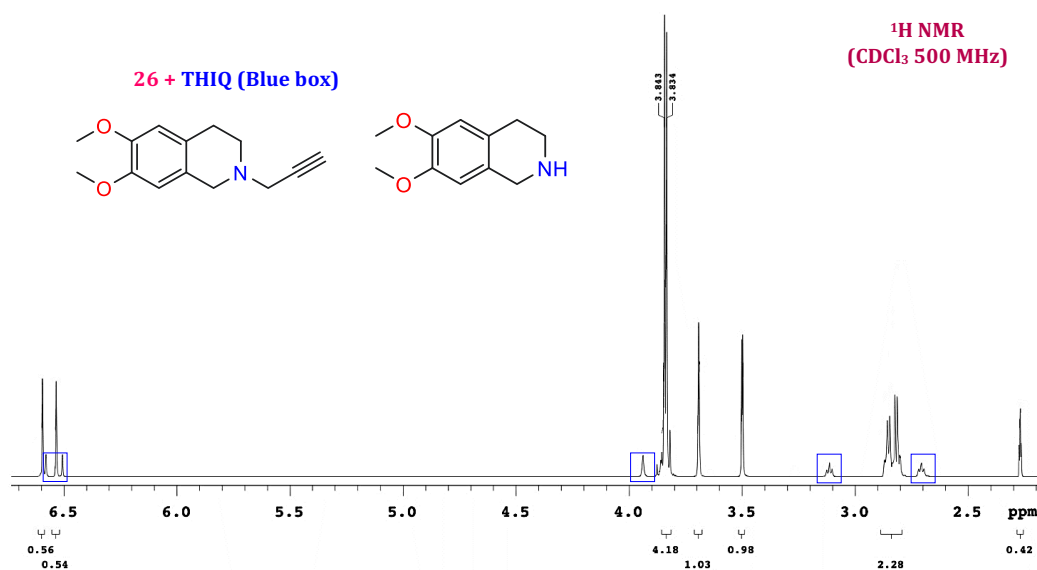
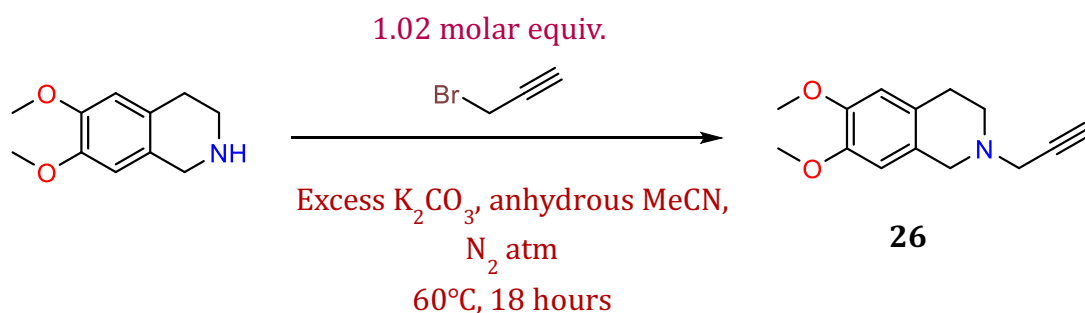


**Figure 29.**  $^1\text{H}$  NMR spectrum of the second attempt crude in re-developing a synthetic scheme. Chemical shifts in blue boxes belong to the unreacted THIQ starting material.

To develop a new synthesis method for **26**, reagents, and solvent used in the original procedure were assessed. First, the solvent used in this reaction was MeCN – a solvent favours  $\text{S}_{\text{N}}2$  type reaction providing polar aprotic conditions. It does not participate in hydrogen bonding with the nucleophile THIQ, so MeCN was proven to be best for synthesising the desired product. Second, the use of an inorganic base  $\text{K}_2\text{CO}_3$  is widely employed in the *N*-alkylation of amines as the base neutralise HBr, which is formed as the reaction proceeds.<sup>56,57,58,59,60,61,62,63</sup> Hence,  $\text{K}_2\text{CO}_3$  continued to be used in this reaction to increase the free amine concentration. The amount of propargyl bromide was strictly controlled using 1.02 molar equivalent to THIQ. In this attempt, the reaction was set to reflux at  $60^\circ\text{C}$ , and the reaction was monitored by running TLC against THIQ to determine the time required for the reaction to complete. After a few trials, the new synthetic scheme with optimal conditions was achieved (**Scheme 2.2.1.2**). This new synthetic scheme yielded exclusively compound mono-*N*-alkylated **26** without needing further purification.



**Scheme 2.2.1.2.** The new S<sub>N</sub>2 alkylation of THIQ with Propargyl Bromide under basic conditions to exclusively yield **26**

### 2.2.3. Develop an exclusively di-*N*, *N*-alkylated synthetic protocol

Before researching a new synthesis for **27**, the old synthetic scheme was re-studied. In the first attempt, the propargyl bromide used was increased to 5 molar equivalents to the THIQ, using the same method as described in the original method. The crude product obtained showed no differences in <sup>1</sup>H NMR than the crude from the original protocol, where both **26** and **27** presented in the mixture. In the second attempt, the reaction was left to stir for 6 hours at room temperature, resulting in the crude with the <sup>1</sup>H NMR spectrum, as seen in **Figure 30**. The obtained spectrum shows the majority of compound **27**. However, some resonances can be seen alongside with small traces of **26**. It was anticipated that the reaction might produce a different compound as a by-product.

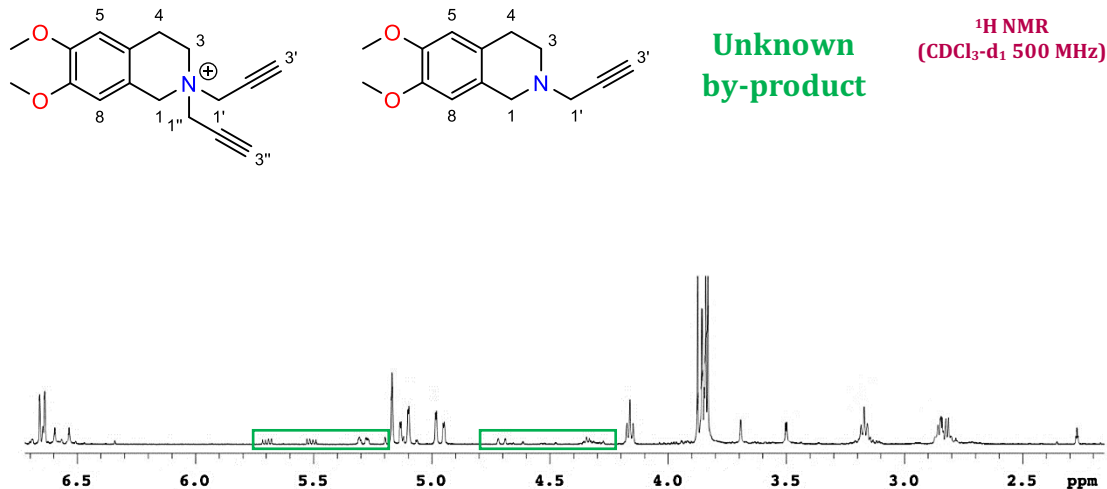


**Figure 30.**  $^1\text{H}$  NMR spectrum of the crude from the second synthesis attempt. Chemical shifts in the green boxes were thought to be an unknown by-product formed in the reaction.

The reaction was repeated using the same reaction conditions except that the reaction time was doubled. Under these conditions, compound **26** was fully consumed in the reaction. However, it was noticed that there are many more resonances observed from the spectrum which indicates **27** was not the only product that formed (**Figure 31**).

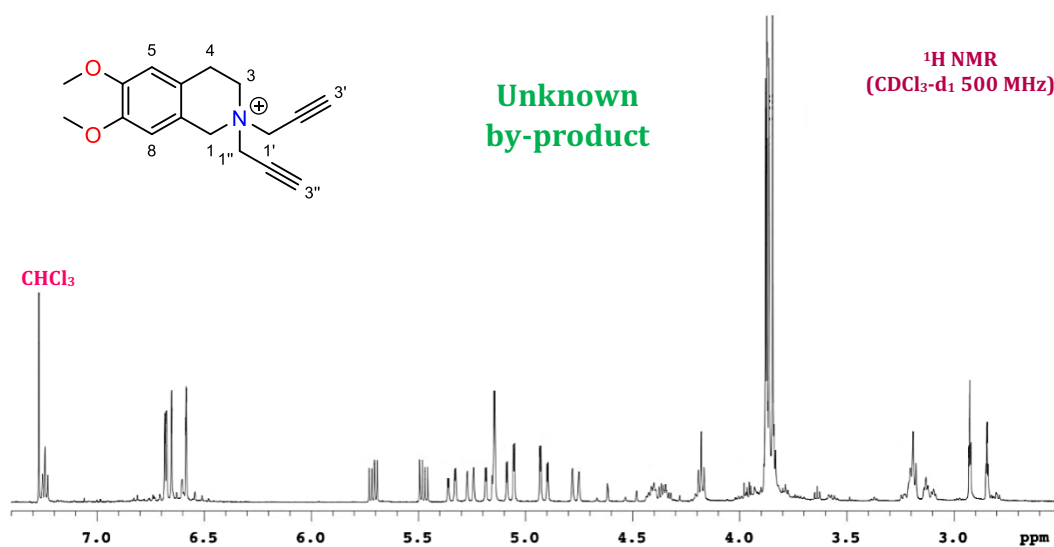


**Figure 31.**  $^1\text{H}$  NMR spectrum of the crude from the third synthesis attempt

The obtained unknown has a massive molecular weight of 922, indicates polymerisation could happen between propargyl bromide and compound **27**. Notably, the initiation and propagation mechanism for the polymerisation of ethynyl pyridinium were proposed by Blumstein *et al.*<sup>64</sup>. According to the study, the polymerisation resulted from the activation of the triple bonds by conjugation of quaternised nitrogen to the  $\alpha$  carbon atom; the conjugation stabilises the carbon anion produced by the nucleophilic attack of the triple bond by the pyridine group, and the carbon anions then initiated the anionic polymerisation. (**Figure 32A**). In another study of Kabanov *et al.*, they reported that some propargyl derivatives such as propargyl bromide, propargyl chloride, and alkyl propargyl sulphates could react with some nitrogen-containing compounds directly, without any catalyst or initiator, to produce polyelectrolyte polyacetylene and poly(propargyl pyridinium bromide). In the presence of excess propargyl bromide and **27**, homopolymerisation could also occur (**Figure 32B**). Though the full mechanism for polymerisation of **27** and propargyl bromide remaining unclear, the unknown formed was anticipated to be a polymerised product as it possesses characteristics of an organic polymer.

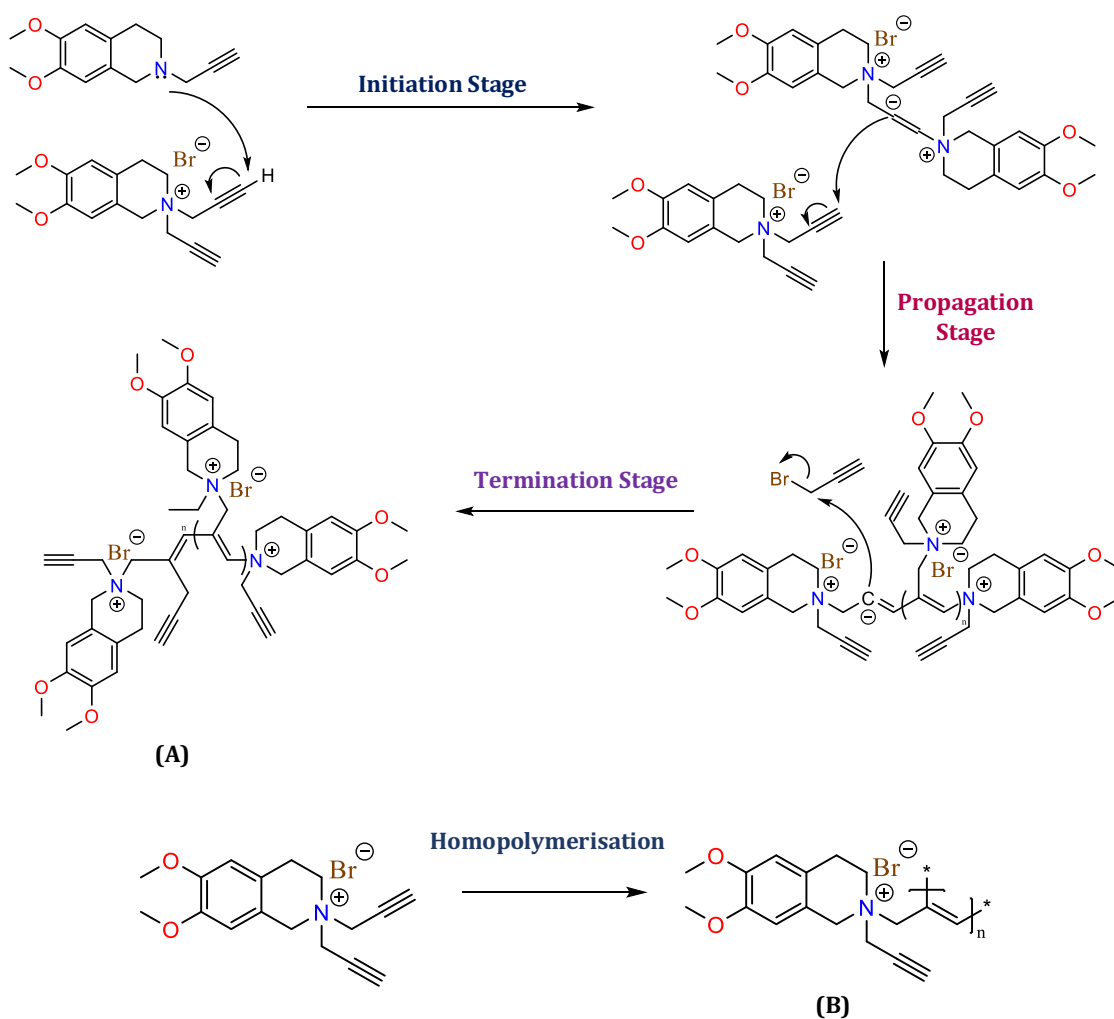


**Figure 32. (A)** Proposed mechanism for Polymerisation of **27**. **(B)** Homopolymerisation of **27**

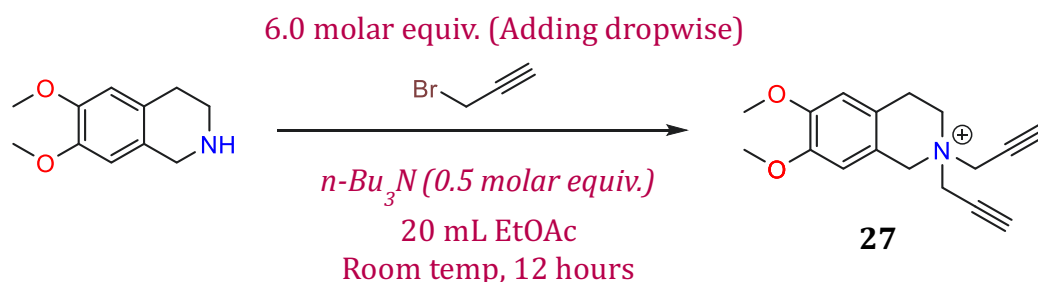
To research for a better synthetic protocol for **27**, assessments on the original procedure were carried out. In the conventional methods for direct alkylation of primary or secondary amines to their quaternary salts, strong inorganic bases such as sodium hydroxide or sodium carbonate, are used to bind the acid-generate liberated from their hydro halide salts, and the equilibria are shifted toward complete alkylation. However, the harsh reaction conditions that required prolonged heating of strongly basic and generally heterogeneous reaction mixtures give rise to undesirable side reactions and, consequently, the low yield is obtained. As observed in the synthetic context of compound **27**, prolonging the reaction with strongly basic  $\text{K}_2\text{CO}_3$  yielded an unknown, which was believed to be a polymerised

product through analysis. To combat this problem,  $K_2CO_3$  must be replaced with an organic base that could homogenise in the reaction.

In the search for a suitable and available organic base, it was noted that the base should fulfil the following requirements. (1) The organic base should have solubilities similar to that of the starting amine. (2) It must have a larger  $pK_a$  value than THIQ to bind, preferably with the acid released during the reaction. (3) It must undergo alkylation at a significantly lower rate than the amines to be quaternised. (4) The acid salt of the organic base and the quaternary ammonium salt **27** should be separable based on their solubilities in common solvents. The choice of the proton acceptor and selecting an appropriate solvent are the two most important factors governing the reaction path. In principle, any organic base that is stronger in base strength and weaker in nucleophilicity than THIQ can be employed to compel the reaction toward complete alkylation. Whereas only slightly greater base strength suffices, substantially lower nucleophilicities than THIQ is preferential. Additionally, the yields of **27** are much dependent on the differences in solubilities between the protonated base and **27** in common solvents. Preferably, a combination of base and reaction solvent was selected to effect precipitation of the desired product **27** or the organic base's hydro halide salts. Since **27** is a quaternary ammonium compound, it is more ionic than acid salts of amines and less soluble in an organic solvent.

After several trials, tributylamine was used as an organic base, the alternative for  $K_2CO_3$ . Tributylamine has a larger  $pK_a$  (10.89) than the starting amine THIQ ( $9.01 \pm 0.20$  at  $25^\circ C$ )<sup>65</sup>. In addition, the severely hindered nature of tributylamine prevents it from forming the acceptor-based alkylated product<sup>66</sup>. Ethyl acetate (EtOAc) was replaced with acetonitrile. As mentioned previously, facilitating solvent's selection must ensure either (1) the desired product **27** being precipitated out from the reaction mixture or (2) the hydro halide salt of tributylamine being crashed out. The hydro halide salts of tributylamine are more soluble in less polar solvents, such as ethyl acetate than compound **27**, thereby affording many instances' effortless isolation of the desired product **27**. Using ethyl acetate as a solvent ensures that compound **27** formed will precipitate out and lose

its ability to undergo polymerisation with propargyl bromide. A new synthetic scheme was developed (**Scheme 2.2.1.3**)



**Scheme 2.2.1.3.** An exhaustive alkylation reaction for the synthesis of *N, N*-dialkylated compound **27**

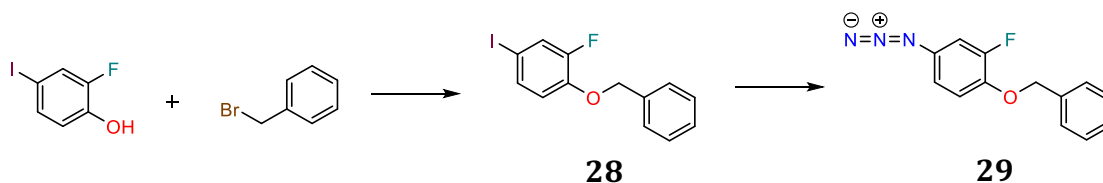
The general procedure simply involves dissolving THIQ, tributylamine, and propargyl bromide in ethyl acetate. A stoichiometric amount of base is important. Although a sufficient amount of proton acceptor must be present to bind the acid released, the excess should be avoided to prevent the formation of the acceptor base alkylated product. In the new synthetic procedure, THIQ (1 molar) was firstly dissolved in 20 mL EtOAc followed by the addition of 0.5 molar equivalent of tributylamine and allowed to stir for 10 minutes at room temperature under an inert atmosphere. The six-fold excess of propargyl bromide was added dropwise. After adding propargyl bromide, a precipitate formed almost immediately. After 12 hours, the solid was removed by filtration, washed with ether and EtOAc, high-vacuumed overnight to afford a crude product. The introduced exhaustive alkylation synthesis of **27** was successful in an one-pot procedure. In the future of synthesising **27** as a precursor, this new protocol can be employed because of its high efficiency, minimal manipulations, and less effort in the reaction workup.

#### 2.2.4. Synthesis of aromatic azides

Upon completing the synthesis of intermediate alkyne precursors, the next step was to carry out the synthesis of an organic azide precursors. Typically, converting a precursor into an organic azide can be quickly done via an  $\text{S}_{\text{N}}2$  reaction with an aliphatic carbon molecule. However, synthesis of aromatic azides by a direct nucleophilic substitution is much harder due to the electron-rich nature of an

aromatic ring. Therefore, other routes of substituting an azide group were explored via two synthetic routes: aryl halide to aryl azide and aryl boronic acids to aryl azide.

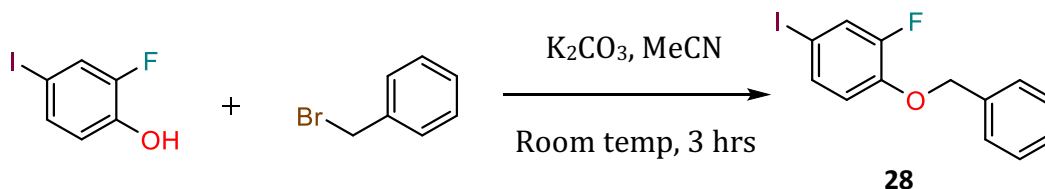
#### 2.2.4.1. Synthesis aryl azides from aryl halides



**Scheme 2.2.4.1.** Proposed synthetic route for the conversion of aryl halide to aryl azide

To access the azide conversion from aryl halide, the scheme **2.2.4.1** was designed. The aryl azide synthesis was carried out with the  $\text{S}_{\text{N}}2$  reaction to construct the ether linkage compound **28**, followed by the proline-copper (I)-catalysed coupling with sodium azide reaction to yield **29** (**0%**).

The first reaction is the  $\text{S}_{\text{N}}2$  alkylation of a benzylic carbon (**Scheme 2.2.4.1a**). A molar equivalent of bromomethylbenzene and 1.02 molar equivalent 2-fluoro-4-iodophenol, excess anhydrous  $\text{K}_2\text{CO}_3$  in 20 mL MeCN, was stirred for 3 hours under an inert atmosphere. The reaction was quenched with water and extracted with  $\text{CHCl}_3$  to afford compound **28** as white flaky crystals (100% yield). A TLC was run prior to confirming the formation of the product. The singlet peak in the  $^1\text{H}$  NMR spectrum with the integral reading of 2 protons at 5.01 ppm indicates the  $-\text{CH}_2$  linkage formation.

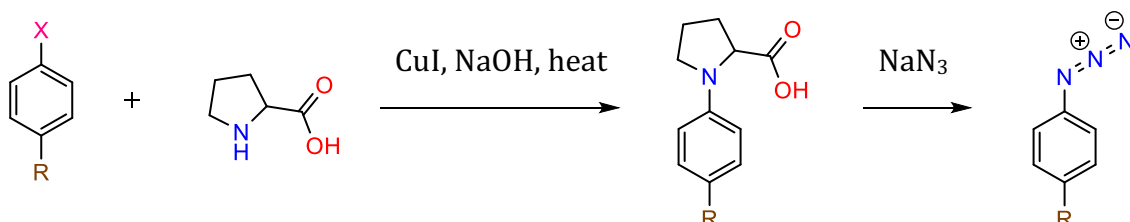


**Scheme 2.2.4.1a.** The  $\text{S}_{\text{N}}2$  alkylation of a bromomethylbenzene with 2-fluoro-4-iodophenol, resulting in an ether product **29**

With the completion of the alkylation product with relatively high yield, the next step was to synthesis an organic aryl azide. The aryl halide starting material has an iodine atom, a good leaving group, which displays the ability to undergo the



$\text{N}_3^-$  substitution on an aromatic ring. To perform the reaction, an Ullmann-type coupling reaction was proposed by Wei Zhu and Dawei Ma (**Scheme 2.2.4.1b**, **Figure 33**). Their work demonstrated that a plethora of aryl iodides and aryl bromides, containing various substituent groups, could be converted to aryl azides<sup>67,68,69,70</sup>.



**Scheme 2.2.4.1b.** The Ullman-type coupling reaction between copper (I)/L-proline and aryl halides for the aryl azides conversion.

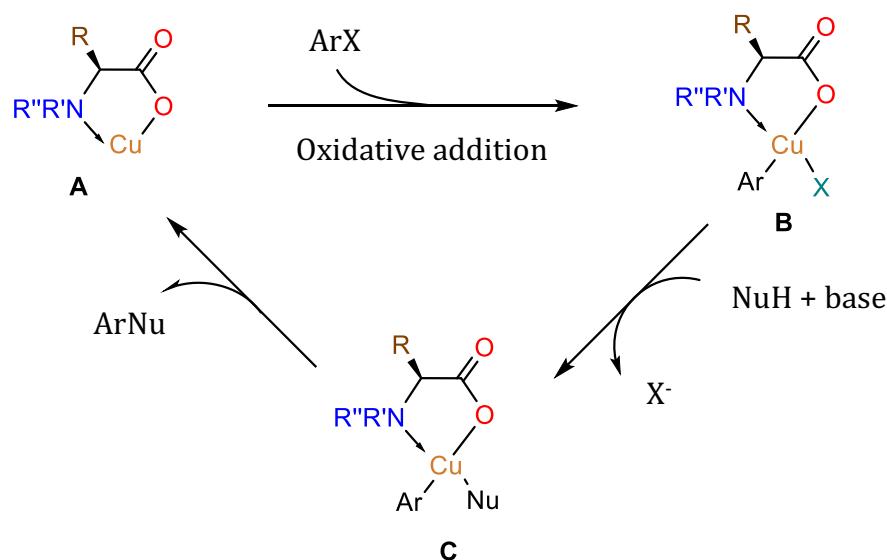


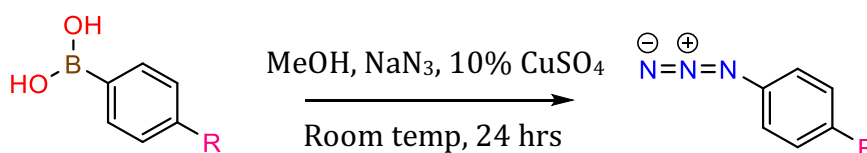
**Figure 33.** Possible catalytic cycle for the amino acid-promoted coupling reactions, proposed by Wei Zhu and Dawei Ma (2011).

Replicating the synthetic protocol, 10% mol CuI, 20% mol L-proline, 10% mol NaOH in a DMSO/ $\text{H}_2\text{O}$  solution with a molar excess of sodium azide was stirred at  $65^\circ\text{C}$  for 24 hours under an inert atmosphere and extracted with ethyl acetate and suspended in 5 mL *i*-PrOH. To test if the reaction had been successful,  $^1\text{H}$  NMR was run and shown no changes in chemical shifts. A TLC run showing the same  $R_f$  of the starting material. The azidation reactions were repeated with increased reaction temperature to  $95^\circ\text{C}$  and using EtOH/ $\text{H}_2\text{O}$  solvent system reported in the paper; however, no product was formed. The reason for the unsuccessful of this reaction could be the structure of an aryl halide is bulkier than any of previously reacted

species reported to have formed an azide, somehow contributing to its lack of reactivity. Another possibility that contributes to the reaction failure is that water in the NaOH solution could act as a good nucleophile to compete with the substitution of the azide ion even if the anhydrous DMSO was used.

#### 2.2.4.2. Aryl boronic acids to aryl azides conversion

After encountering no success with utilising aryl halides in the search for a source of aromatic azides, another pathway to azidation comes through using aryl boronic acids, a commercially available product. The copper (II)-catalysed boronic acid-azide coupling reaction was a powerful transformation that required mild conditions. The copper (II)-catalysed synthesis of aryl azides from arylboronic acids is based on the Chan-Lam coupling of arylboronic acids with N-H containing heteroarenes, aniline, phenols, and amides that employs stoichiometric copper (II) acetate in aprotic solvents and requires a base such as pyridine or triethylamine<sup>71</sup>. Since the sodium azide is sparingly soluble in most aprotic organic solvents, in contrast to the Chan-Lam coupling conditions, protic solvents were used, and the azidation of boronic acids proceeded efficiently in water, methanol, and ethanol<sup>72,73</sup>. It was found that removing the obligate base improves the yield of the conversion (85% - 98%). In a small-scale reaction, this reaction goes to completion within 3 hours at 55°C, under atmospheric condition; but the reaction can also be performed at room temperature if the reaction time is extended to 24 hours, which is preferable when working on scales larger than several millimoles<sup>71</sup>. This type of reaction is conveniently followed colorimetrically as the dark brown solution turns light green as the reaction is completed (**Scheme 2.2.4.2**).



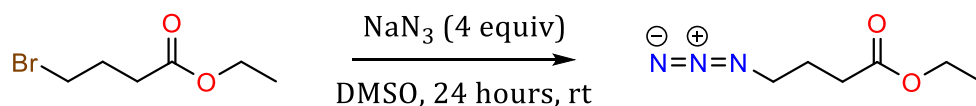
**Scheme 2.2.4.2.** The conversion of aryl boronic acids to aryl azides as described by Tao, C., *et al.* (2007)

The first azidation reaction was performed with (4-benzyloxy-3-fluorophenyl) boronic acid to form **29** in 10 mL MeOH, with 1.5 molar equivalents of  $\text{NaN}_3$  and 10%  $\text{CuSO}_4$ . The reaction was left to stir overnight at room temperature, open atmosphere, extracted with DCM and reconstituted with 5 mL of *i*-PrOH, yielded 97%. The first sign to confirm the reaction reached completion is the light green colour of the reaction mixture. Another way to verify the formation of the azide is through  $^1\text{H}$  NMR. There are no changes in splitting patterns of proton signals. Since the boronic acid group is replaced with the azide ion, it causes the proton signals' chemical shifts on an aromatic ring attached directly to the azide ion to be more deshielded. Upon successful azidation of (4-benzyloxy-3-fluorophenyl) boronic acid, a series of three different azides was also synthesised for further NNMTIs analogues synthesis (**Table 2**).

**Table 2.** Four azides with different substituents at para-position converted from commercially available boronic acids

Entry	Structure
1	
2	
3	
4	

To expand the diversity of analogue libraries, a fifth azide was synthesised via an  $S_N2$  reaction between a sodium azide and the alkyl halide. (**Scheme 2.2.4.2.1**). In addition, current bi-substrate inhibitors (reported in **Chapter 1**) are comprised of three different moieties that occupy separate binding pockets in the NNMT active site, one of which is the amino acid pocket. In the study mentioned in section **1.6.2** and **1.6.6 (Chapter 1)**, compounds bearing a short fatty acid group of 6-7 carbons exhibited the greatest inhibitory activity. This suggested that coupling ethylbutanoate moiety with the core THIQ structure might enhance the inhibitory activity of newly studied NNMTIs analogue series.



**Scheme 2.2.4.2.1.** The  $S_N2$  reaction of ethyl-4-bromobutanoate with sodium azide

### 2.2.5. Copper-Catalysed Azide-Alkyne Cycloaddition reaction to final products

Click chemistry refers to a group of reactions that are fast, simple to use, easy to purify, versatile, regiospecific, and give high product yields<sup>74</sup>. Although several reactions fulfil the criteria, the Copper-Catalysed Azide-Alkyne Cycloaddition (CuAAC) of azides and terminal alkynes to form 1,2,3-triazoles has emerged as the frontrunner. This reaction exclusively yields 1,4-disubstituted products with the assistance of copper (II), making it regiospecific. It typically does not require temperature elevation and can be done in various polar aprotic solvents, including water and over a wide range of pH values 5-12<sup>75</sup>.

Before starting of the cycle, the active Cu (I) is generated from a Cu (II) salt using sodium ascorbate as a reducing agent. The addition of a slight excess of sodium ascorbate prevents the formation of oxidative homocoupling products. At the first stage, Cu (I) reacts with the alkyne to form a terminal  $\sigma$ -acetylide after the terminal proton is removed. In the next step, a  $\sigma$ -bound copper acetylide bearing a  $\pi$ -bound copper coordinates the azide. Once the complex forms, the  $\beta$ -carbon of the acetylide engages in a nucleophilic attack of the N-3 nitrogen atom of the azide, forming a

covalent bond. A cyclisation reaction has now occurred and resulted in an unusual six-membered copper metallacycle where the second copper atom acts as a stabilising donor ligand. In the next stage, ring contraction to a triazolyl-copper derivative is followed by protonolysis that delivers the 1,2,3-triazole ring with a 1,4-disubstituted product and completes the catalytic cycle (**Figure 34**).

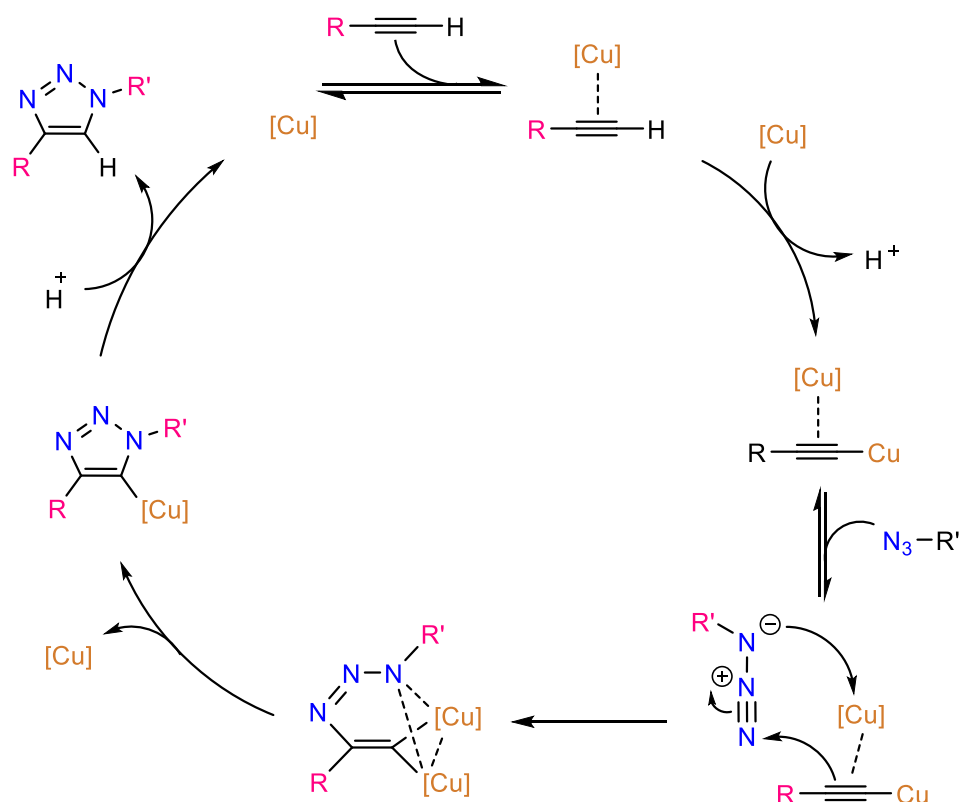
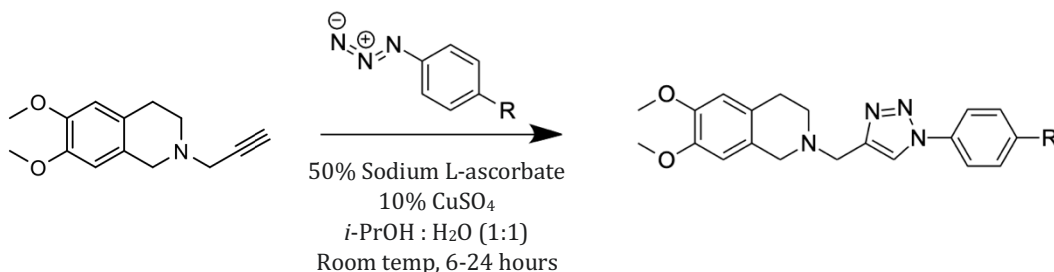


**Figure 34.** Proposed mechanism of CuAAC reaction as described by B. T. Worell, J. A. Malik, V. V. Fokin (2013)

Because of its simplicity and high regioselectivity, the CuAAC reaction was employed to use as a final synthetic route to construct analogue libraries compounds (**Scheme 2.2.5**). The aromatic azide (1.2 molar equivalent) was reacted with the propynyl-derivative of THIQ (1.0 molar equivalent) in the presence of 10%  $CuSO_4 \cdot H_2O$ , 50% sodium ascorbate solution in 10 mL  $i$ -PrOH :  $H_2O$  (1:1). The reaction was stirred at room temperature whilst exposing to air for 6 – 24 hours. The crude product was washed with 0.1 M EDTA to remove the remaining copper, followed by

trituration with cold hexane to remove unreacted azides and afford a pure product as a solid in 23-50% yield.



**Scheme 2.2.5.** The general synthetic scheme for the 1,4-click products

### 2.2.6. Chelating – a useful step to a better Click reaction workup

One of the most prominent disadvantages of Click reaction is a requirement of copper catalyst. For the click reaction product to find a way in new drugs development processes, the copper catalyst must be removed entirely. This may not always be an easy task, but a few research groups have demonstrated some success. For example, the click chemistry reaction developed by Liu *et al.* has shown that using ethylenediaminetetraacetic acid (EDTA) could effectively remove about 98% of the copper by adding an extra step in the synthetic protocol<sup>76</sup>. Furthermore, several research pieces reported that EDTA could be used as a supporter chemical, which can be added to a final reaction mixture after CuAAC, chelating the remained copper and thus facilitating its removal from the desired product reaching copper concentrations down to 0.0005% wt<sup>77,78,79,80,81,82</sup>. EDTA is one of the most well-known chelating agents with six potential sites for binding with metal cations composed of four carboxyls and two amino groups<sup>83</sup>. When equimolar of copper to EDTA or higher concentrations of EDTA is present, it tends to form copper-chelated complexes (**Figure 35**), thus, enhancing homogeneous deposition of coppers in an aqueous solution that can be easily separate by performing liquid-liquid extraction.

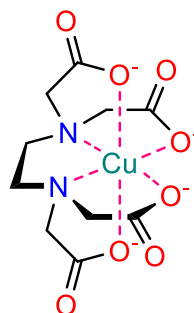


**Figure 35.** Chelation Mechanism of EDTA with Copper

### 2.2.7. Synthesis of an *N*-alkylated click analogue (**FHMxx**)

Five compounds in the **FHMxx** analogue were synthesised and characterised. For the first compound **FHM01**, the  $^1\text{H}$  NMR analysis revealed the presence of the characteristic H-5' triazole proton singlet at 7.92 ppm; integral ratio is 1:1:1 to H-5 and H-8 proton (**Figure 36**). Further evidence of the success of the click reaction is shown by the loss of a terminal alkyne triplet, 1 proton as per the integral. Additionally, the two methylene bridges H-7'' and H-1' are present a singlet, with two protons reading from the integral at 3.92 ppm and 5.21 ppm, respectively. These characteristics convince the formation of a target click product.

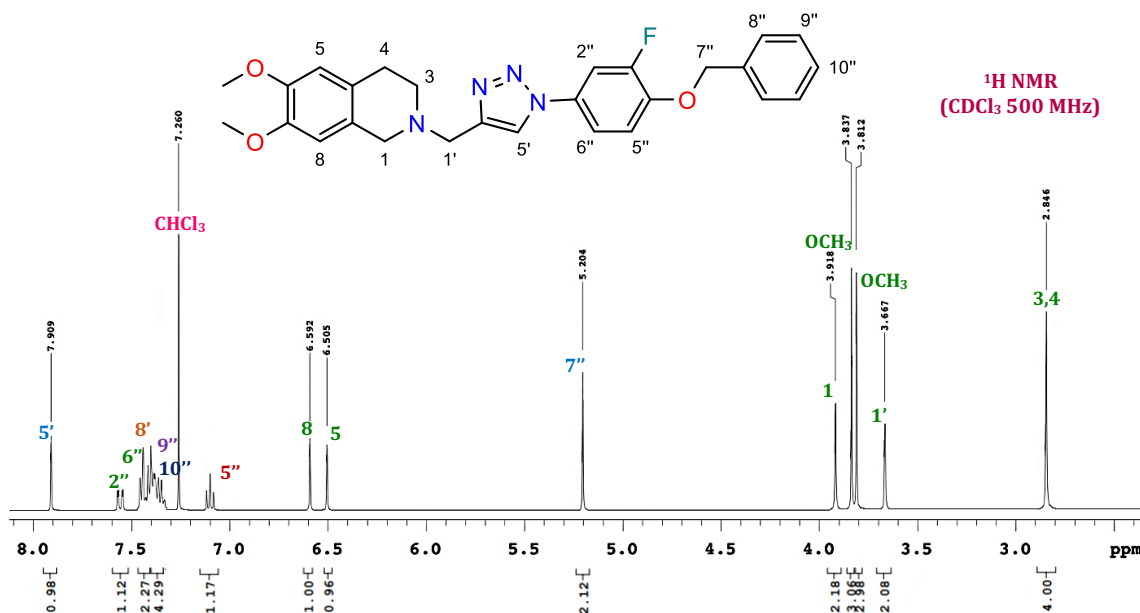


**Figure 36.**  $^1\text{H}$  NMR spectrum of **23 (FHM01)**. The triazole resonance H-5' is detected at 7.91 ppm and loss of terminal alkyne triplet indicates the successful synthesis of a target molecule.

The  $^1\text{H}$  NMR analysis of **FHM02** revealed the characteristic H-5' triazole proton singlet at 7.92 ppm with the reading of one proton (**Figure 37**). Additionally, the protons at H-1', H-1, H-3 and H-4 possess the same characteristics as seen in the spectrum of **FHM01** (**Figure 36**). Also, an extra singlet at 3.86 ppm with the integration of 3 protons correlates with the methoxy substituent on the aromatic ring.

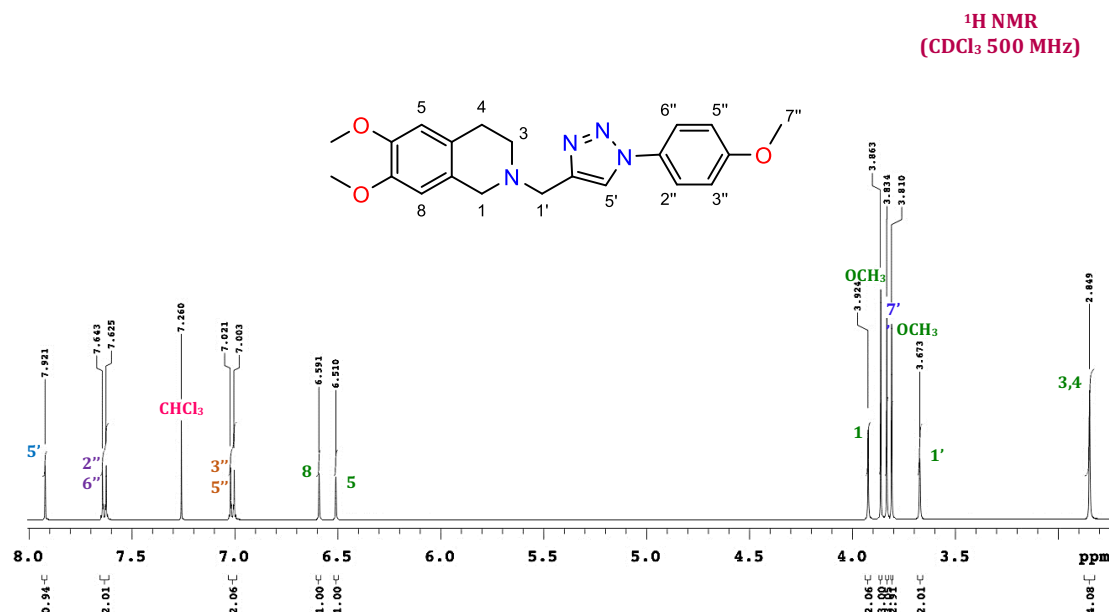


**Figure 37.**  $^1\text{H}$  NMR spectrum of **FHM02**. The triazole resonance H-5' is detected at 7.91 ppm and loss of a terminal alkyne triplet indicates the successful synthesis of a target molecule.

Two more compound with similar structures to **FHM02**, except the substituents at para position on the aromatic ring are  $-\text{OCF}_3$  and  $-\text{COCH}_3$ . Notably, these electron-withdrawing groups can deactivate the aromatic ring system and reduce its nucleophilicity, hence hindering the click reaction to reach the completion within 6 hours time frame. To overcome this problem, these syntheses were performed with the reaction time increased to 24 hours. Unreacted azides were removed by triturating with cold hexane, yielded pure products, as shown in the spectrums in **Figure 38**.  $^1\text{H}$  NMR analysis shows the same characteristics of that reported in **FHM01** and **FHM02**. The only noticeable difference in the NMR spectrum is the change in chemical shifts of H-3'' and H-5''. The inductive effect of  $-\text{OCF}_3$  substituent causes the protons peak of H-3'' and H-5'' to be more deshielded. Thus, the chemical shift can be seen at 7.39 ppm (**Figure 38A**), shifted 0.37 ppm



downfield compared to that reported in **FHM02** (Figure 37). Since the  $-\text{COCH}_3$  group has higher electron negativity than  $-\text{OCF}_3$  and its nature as an electron-withdrawing group possessed by both inductive, and resonance effects, the chemical shifts of H-3'' and H-5'' for this compound are more highly deshielded (Figure 38B) than what seen in the Figure 38A spectrum.

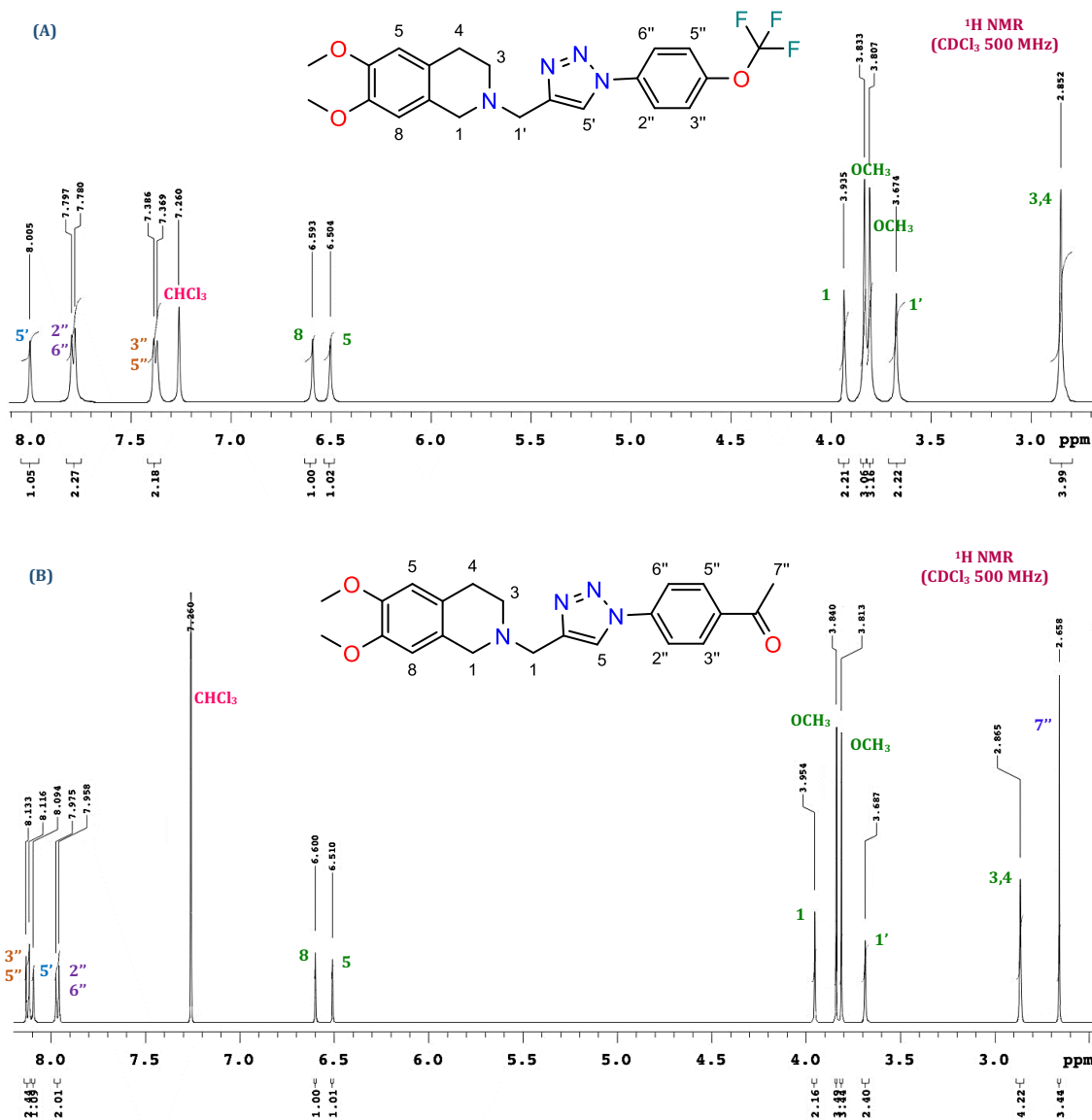
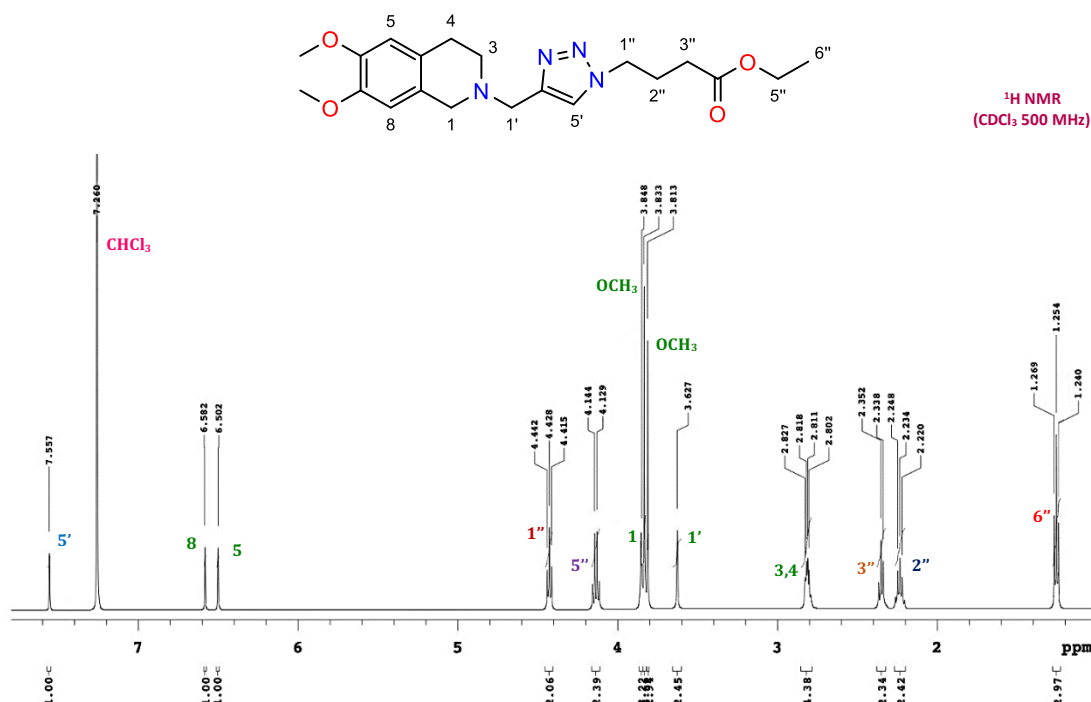


Figure 38. (A)  $^1\text{H}$  NMR spectrum of FHM03. (B)  $^1\text{H}$  NMR spectrum of FHM04.

**FHM05** is the last compound synthesised for this library using the same click reaction as described previously.  $^1\text{H}$  NMR confirmed the final product based on the proton signal of the triazole ring and the loss of an alkynyl proton (**Figure 39**). By replacing the aromatic ring with an aliphatic ester chain, the chemical shift of the H-5' triazole proton is shifted slightly upfield compared to the rest of the **FHMxx** compounds as it experiences lower magnetic field.



Five compounds in the **FHMxx** library were successfully synthesised and characterised from the Click reaction between a mono-*N*-alkylated precursor and synthesised azides. All five products listed in **Table 3** were characterised by  $^1\text{H}$  NMR and  $^{13}\text{C}$  NMR. All compounds display the characteristic H-5' triazole proton singlet from between 7.56 ppm – 8.09 ppm across all structures, confirming the existence of the click product.

**Table 3.** Chemical structures of the **FHMxx** analogues series

ID	Structure
<b>FHM01</b>	
<b>FHM02</b>	
<b>FHM03</b>	
<b>FHM04</b>	
<b>FHM05</b>	

### 2.2.8. Synthesis of an *N, N*-alkylated click analogue (**FHDxx**)

The *N, N*-alkylated compound **27** underwent click reaction with synthesised azides for the construction of the second analogue library. The first compound synthesised was **FHD01**.  $^1\text{H}$  NMR confirmed the final product based on the triazole ring's proton signal and the loss of an alkynyl proton (**Figure 40**). From the NMR analysis, the *N, N*-dialkylated-click-product displays the characteristic H-5',5''' triazole proton singlet at 9.20 ppm, with the reading of 2 protons, shifts downfield by 1.29 ppm compared to the signal observed from the *N*-alkylated-click-product.

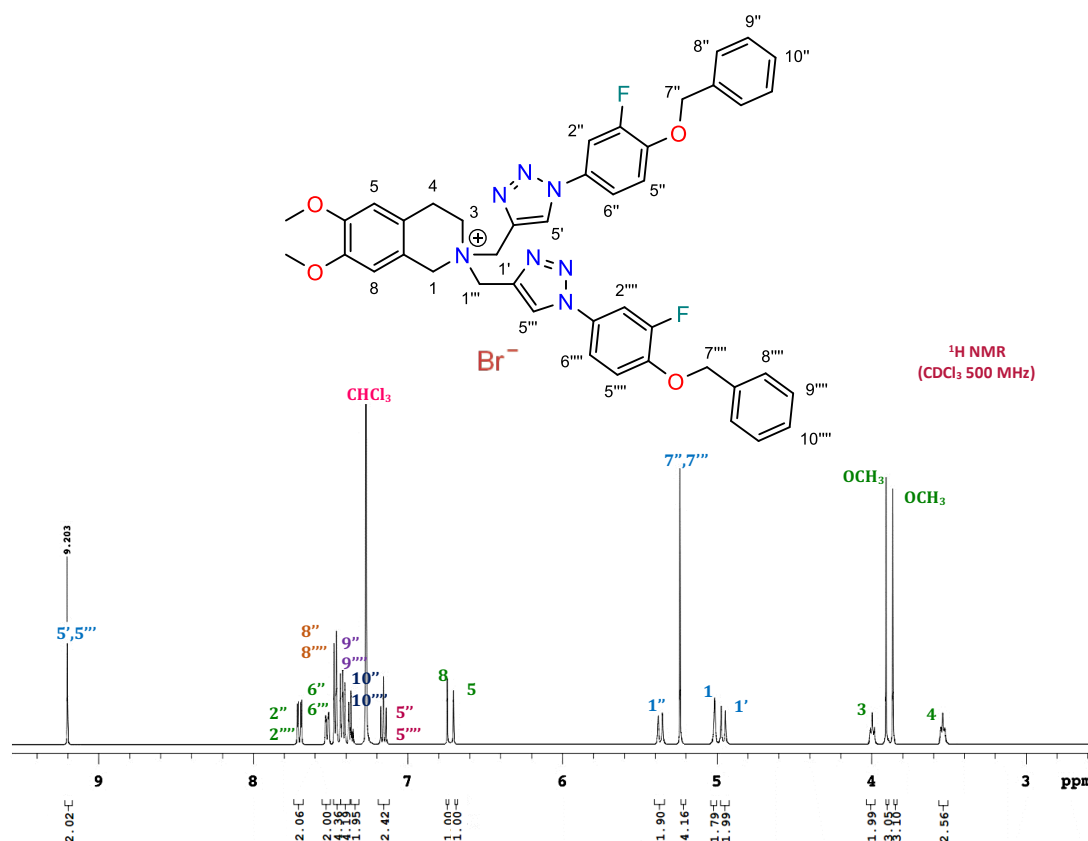


**Figure 40.** <sup>1</sup>H NMR spectrum of **24 (FHD01)**. The triazole resonance H-5',5''' is detected at 9.20 ppm and loss of the terminal alkyne triplet indicates the successful synthesis of a target molecule.

**FHD02** – a parallel compound with **FHM02** was synthesised. <sup>1</sup>H NMR confirmed the final product based on the triazole ring's proton signal and the loss of an alkynyl proton (**Figure 41**). Splitting patterns and chemical shift in this **FHD02** compound possess similar characteristics as seen in the spectrum of **FHD01** (**Figure 40**).

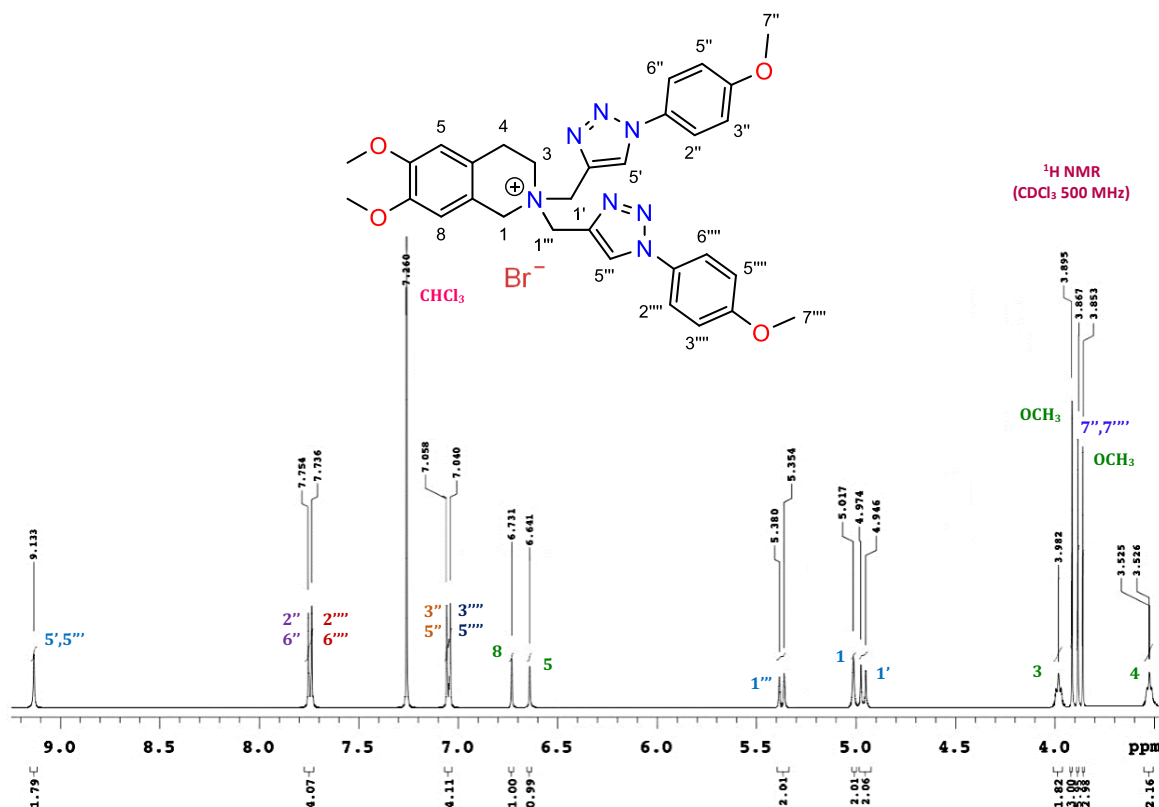


**Figure 41.**  $^1\text{H}$  NMR spectrum of **FHD02**. The triazole resonance H-5',5''' is detected at 9.13 ppm and loss of the terminal alkyne triplet indicates the successful synthesis of a target molecule.

The synthesis of **FHD03** and **FHD04** compounds that used the same azides structure in **FHM03** and **FHM04** was carried out (**Figure 42**). Since prolonging the reaction time was proven to be efficient with compounds containing  $-\text{OCF}_3$  and  $-\text{COCH}_3$  moieties, each mixture of **FHD03** and **FHD04** reactions was stirred for 24 hours at room temperature. Once all the reagents and starting materials were added together, the reaction mixture was cloudy and turned transparent with an oily residue crashed out after 24 hours. It was thought that the oily residue is the click product, but it was the azide based on  $^1\text{H}$  NMR analysis. The reason behind this problem was thought to be the change in polarity of the azide. The fluorinated and acetylated azides are generally less polar than non-fluorinated and non-acetylated derivatives, thus are not favourably soluble in such a polar solvent system (*i*-PrOH and  $\text{H}_2\text{O}$ ) which is supported by the turbidity of the reaction mixture as observations. To overcome this problem, the reactions were heated up to the melting point of the starting azides -  $50^\circ\text{C}$  and allowed to stir for 24 hours. In this attempt, the reaction mixture was less cloudy and remained homogenous after 24

hours of heating. However, as observed in the first attempt, the oily residue was crashed out upon cooling the reaction for further workup, and that was the starting material azide. Several attempts were carried out using the same solvent system with prolonging the reaction time to 48 hours and 72 hours (**Table 5**), but the outcome remained unchanged. With the 72 hours reaction, it was noticed that the solution turned completely dark brown at the 60<sup>th</sup> hour. Upon quenching the reaction with water and extracting the mixture with DCM, the colour of aqueous solution remained dark brown, which is different from the rest of the successful click reaction where the aqueous solution obtained was blue/green. This indicates that the copper salt might have undergone thermal decomposition, thus resulted in an unsuccessful reaction.

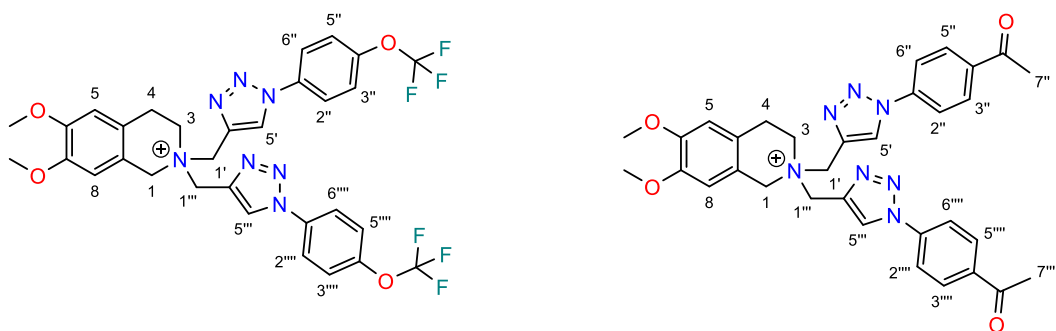


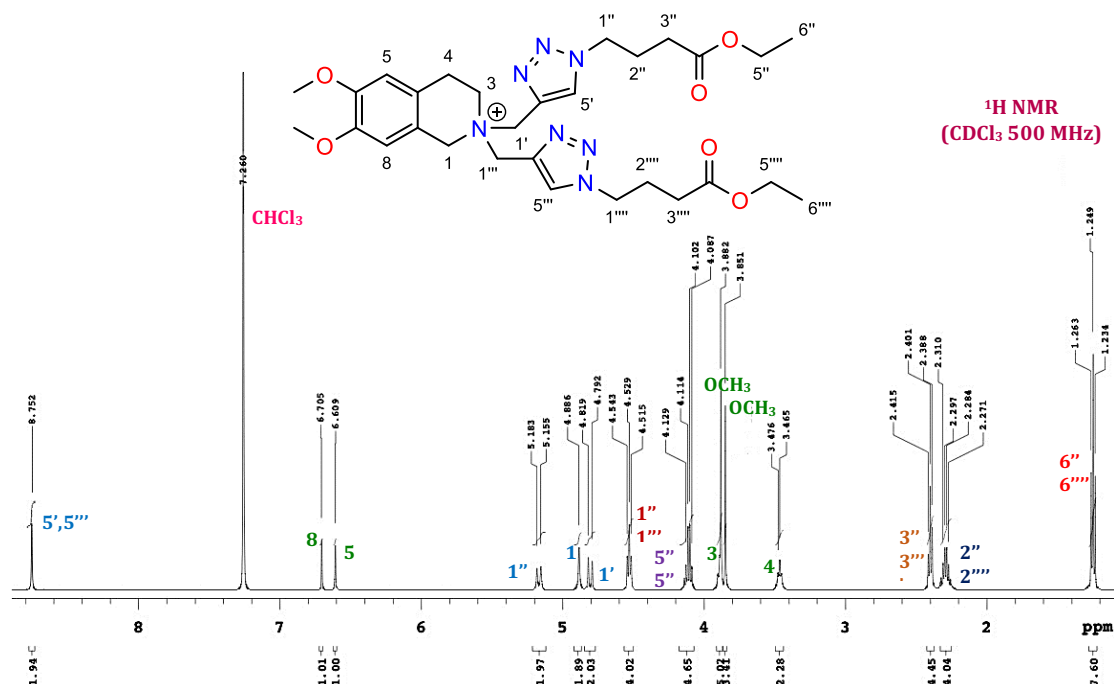
**Figure 42.** Structures of proposed compounds **FHD03** (left) and **FHD04** (right) in the **FHDxx** library.

Since these reactions were believed to be hindered by the solubility of starting azides, it was curious to see if changing the solvent would be helpful. As the CuAAC reaction was proven to work efficiently with various polar aprotic solvents, DMF, MeOH and THF were employed with various attempts and different reaction conditions were reported in **Table 5** below. After several attempts, no click product was recovered except the starting azides. Even though various solvent systems were employed to enhance reactants' and reagents' solubility, none of them could compromise the solubility of all reactants and reagents. Any attempts with different solvents and reaction conditions were failed to find out the best solvent that could produce the expected click products. Due to the time constraint, **FHD03** and **FHD04** were exempted from the **FHDxx** library.

**Table 4.** Reaction conditions for the synthesis of **FHD03** and **FHD04**

Attempt	Solvent	Temp	Time	Attempt	Solvent	Temp	Time
<b>1</b>	<i>i</i> -PrOH : H <sub>2</sub> O (1:1)	Rt	24 hrs	<b>10</b>	MeOH : H <sub>2</sub> O (1:1)	50°C	24 hrs
<b>2</b>	<i>i</i> -PrOH : H <sub>2</sub> O (1:1)	50°C	24 hrs	<b>11</b>	MeOH : H <sub>2</sub> O (7:3)	Rt	24 hrs
<b>3</b>	<i>i</i> -PrOH : H <sub>2</sub> O (1:1)	50°C	48 hrs	<b>12</b>	MeOH : H <sub>2</sub> O (7:3)	50°C	24 hrs
<b>4</b>	<i>i</i> -PrOH : H <sub>2</sub> O (1:1)	50°C	72 hrs	<b>13</b>	MeOH : H <sub>2</sub> O (8:2)	Rt	48 hrs
<b>5</b>	DMF	Rt	24 hrs	<b>14</b>	MeOH : H <sub>2</sub> O (8:2)	50°C	48 hrs
<b>6</b>	DMF	50°C	24 hrs	<b>15</b>	MeOH : H <sub>2</sub> O (9:1)	Rt	72 hrs
<b>7</b>	DMF	50°C	48 hrs	<b>16</b>	MeOH : H <sub>2</sub> O (9:1)	50°C	72 hrs
<b>8</b>	DMF	50°C	72 hrs	<b>17</b>	THF	rt	24 hrs
<b>9</b>	MeOH : H <sub>2</sub> O (1:1)	Rt	24 hrs	<b>18</b>	THF	50°C	24 hrs

The compound **FHD05**, last in the **FHDxx** library was made with the aliphatic ester replaced the aromatic ring on the compound's right-hand side, the same structure as seen in **FHM05**. From the NMR analysis, the *N,N*-dialkylated-click-product displays the characteristic H-5',5''' triazole proton singlet at 8.75 ppm, with the reading of 2 protons, shifts dramatically upfield by 3.70 ppm compared to the signal observed from **FHD01** and **FHD02** (**Figure 43**). All the signals observed for the aliphatic ester appear to have the same splitting patterns seen in **FHM05**. The integration is double since the product contains two identical alkyl moieties. The protons signal at H-4 is more shielded, thus overlapping with one of the methoxy peaks. Other than that, the rest of the resonances possess the same characteristics as analysed for **FHD01** and **FHD02**.

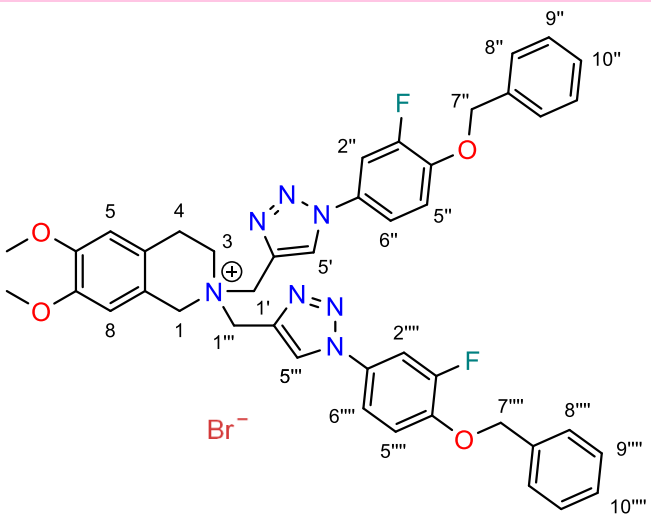
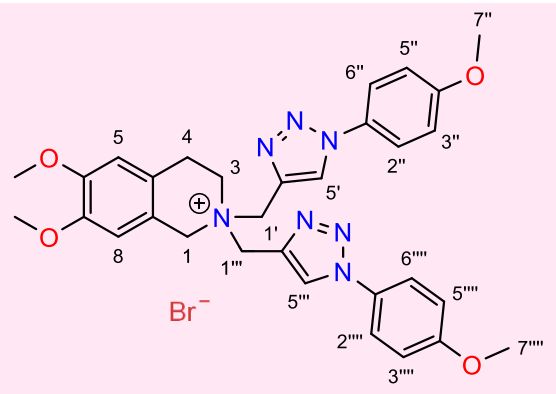
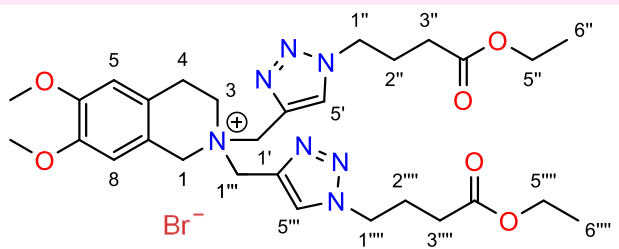


**Figure 43.** <sup>1</sup>H NMR spectrum of **FHD05**. The triazole resonance H-5',5''' is detected at 8.75 ppm and loss of the terminal alkyne triplet indicates the successful synthesis of a target molecule.



Three compounds in the **FHDxx** library were synthesised and characterised. All three products listed in **Table 5** were characterised by  $^1\text{H}$  NMR and  $^{13}\text{C}$  NMR. All compounds display the characteristic H-5' and H-5''' triazole proton singlet from between 8.75 ppm – 9.21 ppm across all structures, confirming the existence of the click product.

**Table 5.** Chemical structures of the **FHDxx** analogue series

ID	Structure
FHD01	
FHD02	
FHD05	

## 2.3. Experimental

### 2.3.1. General experimental

#### 2.3.1.1. Proton ( $^1\text{H}$ ) Nuclear Magnetic Resonance (NMR) Spectroscopy

$^1\text{H}$  NMR spectra were recorded on an Agilent 500 MHz spectrometer in deuterated chloroform ( $\text{CHCl}_3$ ) containing 0.03% v/v tetramethyl silane (TMS) unless otherwise specified. All samples were either referenced relative to the  $\text{CHCl}_3$  chemical resonance at 7.26 ppm or TMS chemical resonance ( $\delta$ ) at 0 part-per-million (ppm). Proton resonances were assigned as chemical shift (multiplicity, coupling constant(s), the number of protons, proton assignment). Multiplicities are reported as m (multiplet), s (singlet), br s (broad singlet), d (doublet), t (triplet), q (quartet), quint (quintet), n (nonet), dd (doublet of doublets), dt (doublet of triplets), td (triplet of doublets), qd (a quartet of doublets), qt (a quartet of triplets), dsex (doublet of sextets), dsep (doublet of septets) and ddd (doublet of doublets of doublets). All  $J$ -coupling constants are provided in units of Hz (Hertz). NMR assignments were based on COSY, HSQC, HMBC experiments and are numbered according to the systematic name.

#### 2.3.1.2. Carbon ( $^{13}\text{C}$ ) NMR Spectroscopy

$^{13}\text{C}$  NMR spectra were recorded on an Agilent 125 MHz spectrometer in deuterated chloroform ( $\text{CHCl}_3$ ) containing 0.03% v/v tetramethyl silane (TMS) unless otherwise specified. All samples were referenced relative to the  $\text{CHCl}_3$  chemical resonance at 77.36 ppm. Carbon resonances were assigned as chemical shift (carbon assignment). NMR assignments were based on COSY, HSQC, HMBC experiments and are numbered according to the systematic name

#### 2.3.1.3. High-Resolution Mass Spectroscopy (HRMS)

High-resolution mass spectra were obtained on an Agilent 6510 Accurate-Mass Q-TOF Mass Spectrometer, equipped with an electrospray ionisation source (ESI) using an HPLC Grade methanol solvent system. HRMS were obtained *in lieu* of elemental analysis, with NMR used to determine purity.

#### 2.3.1.4. Column Chromatography

Compounds were purified by column chromatography using either Merck flash neutral alumina or silica gel (40 – 63  $\mu\text{m}$ ) packed as a slurry in the eluent. Separations were performed using a 35 mm diameter column and the solvent system of (DCM: MeOH 50:50 to 90:10), either by the gravity, elution by compressed air or vacuum.

#### 2.3.1.5. Thin Layer Chromatography (TLC)

TLC analysis was performed using aluminium backed Merck 60 GF<sub>254</sub> silica gel or Merck 60 GF<sub>254</sub> neutral alumina gel TLC plates (Layer thickness 250  $\mu\text{m}$ ). The progress of reactions was monitored, and separation methods were developed with the stated chromatography solvent system. UV detection at 24 nm and KMnO<sub>4</sub> staining was used to develop the plates.

#### 2.3.1.6. Melting Points

A Gallenkamp Melting Point Apparatus was used to collect the melting points of all products, listed in Degrees Celsius ( $^{\circ}\text{C}$ ).

#### 2.3.1.7. High Vacuum

A Dynavac VRD-8 Vacuum Pump (8m<sup>3</sup>/hr) supplied high vacuum for solvent evaporation. A BUCHI Rotavapour R-210 provided all necessary rotary evaporation during solvent removal and drying.

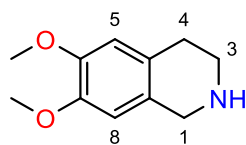
#### 2.3.1.8. Reagents and Solvents

Reagents and analytical grade solvents for all syntheses described in chapter 2 were purchased from Sigma-Aldrich (Castle Hill, NSW, Australia); the precursor for the synthesis of THIQ was purchased from Chem-Supply (Gillman, SA, Australia); boronic acids precursors were purchased from Boron Molecular (Noble Park, VIC 3174) and Fluoro Chem (Derbyshire, United Kingdom). All were used  $\geq 95\%$  purity and were used without further purification.

### 2.3.2. Chemical Reaction Procedures

#### 2.3.2.1. Synthesis of the THIQ core structure – a primary scaffold of NNMTIs

##### Synthesis of 6,7-dimethoxy-1,2,3,4-tetrahydroisoquinoline (25)

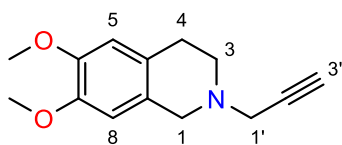


To a flask containing 3,4-dimethoxyphenethylamine (3.00 g, 16.5 mmol), was added dropwise formic acid (10 mL). The reaction mixture was stirred at 0°C for 15 minutes until the solution turned orange and then paraformaldehyde (0.50 g, 16.5 mmol) was added. The mixture was heated to 55°C and stirred for 18 hours, with a drying tube attached to the condenser. The excess formic acid was removed in *vacuo*. 1.0 M NaOH was added to the residue until pH 12 and the crude product was extracted with DCM (2 x 25 mL). The combined organic phases were washed with brine solution (30 mL) and dried over anhydrous K<sub>2</sub>CO<sub>3</sub>. Removal of the solvent in *vacuo* yielded the pure product as a pale-yellow solid (2.91 g, 92%, *R*<sub>f</sub> = 0.38 in 10% MeOH: DCM, m.p. 81°C). HRMS (EI) Calcd for C<sub>11</sub>H<sub>15</sub>NO<sub>2</sub> [M+H]<sup>+</sup> 194.2427. Found *m/z* 194.2423.

<sup>1</sup>H NMR (CDCl<sub>3</sub>-d<sub>1</sub>, 500 MHz) δ: 6.58 (s, 1H, H-8), 6.51 (s, 1H, H-5), 3.96 (s, 2H, H-1), 3.85 (s, 3H, OCH<sub>3</sub>), 3.84 (s, 3H, OCH<sub>3</sub>), 3.12 (t, *J* = 6.0 Hz, 2H, H-3), 2.71 (t, *J* = 6.0 Hz, 2H, H-4).

<sup>13</sup>C NMR (CDCl<sub>3</sub>-d<sub>1</sub>, 125 MHz) δ: 56.2 (OCH<sub>3</sub>), 146.9 (C), 148.6 (C), 111.5 (CH), 108.5 (CH), 125.2 (C), 28.0 (CH<sub>2</sub>), 47.3 (CH<sub>2</sub>), 43.6 (CH<sub>2</sub>).

##### Synthesis of 6,7-dimethoxy-2-prop-2-yn-1-yl-3,4-dihydro-1*H*-isoquinoline (26)



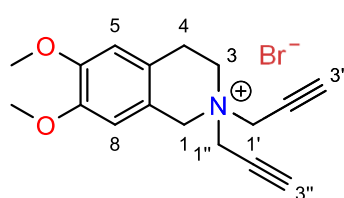
To a flask, 6,7-Dimethoxy-1,2,3,4-tetrahydroisoquinoline (1.00 g, 5.17 mmol), excess anhydrous K<sub>2</sub>CO<sub>3</sub> (3.00 g, 21.74 mmol), and anhydrous MeCN (20 mL) was stirred under N<sub>2</sub> for 5 minutes. To the reaction mixture was added dropwise propargyl bromide (0.4 mL, 628 mg, 5.27 mmol, 1.02 equiv.). The mixture was heated to 65°C and stirred for 18 hours with the N<sub>2</sub> flow attached on top of the condenser. The reaction was quenched with water (40 mL), 1 M NaOH (20 mL) and the crude product was extracted with CHCl<sub>3</sub> (3 x 20 mL). The combined organic phases were washed with brine solution (30 mL) and dried over anhydrous K<sub>2</sub>CO<sub>3</sub>. Removal of the solvent in *vacuo* yielded the pure product as an oily residue,

solidified under high vacuum (1.07 g, 90%,  $R_f$  = 0.61 in 10% MeOH: DCM, m.p. sublimed). HRMS (EI) Calcd for  $C_{14}H_{17}NO_2$   $[M+H]^+$  232.1332. Found  $m/z$  232.1333.

$^1H$  NMR ( $CDCl_3$ - $d_1$ , 500 MHz)  $\delta$ : 6.59 (s, 1H, H-8), 6.54 (s, 1H, H-5), 3.85 (s, 3H,  $OCH_3$ ), 3.84 (s, 3H,  $OCH_3$ ), 3.69 (s, 2H, H-1), 3.50 (d,  $J$  = 2.5 Hz, 2H, H-1'), 2.82 (dd,  $J$  = 11.5, 5.5 Hz, 4H, H-3, H-4), 2.27 (t,  $J$  = 2.5 Hz, 1H, H-3').

$^{13}C$  NMR ( $CDCl_3$ - $d_1$ , 125 MHz)  $\delta$ : 147.8 (C-7), 147.6 (C-6), 126.4 (C-9), 125.7 (C-10), 111.3 (CH-8), 109.4 (CH-5), 79.0 (C-2'), 73.2 (CH-3'), 55.9 ( $OCH_3$ ), 55.8 ( $OCH_3$ ), 53.9 ( $CH_2$ -1), 49.8 ( $CH_2$ -3), 46.7 ( $CH_2$ -1'), 28.8 ( $CH_2$ -4).

### Synthesis of 6,7-dimethoxy-2,2-di(prop-2-yn-1-yl)-1,2,3,4-tetrahydroisoquinolin-2-ium bromide (27)



To a flask, 6,7-Dimethoxy-1,2,3,4-tetrahydroisoquinoline (1.00 g, 5.17 mmol), tributylamine ( $Bu_3N$ ) (0.48 g, 0.62 mL, 2.6 mmol) and EtOAc (20 mL) were stirred under  $N_2$  for 10 minutes. To the reaction mixture was added dropwise propargyl bromide (2.35 mL, 3.69 g, 31.02 mmol, 6.0 molar equiv.). The mixture was stirred at room temperature for 12 hours. The solid that formed was removed by filtration and washed with ether (1 x 10 mL) and EtOAc (2 x 10 mL). The solid material was collected, and vacuum dried at ambient temperature to afford the pure product as a flaky white crystal (0.826 g, 3.06 mmol, 78%, m.p. sublimed). HRMS (EI) Calcd for  $C_{17}H_{20}NO_2$   $[M]^+$  270.1489. Found  $m/z$  270.1488.

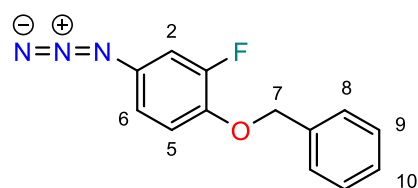
$^1H$  NMR ( $CDCl_3$ - $d_1$ , 500 MHz)  $\delta$ : 6.67 (s, 1H, H-8), 6.65 (s, 1H, H-5), 5.11 (s, 2H, H-1), 5.23 (dd,  $J$  = 16.3, 2.5 Hz, 2H, H-1'), 4.88 (dd,  $J$  = 16.3, 2.5 Hz, 2H, H-1''), 4.16 (t,  $J$  = 6.5 Hz, 2H, H-3), 3.86 (s, 3H,  $OCH_3$ ), 3.85 (s, 3H,  $OCH_3$ ), 3.17 (t,  $J$  = 6.5 Hz, 2H, H-4), 2.95 (t,  $J$  = 2.5 Hz, 2H, H-3', 3'')

$^{13}C$  NMR ( $CDCl_3$ - $d_1$ , 125 MHz)  $\delta$ : 149.9 (C-7), 149.2 (C-6), 120.1 (C-9), 116.9 (C-10), 110.9 (CH-8), 109.8 (CH-5), 82.1 (C-2', 2''), 70.61 (CH-3', 3''), 56.2 ( $OCH_3$ ), 56.1 ( $OCH_3$ ), 58.6 ( $CH_2$ -1), 54.7 ( $CH_2$ -3), 50.1 ( $CH_2$ -1', 1''), 23.4 ( $CH_2$ -4).

### 2.3.2.2. General synthesis of aryl azides from aryl boronic acids from the Copper(II)-catalysed conversion (28)

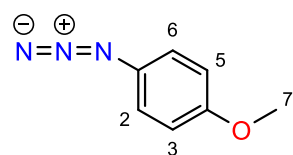
To a solution of organic boronic acid (0.2 g, 0.81 mmol) in MeOH (10 mL), was added copper(II) sulphate (28 mg, 0.11 mmol) and sodium azide (110 mg, 1.69 mmol). The mixture was stirred at room temperature for 24 hours whilst exposed to air. The mixture was then quenched with water (25 mL) and extracted with DCM (2 x 15 mL). The combined organic extracts were washed with brine (20 mL) and dried over anhydrous MgSO<sub>4</sub>. The solvent was removed in *vacuo*. The crude liquid product was reconstituted with *i*-PrOH (5 mL). The solution of crude azide was used in the next reaction step without further purification. The aryl azide solution was kept in a vial with aluminium cover and stored at -20°C.

#### 1-azido-4-(benzyloxy)-3-fluorobenzene

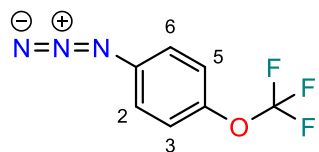


Removal of the solvent in *vacuo* yielded a pure product as dark brown liquid (197 mg, 0.81 mmol, 100%). <sup>1</sup>H NMR (CDCl<sub>3</sub>-d<sub>1</sub>, 500 MHz)  $\delta$ : 7.60 (d, *J* = 8.5 Hz, 1H, H-6), 7.50 (d, *J* = 8.5 Hz, 1H, H-2), 7.45 (d, *J* = 7.5 Hz, 1H, H-8), 7.40 (t, *J* = 7.5 Hz, 2H, H-9), 7.36 (t, *J* = 7.5 Hz, 2H, H-10), 7.11 (t, *J* = 8.5 Hz, 1H, H-5), 5.21 (s, 2H, H-7). <sup>13</sup>C NMR (CDCl<sub>3</sub>-d<sub>1</sub>, 125 MHz)  $\delta$ : 155.2 (C), 150.3 (C), 138.4 (C), 136.7 (C), 128.9 (CH), 128.5 (CH), 127.9 (CH), 123.7 (CH), 121.7 (CH), 105.6 (CH), 70.8 (CH<sub>2</sub>).

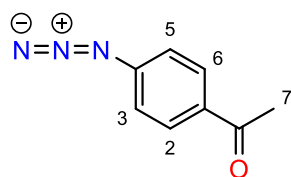
#### 1-azido-4-methoxybenzene



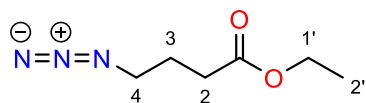
Removal of the solvent in *vacuo* yielded a pure product as brown liquid (196 mg, 100%). <sup>1</sup>H NMR (CDCl<sub>3</sub>-d<sub>1</sub>, 500 MHz)  $\delta$ : 6.96-6.93 (m, 2H, H-5,6), 6.89-6.83 (m, 2H, H-2,3), 3.78 (s, 3H, H-7). <sup>13</sup>C NMR (CDCl<sub>3</sub>-d<sub>1</sub>, 125 MHz)  $\delta$ : 156.9 (C), 150.8 (C), 125.1 (CH), 114.6 (CH), 55.5 (CH<sub>3</sub>).

**1-azido-4-(trifluoromethoxy)benzene**

Removal of the solvent in *vacuo* yielded a pure product as light brown liquid (196 mg, 100%).  $^1\text{H}$  NMR ( $\text{CDCl}_3\text{-d}_1$ , 500 MHz)  $\delta$ : 7.78 (d,  $J$  = 8.5 Hz, 2H, H-5,6), 7.37 (d,  $J$  = 8.5 Hz, 2H, H-2,3).  $^{13}\text{C}$  NMR ( $\text{CDCl}_3\text{-d}_1$ , 125 MHz)  $\delta$ : 150.8 (C), 148.3, (C), 125.1 (CH), 121.0 (C), 115.1 (CH).

**1-(4-azidophenyl)ethan-1-one**

Removal of the solvent in *vacuo* yielded a pure product as dark yellow liquid (196 mg, 100%).  $^1\text{H}$  NMR ( $\text{CDCl}_3\text{-d}_1$ , 500 MHz)  $\delta$ : 7.97 (d,  $J$  = 8.7 Hz, 2H, H-5,6), 7.09 (d,  $J$  = 8.7 Hz, 2H, H-2,3), 2.59 (s, 3H, H-7).  $^{13}\text{C}$  NMR ( $\text{CDCl}_3\text{-d}_1$ , 125 MHz)  $\delta$ : 196.6 (C), 150.8 (C), 132.6 (C), 130.4 (CH), 122.3 (CH), 26.4 ( $\text{CH}_3$ ).

**Ethyl-4-azidobutanoate**

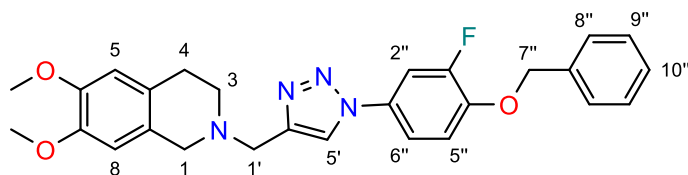
To a flask containing DMSO (25 mL) was added methyl-5-bromopentanoate (0.2 g, 1.025 mmol) and  $\text{NaN}_3$  (0.2 g, 3.076 mmol). The mixture was stirred at room temperature for 24 hours whilst exposed to air. The mixture was extracted with EtOAc (2 x 15 mL). The combined organic extracts were washed with  $\text{H}_2\text{O}$  (5 x 25 mL) and dried over  $\text{Na}_2\text{CO}_3$ . Removal of the solvent in *vacuo* yielded a pure product as a transparent liquid (0.15 g, 93%). The  $^1\text{H}$  NMR spectrum of the product was in good agreement with previously reported data for a pure product.<sup>84</sup>

**2.3.2.3. Standard Copper-Catalysed Azide-Alkyne Cycloaddition reaction conditions**

To a flask, the *i*-PrOH/azide solution (5 mL, 190 mg, 0.78 mmol), 6,7-dimethoxy-2-prop-2-ynyl-3,4-dihydro-1*H*-isoquinoline (150 mg, 0.65 mmol),  $\text{CuSO}_4 \cdot 5\text{H}_2\text{O}$  (14.95 mg, 0.6 mmol), excess sodium ascorbate (268 mg, 1.35 mmol) and water (5 mL) were stirred at room temperature for 6-24 hours or until the colour of the reaction mixture turned from dark brown to completely green. The mixture was quenched with water (25 mL). To a reaction mixture was added 0.1 M EDTA (25 mL) and stirred for 15 minutes then extracted with  $\text{CHCl}_3$  (3 x 20 mL). The

combined organic extract was washed with 0.1M EDTA (5 x 10 mL) and brine (1 x 30 mL) then dried over anhydrous Na<sub>2</sub>CO<sub>3</sub>.

**6,7-dimethoxy-2-((1-(4-(benzyloxy)-3-fluorophenyl)-1*H*-1,2,3-triazol-4-yl)methyl)-1,2,3,4-tetrahydroisoquinoline (23) – FHM01**

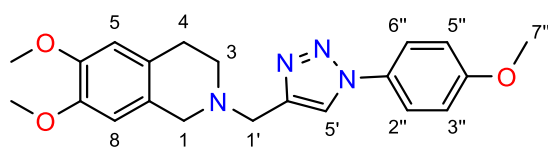


Removal of the solvent in *vacuo* yielded the pure product as a dark army solid (286 mg, 93%, *R<sub>f</sub>* = 0.5). HRMS (EI) Calcd

for C<sub>27</sub>H<sub>27</sub>FN<sub>4</sub>O<sub>3</sub> [M+H]<sup>+</sup> 475.2139. Found *m/z* 475.2139. <sup>1</sup>H NMR (CDCl<sub>3</sub>-d<sub>1</sub>, 500 MHz) δ: 7.91 (s, 1H, H-5'), 7.60 (d, *J* = 8.5 Hz, 1H, H-6''), 7.50 (d, *J* = 8.5 Hz, 1H, H-2''), 7.45 (d, *J* = 7.5 Hz, 1H, H-8''), 7.40 (t, *J* = 7.5 Hz, 2H, H-9''), 7.36 (t, *J* = 7.5 Hz, 2H, H-10''), 7.11 (t, *J* = 8.5 Hz, 1H, H-5''), 6.59 (s, 1H, H-5), 6.51 (s, 1H, H-8), 5.21 (s, 2H, H-7''), 3.92 (s, 2H, H-1), 3.85 (s, 3H, OCH<sub>3</sub>), 3.83 (s, 3H, OCH<sub>3</sub>), 3.67 (s, 2H, H-1'), 2.85 (s, 4H, H-3, 4).

<sup>13</sup>C NMR (CDCl<sub>3</sub>-d<sub>1</sub>, 125 MHz) δ: 153.8 (C), 151.8 (C), 149.7 (C), 148.9 (C), 147.5 (C), 136.0 (C), 135.7 (C), 129.7 (C), 128.8 (CH), 128.4 (CH), 127.5 (CH), 127.3 (CH), 117.4 (C), 116.4 (CH), 115.9 (CH), 110.9 (CH), 109.9 (CH), 109.7 (CH), 71.6 (CH<sub>2</sub>), 64.4 (CH<sub>2</sub>), 59.5 (CH<sub>2</sub>), 56.1 (CH<sub>3</sub>), 56.0 (CH<sub>3</sub>), 55.7 (CH<sub>2</sub>), 53.2 (CH<sub>2</sub>), 152.2 (q, *J* = 247.4 Hz), 116.7 (q, *J* = 19 Hz), 145.3 (q, *J* = 10.8 Hz), 131.0 (q, *J* = 6.5), 124.4 (q, *J* = 3.3 Hz).

**6,7-dimethoxy-2-((1-(4-methoxyphenyl)-1*H*-1,2,3-triazol-4-yl)methyl)-1,2,3,4-tetrahydroisoquinoline – FHM02**



Removal of the solvent in *vacuo* yielded a crude product as a dark brown solid. The crude was triturated with cold hexane (4

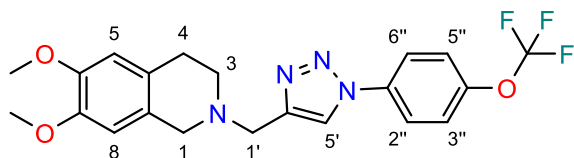
x 5 mL), resulted in the pure product as a light brown solid (47 mg, 19%, *R<sub>f</sub>* = 0.5). HRMS (EI) Calcd for C<sub>21</sub>H<sub>24</sub>N<sub>4</sub>O<sub>3</sub> [M+H]<sup>+</sup> 381.1921. Found *m/z* 381.1921. <sup>1</sup>H NMR (CDCl<sub>3</sub>-d<sub>1</sub>, 500 MHz) δ: 7.93 (s, 1H, H-5'), 7.63 (d, *J* = 8.5 Hz, 2H, H-2'',6''), 7.01 (d, *J* = 8.5 Hz, 2H, H-3'',5''), 6.60 (s, 1H, H-5), 6.51 (s, 1H, H-8), 3.93 (s, 2H, H-1), 3.87 (s, 3H, OCH<sub>3</sub>), 3.84 (s, 3H, OCH<sub>3</sub>), 3.81 (s, 3H, H-7''), 3.68 (s, 2H, H-1'), 2.85 (s, 4H, H-3,4).

<sup>13</sup>C NMR (CDCl<sub>3</sub>-d<sub>1</sub>, 125 MHz) δ: 159.8 (C), 147.6 (C), 147.3 (C), 145.6 (C), 130.6 (C), 126.3 (C), 125.9 (C), 122.1 (CH), 120.9 (CH), 119.9 (CH), 118.1 (CH), 114.8 (CH),



111.4 (CH), 109.5 (CH), 55.9 (CH<sub>2</sub>), 55.8 (CH<sub>2</sub>), 55.6 (CH<sub>3</sub>), 55.5 (CH<sub>3</sub>), 55.4 (CH<sub>3</sub>), 53.3 (CH<sub>2</sub>), 28.7 (CH<sub>2</sub>)

**6,7-dimethoxy-2-((1-(4-(trifluoromethoxy)phenyl)-1*H*-1,2,3-triazol-4-yl)methyl)-1,2,3,4-tetrahydroisoquinoline – FHM03**

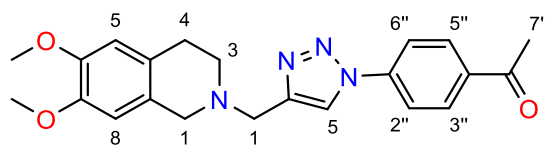


Removal of the solvent in *vacuo* yielded a crude product as a dark brown solid.

The crude was triturated with cold hexane (4 x 5 mL), resulted in the pure product as a dark brown crystalline powder (57 mg, 21%, *R<sub>f</sub>* = 0.5). HRMS (EI) Calcd for C<sub>21</sub>H<sub>21</sub>F<sub>3</sub>N<sub>4</sub>O<sub>3</sub> [M+H]<sup>+</sup> 435.1638. Found *m/z* 435.1639. <sup>1</sup>H NMR (CDCl<sub>3</sub>-d<sub>1</sub>, 500 MHz) δ: 8.01 (s, 1H, H-5'), 7.78 (d, *J* = 8.5 Hz, 2H, H-2'',6''), 7.37 (d, *J* = 8.5 Hz, 2H, H-3'',5''), 6.59 (s, 1H, H-5), 6.50 (s, 1H, H-8), 3.94 (s, 2H, H-1), 3.83 (s, 3H, OCH<sub>3</sub>), 3.81 (s, 3H, OCH<sub>3</sub>), 3.67 (s, 2H, H-1'), 2.85 (s, 4H, H-3,4).

<sup>13</sup>C NMR (CDCl<sub>3</sub>-d<sub>1</sub>, 125 MHz) δ: 159.8 (C), 147.6 (C), 147.3 (C), 145.6 (C), 130.6 (C), 126.3 (C), 125.9 (C), 122.1 (CH), 120.9 (CH), 119.9 (CH), 118.1 (CH), 114.8 (CH), 111.4 (CH), 109.5 (CH), 55.9 (CH<sub>2</sub>), 55.8 (CH<sub>2</sub>), 55.6 (CH<sub>3</sub>), 55.5 (CH<sub>3</sub>), 55.4 (C), 53.3 (CH<sub>2</sub>), 28.7 (CH<sub>2</sub>), 134.5 (q, *J* = 240 Hz), 125.6 (q, *J* = 30 Hz), 122 (q, *J* = 2 Hz).

**1-(4-(4-((6,7-dimethoxy-3,4-dihydroisoquinolin-2(1*H*)-yl)methyl)-1*H*-1,2,3-triazol-1-yl)phenyl)ethan-1-one – FHM04**

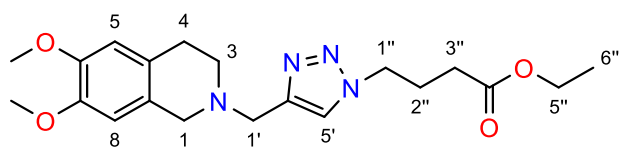


Removal of the solvent in *vacuo* yielded a crude product as a dark brown solid. The crude was triturated with cold hexane (4

x 5 mL), resulted in the pure product as a light brown solid (48 mg, 20%, *R<sub>f</sub>* = 0.5). HRMS (EI) Calcd for C<sub>22</sub>H<sub>24</sub>N<sub>4</sub>O<sub>3</sub> [M+H]<sup>+</sup> 393.1921. Found *m/z* 393.1921. <sup>1</sup>H NMR (CDCl<sub>3</sub>-d<sub>1</sub>, 500 MHz) δ: 8.13 (d, *J* = 8.5 Hz, 2H, H-5'',3''), 8.09 (s, 1H, H-5'), 7.98 (d, *J* = 8.5 Hz, 2H, H-2'',6''), 6.60 (s, 1H, H-5), 6.51 (s, 1H, H-8), 3.95 (s, 2H, H-1), 3.84 (s, 3H, OCH<sub>3</sub>), 3.81 (s, 3H, OCH<sub>3</sub>), 3.69 (s, 2H, H-1'), 2.87 (s, 4H, H-3,4), 2.66 (s, 3H, H-7'').

<sup>13</sup>C NMR (CDCl<sub>3</sub>-d<sub>1</sub>, 125 MHz) δ: 197.0 (C), 148.2 (C), 146.7 (C), 141.2 (C), 136.7 (C), 132.8 (C), 128.8 (CH), 126.5 (C), 122.5 (CH), 119.1 (CH), 111.4 (CH), 108.3 (CH), 62.4 (CH<sub>2</sub>), 57.2 (CH<sub>2</sub>), 56.1 (CH<sub>3</sub>), 56.0 (CH<sub>3</sub>), 54.5 (CH<sub>2</sub>), 27.3 (CH<sub>2</sub>), 26.6 (CH<sub>3</sub>).

**Ethyl-4-((6,7-dimethoxy-3,4-dihydroisoquinolin-2(1H)-yl)methyl)-1H-1,2,3-triazol-1-yl)butanoate – FHM05**

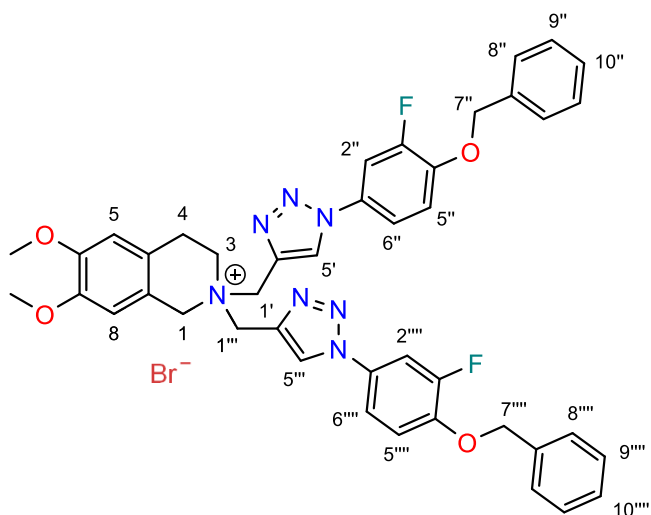


Removal of the solvent in *vacuo* yielded a crude product as a dark brown solid. The crude was

trituated with cold hexane (4 x 5 mL), resulted in the pure product as a dark brown solid (67 mg, 40%,  $R_f$  = 0.5). HRMS (EI) Calcd for  $C_{20}H_{28}N_4O_4$   $[M+H]^+$  389.2183. Found  $m/z$  389.2183.  $^1H$  NMR ( $CDCl_3$ - $d_1$ , 500 MHz)  $\delta$ : 7.56 (s, 1H, H-5'), 6.58 (s, 1H, H-8), 6.50 (s, 1H, H-5), 4.3 (t,  $J$  = 7.0 Hz, 2H, H-1''), 4.14 (q,  $J$  = 7.0 Hz, 2H, H-5''), 3.85 (s, 2H, H-1), 3.83 (s, 3H,  $OCH_3$ ), 3.81 (s, 3H,  $OCH_3$ ), 3.62 (s, 2H, H-1'), 2.81 (s, 4H, H-3,4), 2.35 (t,  $J$  = 7.0 Hz, 2H, H-3''), 2.247 (quint,  $J$  = 7.0 Hz, 2H, H-2''), 1.27 (t,  $J$  = 7.0 Hz, 3H, H-6'').

$^{13}C$  NMR ( $CDCl_3$ - $d_1$ , 125 MHz)  $\delta$ : 174.1 (C), 148.6 (C), 146.9 (C), 137.5 (C), 125.9 (C), 125.4 (CH), 125.2 (C), 111.0 (CH), 109.4 (CH), 56.2 ( $CH_3$ ), 54.4 ( $CH_2$ ), 53.7 ( $CH_2$ ), 51.8 ( $CH_3$ ), 49.6 ( $CH_2$ ), 49.4 ( $CH_2$ ), 31.1 ( $CH_2$ ), 28.3 ( $CH_2$ ), 24.3 ( $CH_2$ ).

**2,2-bis((1-4-(benzyloxy)-3-fluorophenyl)-1H-1,2,3-triazol-4-yl)methyl)-6,7-dimethoxy-1,2,3,4-tetrahydroisoquinolinium bromide (24) – FHD01**



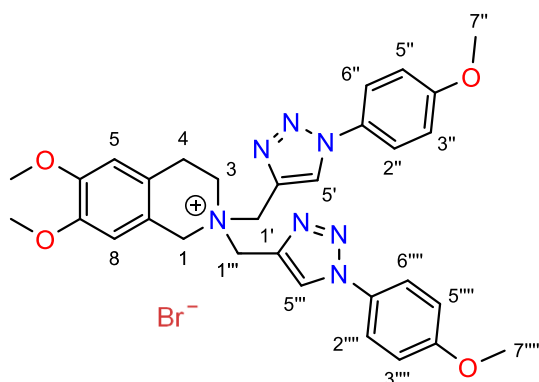
The title compound was prepared from 6,7-dimethoxy-2,2-di(prop-2-yn-1-yl)-1,2,3,4-tetrahydroisoquinolin-2-ium (100 mg, 0.37 mmol) and azide (190 mg, 0.78 mmol) in *i*-PrOH (5 mL), using a similar method to that described general synthetic procedure above. The mixture was quenched with  $H_2O$  (25 mL)

and extracted with  $CHCl_3$  (3 x 20 mL). The organic extracts were dried over  $Na_2CO_3$ . Removal of the solvent in *vacuo* yielded the pure product as a light army solid (223 mg, 0.29 mmol, 80%,  $R_f$  = 0.31, m.p. 236.7°C). HRMS (EI) Calcd for  $C_{43}H_{40}F_2N_7O_4^+$   $[M]^+$  756.3104. Found  $m/z$  756.3104.

$^1\text{H-NMR}$  ( $\text{CDCl}_3\text{-d}_1$ , 500 MHz)  $\delta$ : 9.20 (s, 2H, H-5',5'''), 7.71 (d,  $J$  = 8.5 Hz, 2H, H-6'',6'''), 7.53 (d,  $J$  = 8.5 Hz, 2H, H-2'',2'''), 7.46 (d,  $J$  = 7.5 Hz, 4H, H-8'',8'''), 7.44 (t,  $J$  = 7.0 Hz, 4H, H-9'',9'''), 7.35 (t,  $J$  = 7.0 Hz, 2H, H-10'',10'''), 7.15 (t,  $J$  = 8.5 Hz, 2H, H-5'',5'''), 6.74 (s, 1H, H-8), 6.67 (s, 1H, H-5), 5.36 (d,  $J$  = 14 Hz, 2H, H-1'), 5.24 (s, 4H, H-7'',7'''), 5.02 (s, 4H, H-1), 4.96 (d,  $J$  = 14 Hz, 2H, H-1'''), 3.96 (t,  $J$  = 6.0 Hz, 2H, H-3), 3.88 (s, 3H,  $\text{OCH}_3$ ), 3.84 (s, 3H,  $\text{OCH}_3$ ), 3.51 (t,  $J$  = 6.0 Hz, 2H, H-4).

$^{13}\text{C-NMR}$  ( $\text{CDCl}_3\text{-d}_1$ , 125 MHz)  $\delta$ : 160.8 (C), 155.9 (C), 153.9 (C), 149.7 (C), 148.9 (C), 135.7 (C), 130.3 (CH), 128.8 (CH), 128.5 (CH), 127.5 (CH), 126.1 (CH), 121.0 (C), 117.9 (C), 117.5 (C), 111.8 (CH), 110.9 (CH), 109.9 (CH), 103.8 (CH), 70.8 ( $\text{CH}_2$ ), 60.4 ( $\text{CH}_2$ ), 59.2 ( $\text{CH}_2$ ), 56.1 ( $\text{CH}_3$ ), 56.0 ( $\text{CH}_3$ ), 55.5 ( $\text{CH}_2$ ), 52.9 ( $\text{CH}_2$ ), 152.2 (q,  $J$  = 247.4 Hz), 116.7 (q,  $J$  = 19 Hz), 145.3 (q,  $J$  = 10.8 Hz), 131.0 (q,  $J$  = 6.5), 124.4 (q,  $J$  = 3.3 Hz).

**6,7-dimethoxy-2,2-bis((1-(4-methoxyphenyl)-1H-1,2,3-triazol-4-yl)methyl)-1,2,3,4-tetrahydroisoquinolin-2-ium bromide – FHD02**



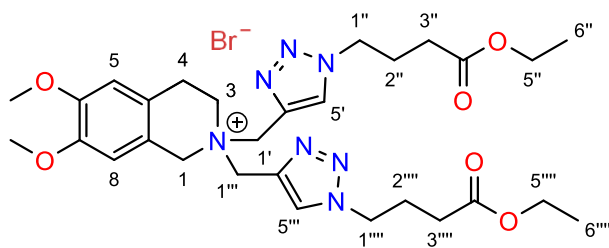
The title compound was prepared from **27** (100 mg, 0.37 mmol) and 1-azido-4-methoxybenzene (200 mg, 0.70 mmol) in *i*-PrOH :  $\text{H}_2\text{O}$  (10 mL, 1:1), using a similar method to that described above for the synthesis of **FHD01**. Removal of the solvent in *vacuo* yielded a crude product

as a light army crystalline solid. The crude product was triturated with cold hexane (4 x 5 mL), resulted in a pure product as a light army crystalline powder (78 mg, 37%,  $R_f$  = 0.5). HRMS (EI) Calcd for  $\text{C}_{31}\text{H}_{34}\text{N}_7\text{O}_4^+$   $[\text{M}]^+$  568.2666. Found  $m/z$  568.2666.

$^1\text{H-NMR}$  ( $\text{CDCl}_3\text{-d}_1$ , 500 MHz)  $\delta$ : 9.13 (s, 2H, H-5',5'''), 7.75 (d,  $J$  = 8.5 Hz, 4H, H-2'',2''',6'',6'''), 7.06 (d,  $J$  = 8.5 Hz, 4H, H-3'',3''',5'',5'''), 6.73 (s, 1H, H-5), 6.64 (s, 1H, H-8), 5.38 (d,  $J$  = 13 Hz, 2H, H-1'), 5.02 (s, 2H, H-1), 4.97 (d,  $J$  = 14 Hz, H-1'''), 3.98 (t,  $J$  = 6.0 Hz, 2H, H-3), 3.89 (s, 3H,  $\text{OCH}_3$ ), 3.87 (s, 6H, H-7'',7'''), 3.85 (s, 3H,  $\text{OCH}_3$ ), 3.53 (t,  $J$  = 6.0 Hz, 2H, H-4).

$^{13}\text{C}$ -NMR ( $\text{CDCl}_3\text{-d}_1$ , 125 MHz)  $\delta$ : 160.6 (C), 146.9 (C), 146.7 (C), 132.8 (C), 130.5 (C), 129.1 (C), 122.3 (CH), 121.3 (C), 119.1 (CH), 114.3 (CH), 111.6 (CH), 111.4 (CH), 66.3 (CH<sub>2</sub>), 60.5 (CH<sub>2</sub>), 56.1 (CH<sub>3</sub>), 56.0 (CH<sub>3</sub>), 55.8 (CH<sub>3</sub>), 53.5 (CH<sub>2</sub>), 25.1 (CH<sub>2</sub>).

**6,7-dimethoxy-2,2-bis((1-(5-methoxy-5-oxopentyl)-1*H*-1,2,3-triazol-4-yl)methyl)-1,2,3,4-tetrahydroisoquinolin-2-ium bromide – FHD03**



The title compound was prepared from **27** (80 mg, 0.29 mmol) and ethyl-4-azidobutanoate (160 mg, 0.60 mmol) in MeOH : H<sub>2</sub>O (10 mL, 1:1), using a similar method to that

described above for the synthesis of **FHD01**. Removal of the solvent in *vacuo* yielded a crude product as a yellow solid. The crude product was triturated with cold hexane (4 x 5 mL), resulted in a pure product as a yellow solid (78 mg, 48%, *R*<sub>f</sub> = 0.5). HRMS (EI) Calcd for C<sub>29</sub>H<sub>42</sub>N<sub>7</sub>O<sub>6</sub><sup>+</sup> [M]<sup>+</sup> 584.3191. Found *m/z* 584.3191.

$^1\text{H}$ -NMR ( $\text{CDCl}_3\text{-d}_1$ , 500 MHz)  $\delta$ : 8.75 (s, 2H, H-5',5'''), 6.71 (s, 1H, H-8), 6.61 (s, 1H, H-5), 5.18 (d, *J* = 14 Hz, 2H, H-1'), 4.89 (s, 2H, H-1), 4.82 (d, *J* = 13.5 Hz, 2H, H-1'''), 4.53 (t, *J* = 7.0 Hz, 4H, H-1'',1'''), 4.10 (q, *J* = 7.5 Hz, 4H, H-5'',5'''), 3.89 (t, *J* = 5.5 Hz, 2H, H-3), 3.88 (s, 1H, OCH<sub>3</sub>), 3.85 (s, 1H, OCH<sub>3</sub>), 3.47 (t, *J* = 5.5 Hz, 2H, H-4), 2.40 (t, *J* = 7.0 Hz, 4H, H-3'',3'''), 2.29 (quint, *J* = 6.5 Hz, 4H, H-2'',2'''), 1.25 (t, *J* = 7.0 Hz, 6H, H-6'',6''').

$^{13}\text{C}$ -NMR ( $\text{CDCl}_3\text{-d}_1$ , 125 MHz)  $\delta$ : 174.1 (C), 148.6 (C), 148.3 (C), 137.5 (C), 135.8 (C), 127.5 (C), 125.4 (CH), 111.0 (CH), 110.9 (CH), 65.3 (CH<sub>2</sub>), 61.8 (CH<sub>2</sub>), 58.8 (CH<sub>2</sub>), 56.2 (CH<sub>3</sub>), 51.8 (CH<sub>3</sub>), 49.4 (CH<sub>2</sub>), 31.1 (CH<sub>2</sub>), 28.6 (CH<sub>2</sub>), 24.3 (CH<sub>2</sub>).

**2.3.2.4. Isolation procedure of a crude mixture obtained from the THIQ *N*-alkylation reaction**

To the crude mixture of *N*-alkylated product and *N,N*-dialkylated product was added water (50 mL) and sonicated for 5 minutes. The undissolved solid was collected and reconstituted in DCM (20 mL). The filtrate was extracted with DCM (2 x 15 mL). The combined organic extract was dried over anhydrous K<sub>2</sub>CO<sub>3</sub>. The solvent was removed to afford a pure *N*-alkylation product as an orange solid.

The filtrate was collected to remove water in *vacuo* (water bath temperature: 70°C, atm: 65 mbar) until the yellow residue appeared. The yellow residue was reconstituted with 25 mL DCM and dried over anhydrous K<sub>2</sub>CO<sub>3</sub>. The solvent was removed, yielded pure *N,N*-dialkylated product as a yellow solid. The pure *N,N*-dialkylated product could also be obtained from freeze-drying the aqueous solution after the second extraction.

## Chapter 3      *In vitro* assessment of NNMT inhibitory activity

### 3.1. Introduction

Using the synthetic procedures developed in **Chapter 2**, a library of 5 mono-alkylated and 3 di-alkylated THIQ analogues were prepared in sufficient yield and purity to allow *in vitro* evaluation of their NNMT inhibitory activities. There are several different NNMT inhibition assays reported in the literature, and each has important advantages and disadvantages. In the following section, each class of NNMT assay is described in order to select the most appropriate assay to use for subsequent testing of the THIQ library

### 3.2. Screening methods to determine the inhibitory activity of NNMTIs

One of the key challenges of running an NNMT inhibition assay is to monitor the progress of the enzymatic reaction. To date, the NNMT assays that have been developed can be split into two broad classes based on the technique used to detect the reaction product. The first NNMT assay developed used LC-MS for product detection, and subsequent assays have relied on fluorescence-based techniques.

#### 3.2.1. HPLC-MS based NNMT assay

Haren *et al.* described an HPLC-MS based assay in 2017<sup>5</sup>. In this assay, each test compound was incubated with NNMT for 5 minutes, over a concentration range of 10 nM to 5000  $\mu$ M with 550 nM NNMT in 50 mM Tris buffer (pH 8.6). The reaction was initiated by adding a NAM/SAM mixture (10 and 200  $\mu$ M, respectively) and left to react for 10 minutes. Reaction aliquots were quenched by addition of acetonitrile, and 10  $\mu$ M the amount of MNA that was formed by the enzymatic reaction was quantified by HPLC. While this assay did allow conveniences in sample workup and offers excellent separation efficiency, shorter run times and higher sample throughput, this assay was time-consuming because it relied in HPLC analysis, which laborious. In addition, this assay is not amenable for high throughput screening (HTS) applications.

### 3.2.2. Fluorescent-based assay

Fluorescent analysis, on the other hand, requires no further method development and is more readily accessible with greater consistency and less delay.

#### 3.2.2.1. NAM-coupled fluorescent assay

The principle of NAM-coupled fluorescent analysis relies on the MNA formed during the NNMT reaction, which reacts with acetophenone in KOH and formic acid to produce a fluorescent product: *N*-methyl-2,7-naphthyridin-1(2*H*)-one (**Figure 44**). Different concentrations of inhibitors were pre-incubated with NNMT for 30 minutes at 37°C. A mixture of 6  $\mu$ M NAM and 7  $\mu$ M SAM was added and incubated for 60 minutes. The reaction is quenched by adding a solution of ethanol: acetophenone (EtOH: ACP 75:25) and 5M KOH in 50% EtOH and incubated for 15 minutes. An aliquot of 100  $\mu$ L HCOOH 60% is added. After 60 minutes of incubation at 37°C, the fluorescent product was measured using a Tecan reader with excitation wavelength at 375 nm and emission wavelength at 430 nm<sup>85</sup>. While this assay was suitable for HTS and no method developments were needed, it requires complex buffer systems, tedious workup and derivatisation reactions, long run times, and may give false positive results.

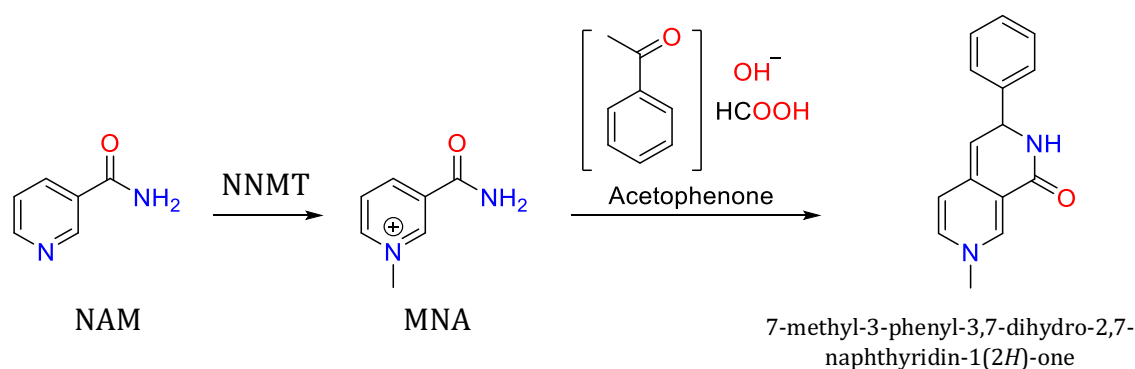


**Figure 44.** The reaction of NAM in the presence of NNMT and SAM-forming product MNA. MNA is further treated with acetophenone in the presence of KOH and HCOOH to give *N*-methyl-2,7-naphthyridine-1(2*H*)-one in the fluorescent *in vitro* assay.

### 3.2.2.2. SAH-coupled fluorescent-based assay

This method is an enzyme-coupled colourimetric assay that examines the enzymatic activity by-product SAH<sup>86,87,88</sup>. This assay employs a similar mechanism to the well-known Ellman assay, a colourimetric method based on the amount of thiocholine released. The thiocholine released is quantified colourimetrically by its reaction with 5,5'-bisdithionitrobenzoic acid (DNTB). The product is an orange-coloured compound with a maximum absorbance at 490 nm (**Figure 45**).

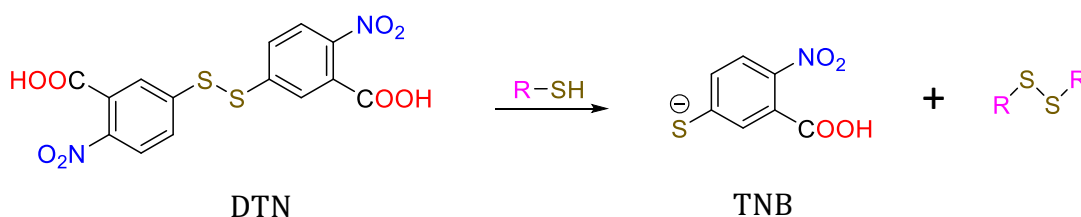


**Figure 45.** The schematic reaction of Ellman's Assay

For this assay, different concentrations of inhibitors were incubated with the enzyme, and the reaction can then be initiated by adding SAM and substrate NAM, and further incubated for 15 minutes at 37°C. To the reaction mixture, a mixture of two enzyme and Thiol Detecting Probe was added, and the fluorescent signal was measured at Ex/Em = 392/482 nm. In a different approach, Ellman's reagent was added as a quench solution to convert homocysteine to 5-thio-2-nitrobenzoic acid (TNB), the absorbance of which can be measured at 412 nm (**Figure 46**). This assay is a simple, sensitive, and rapid tool to screen potential inhibitors of NNMT. However, unpredictable background detection of SAM auto decompose to SAH is possible, leading to false-positive results<sup>5</sup>.



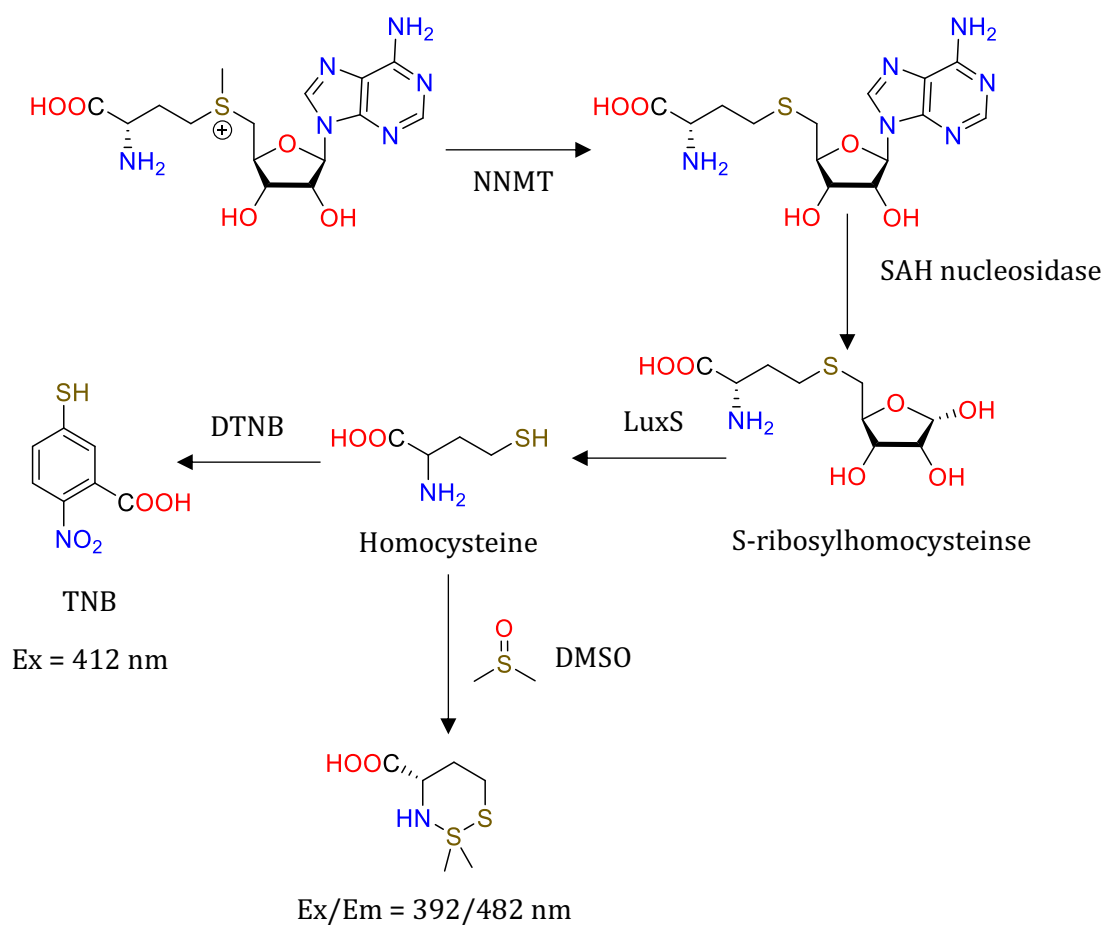


**Figure 46.** The reaction of SAH with DTNB and DMSO as two biological assay reaction routes

### 3.2.2.3. Noncoupled fluorescent-based assay

Relying upon the NNMT selective substrate quinoline that is methylated by SAM to form 1-methylquinolinium (1-MQ) with characteristic fluorescent properties, this assay was firstly developed by Neelakantan *et al.* in 2017<sup>85</sup>. This assay was performed at room temperature and initiated by adding a mixture of substrate SAM and quinoline to the enzyme solution. The product 1-MQ is fluoresced and can be measured at Ex/Em = 330/405 nm (**Figure 47**). This assay is simple, quick, provide quantitative read-out of fluorescent signal and does not require tedious reaction work-up. This suggests its applicability for HTS of chemical libraries to identify novel NNMTIs. Having more advantages than other fluorescent-

based assays, this noncoupled fluorescent assay was employed to perform the *in vitro* biological protein-ligand assays in this project.

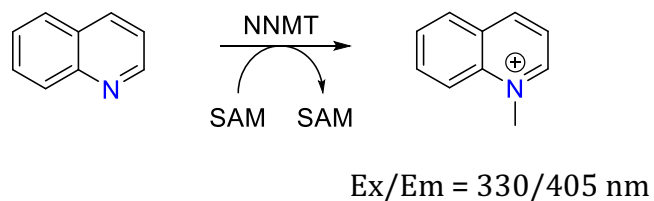


**Figure 47.** Noncoupled fluorescent-based assay reaction

### 3.3 Attempted assessment of NNMT inhibitory activity using Non-coupled fluorescent-based assay

The noncoupled fluorescent-based assay was first developed by Neelakantan *et al.*<sup>85</sup>. This assay mechanism is based on the enzymatic activity of NNMT, where substrate NAM is replaced with Quinoline to product 1-MQ as a fluorescent product that can be detected using the plate reader. Due to the assay's simplicity, it was employed as a primary method to determine the inhibitory activity of synthesised NNMTIs. After reviewing all the methods, each component's concentration to be made as stock solutions and final concentrations per well are gathered in **Table 6A**.

**Table 6A.** Concentrations of all components that need to be prepared and reported final concentration per well.

Component	Final concentration per well	Stock solutions concentration
NNMT	2.994 µg/mL = 110 nM	11.976 µg/mL
Tris HCl Buffer	5 mM, pH 8.6	5 mM, pH 8.6 *
DTT	1 mM	4 mM
SAM	10 µM	80 µM
Quinoline	100 µM	800 µM

\* 5 mM Tris HCl pH 8.6 was made in a large batch and used to prepare SAM stock solution and dilute Quinoline working solution. Doing this ensures Tris HCl buffer's concentration to be kept constant and reduce the complication in preparing stock solutions.

**Table 6B.** Outline of the assay

Total % DMSO	0% DMSO	0% DMSO	0% DMSO	0% DMSO	0.1% DMSO
	NNMT Blank	Quinoline Blank	SAM Blank	Control	Solvent Control
Solution (µL)	A1	A2	A3	A4	A5
Buffer	75	87.5	87.5	50	50*
NNMTIs	-	-	-	-	-
NNMT	25	-	-	25	25
SAM	-	-	12.5	12.5	12.5
Quinoline	-	12.5	-	12.5	12.5
Total V.	100	100	100	100	100

\*5 mM Tris (pH 8.6) with 0.1% DMSO was prepared to specifically be used for this well as NNMT was proven to work effectively as low as 0.2% DMSO.

Before starting the inhibition study, enzyme activity assay was first performed to validate the results reported in the work of Neelakantan *et al.* The first attempt was carried out using following the assay outline in **Table 6B**. The NNMT, SAM and Substrate Quinoline were thawed at room temperature. The assay was performed at room temperature (25°C) in Buffer consisting of 5 mM Tris (pH 8.6)

and 1 mM DTT. Solution of NNMT and buffer was added to each well and the reactions were initiated by adding the mixture of SAM and Quinoline. The reaction progress was immediately monitored using a Tecan 96-well plate reader, and the reaction data were collected approximately every fifteen seconds for 15 minutes. The 1-MQ reaction product production in each well was monitored by recording fluorescence emission intensities at 405 nm and excitation wavelength ( $\lambda_{\text{ex}}$ ) of 330 nm) with detector excitation and emission slit widths positioned at 5 nm. However, no fluorescent signals were detected compared to the readings collected from the NNMT, SAM and Quinoline blank wells (**Figure 48**).

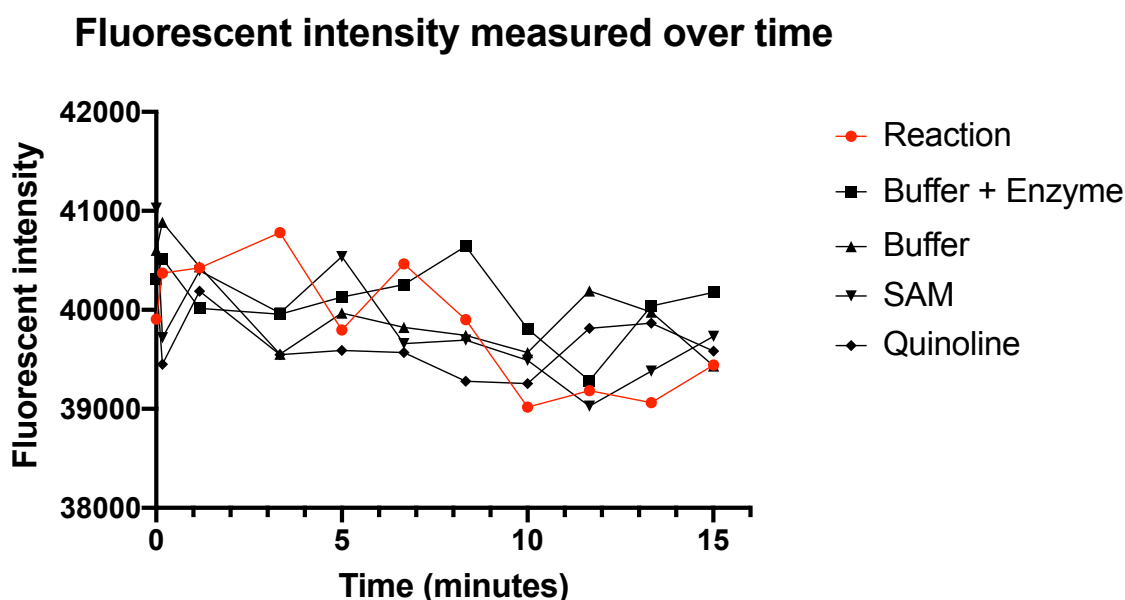


**Figure 48.** Fluorescent intensity measured over 15 minutes

Various attempts with slight changes to the method and adding each component to the well plate were carried out as outlined in **Table 7**. Quinoline was incubated with the enzyme solution for 5-10 minutes at 25 and 37°C. The reactions were initiated by adding SAM and put to read immediately. Adding Quinoline separately from the SAM to the enzyme was thought to allow it binds preferentially with the enzyme receptors; hence the reaction would be more likely to occur once SAM is added. In addition, various assays in increasing the concentration of NNMT, SAM and Quinoline to 1.5, 2.0 and 3.0 folds were performed (**Table 10**) However, the obtained results remain unchanged, with no 1-MQ signals being detected.

**Table 7.** Changes in the procedure of the enzyme activity assay

Method	Changes in procedure
<i>Original</i>	<i>NNMT at 25°C ⇒ Mixture of SAM and Quinoline added ⇒ Read</i>
<b>1</b>	NNMT + Quinoline was incubated at 25°C for 5 minutes ⇒ SAM added ⇒ Read
<b>2</b>	NNMT + Quinoline was incubated at 25°C for 10 minutes ⇒ SAM added ⇒ Read
<b>3</b>	NNMT + Quinoline was incubated at 37°C for 5 minutes ⇒ SAM added ⇒ Read
<b>4</b>	NNMT + Quinoline was incubated at 37°C for 10 minutes ⇒ SAM added ⇒ Read

**Table 8.** Change in concentration of NNMT, SAM and Quinoline

Variable	Increase in Concentration		
	NNMT	SAM	Quinoline
<b>NNMT</b>	x 1.5, x 2.0, x 3.0	-	-
<b>SAM</b>	-	x 1.5, x 2.0, x 3.0	-
<b>Quinoline</b>	-	-	x 1.5, x 2.0, x 3.0

A problem that could be the cause of this is the enzyme. Since the enzyme was purchased and stored for more than 1.5 years (the supplier recommends using the enzyme within 6-12 months of purchasing), it could decompose and cannot function. A new enzyme was purchased, and the experiments were repeated, but the obtained results remain unchanged. This proved the enzyme was not the cause of the unsuccessful assay.

Another possible reason for the enzyme assay to not work as expected is the quality of SAM – a methyl donor. In the search for SAM stability and stabilisation information, there was some useful information that came across. The study of Kawahara *et al.* claimed that SAM is very unstable at room temperature and in basic conditions<sup>89</sup>. A similar discovery was also reported in the work of Matos *et al.*<sup>90</sup>. It was asserted that SAM solution must be prepared in the solution with pH 3-5, containing an excess of large-size, non-nucleophilic counterions, such as tosylate or sulphate. A recent work in synthesising and testing NNMTIs of Policapro *et al.*<sup>48</sup> reported the preparation of SAM working solution from SAM.HCl purchased from Sigma in solution consists of 10% EtOH, 0.005 M H<sub>2</sub>SO<sub>4</sub>, pH 4.0. New SAM working solution was prepared accordingly. The assays were performed but no fluorescent signal was detected (**Figure 49**).

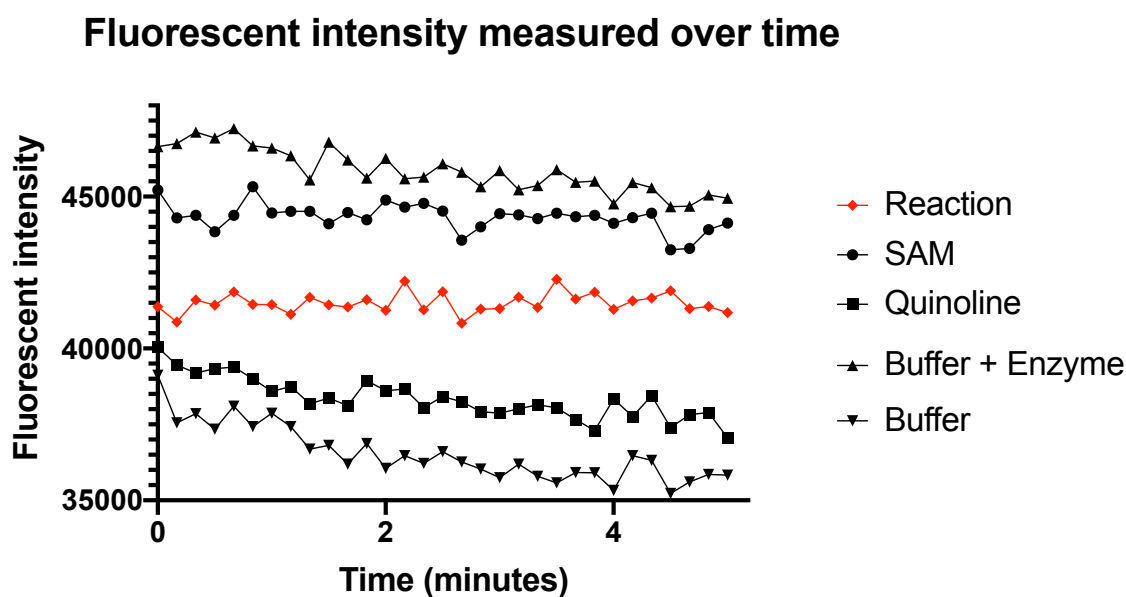


**Figure 49.** Fluorescent intensity measured over time. The reaction was performed with new NNMT and SAM solution

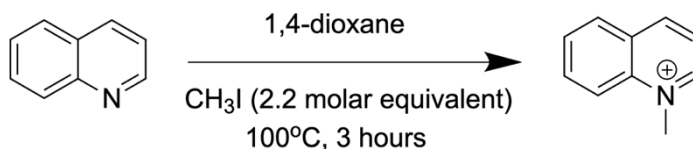
### 3.2.3. Assessment of NNMT assay sensitivity and limit of detection

Despite several modifications of the assay procedure and use of fresh enzyme, detection of 1-MQ could not be achieved. One potential explanation for this may be the limit of detection of the plate reader used. It is possible that 1-MQ was being generated in the assays, but at concentration not high enough to be detected by the plate reader.

From the reported procedure, a theoretical concentration of 1-MQ that could be generated in the enzymatic reaction is 10  $\mu$ M, and it could be possibly lower when performing an actual experiment. Therefore, to better understand why the assay did not give any signals as described in the original method, a study of 1-MQ detection limits was carried out. To achieve this, solutions of 1-MQ at concentrations ranging from 1.0  $\mu$ M – 10 mM were prepared and measured directly in the plate reader.

#### 3.2.3.1. Synthesis of 1-MQ

Prior to conducting the study, a pure sample of 1-MQ was first synthesised, as shown in **Scheme 3.3.1.2**. 1-MQ was prepared in a one-step procedure in which quinoline was reacted with iodomethane at 100°C for 3 hours. The reaction mixture was cool down in an ice bath and filtered to collect the precipitate. The precipitate product was washed with diethyl ether (3 x 30 mL) and cold hexanes (2 x 30 mL) and dried in *vacuo*. The  $^1\text{H}$  NMR proton of 1-MQ was obtained (**Figure 50**). The most prominent peak to confirm the formation of the 1-MQ product is a strong singlet peak detected at 4.92 ppm.



**Scheme 3.3.1.2** Synthesis of 1-MQ product

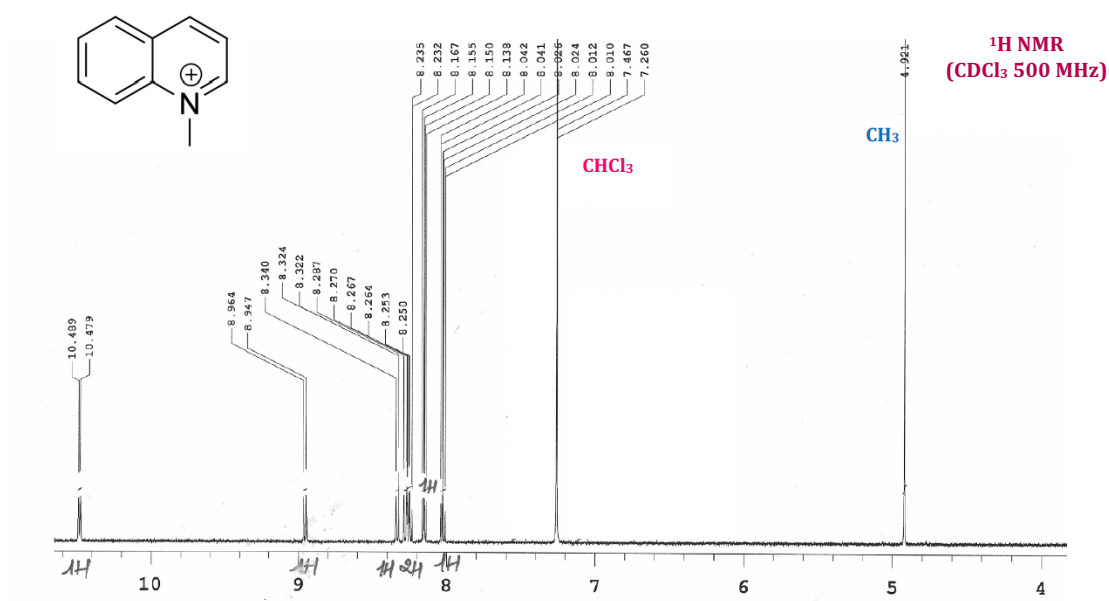
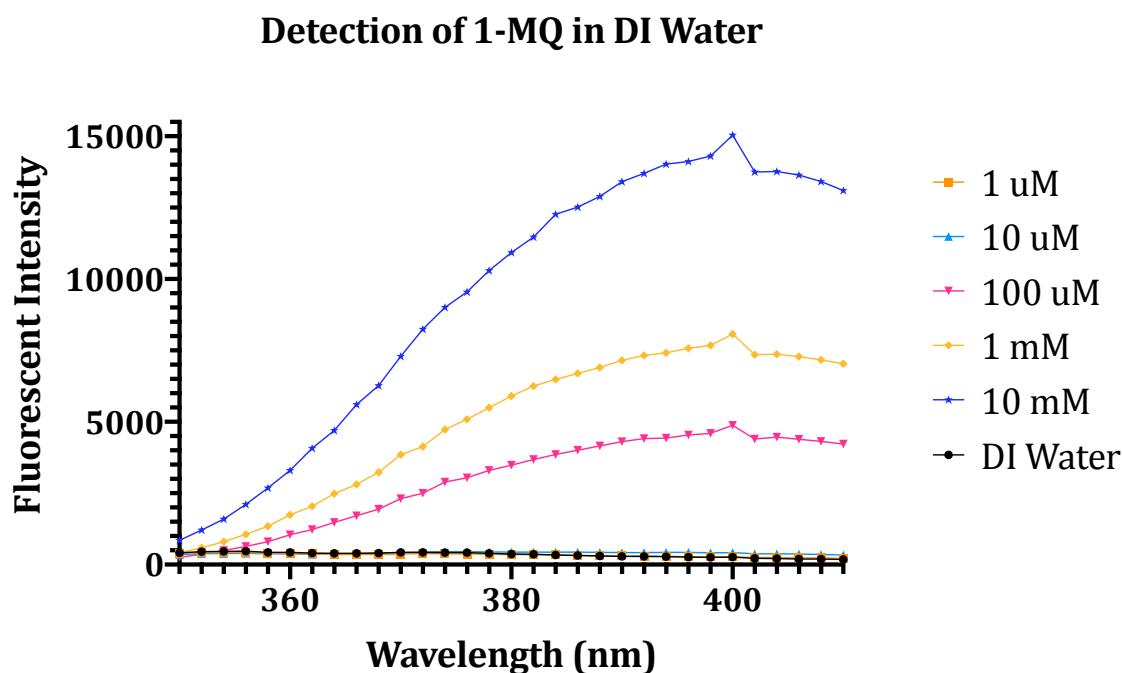


**Figure 50.**  $^1\text{H}$  NMR spectrum of the synthesised product 1-MQ

### 3.2.3.2. Plate reader detection of 1-MQ in various solvent systems

To assess the sensitivity of the plate reader various concentrations of synthetic 1-MQ were prepared in deionised (DI) water, 5 mM Tris Buffer HCl and assay solution (containing SAM, Quinoline, Buffer and NNMT). With 1-MQ solutions prepared in water, the fluorescent intensity scan was shown in **Figure 51**. At the concentration of 10 mM, the highest fluorescent intensity was observed. Decreased in fluorescent intensity was observed with lower 1-MQ concentrations. At 1  $\mu$ M of 1-MQ, there were no signals that could be seen. The obtained results suggest that the detection range of 1-MQ in water is between 10  $\mu$ M and 10 mM.



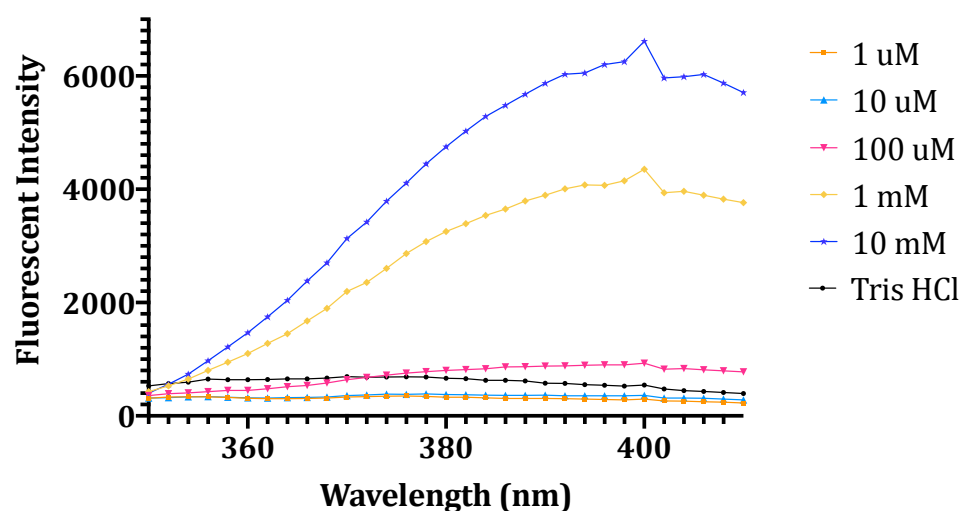
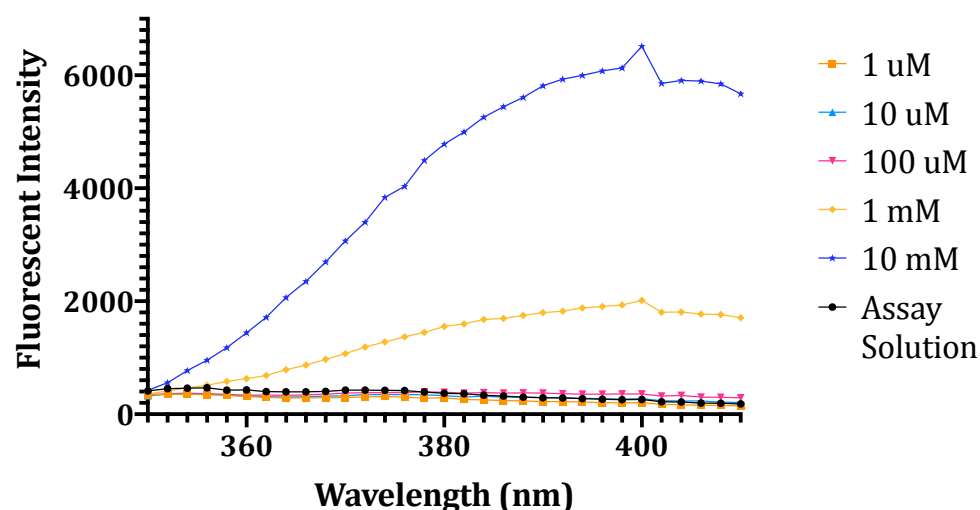


**Figure 51.** Detection of various concentrations of 1-MQ prepared in DI water

Two other sets of 1-MQ solutions were prepared in 5 mM Tris HCl buffer and assay solution to find out if the same effects is observed as seen in **Figure 51**. In 5 mM Tris HCl buffer, the detection limit range marked suppression, with 1 mM and 10 mM as a lower and an upper detection limit respectively (**Figure 52A**). The signals of remaining tested concentrations were as low as the control blank with the maximum emission wavelength observed between 360 nm and 380 nm. These effects were also seen in the last data set, where 1-MQ solutions were prepared in the assay solution (**Figure 52B**). These results are consistent with a previous study on fluorescence polarisation-based assay that claimed that noncoupled fluorescent-based assays have an extremely low signal-to-noise ratio which hinders<sup>91</sup>.

Since 1-MQ signal significantly decreased in the presence of Tris Buffer, it is suspected that Tris HCl might interfere with the fluorescent signal. In a recent publication on 1-MQ quenching mechanisms, Flor *et al.* claimed that a pair of alcohol molecules with increase in concentration can quench the excited cation of 1-MQ to form emissive exciplexes  $1\text{-MQ}^+\cdot\text{RO}^+\cdot\text{ROH}_2^+$ , reduces in fluorescent intensity<sup>92</sup>. Tris buffer is an alcohol with three hydroxy groups and that it is possible to interact with the 1-MQ formed, resulted in decrease fluorescent intensity as seen in **Figure 54**. Since the enzymatic reaction could only theoretically produce 10  $\mu\text{M}$  of 1-MQ; and

the detection concentration is 100-1000 folds higher, it is impossible to perform the assay with such high concentrations in the well plate due to solubility issues. Combining the obtained results and evidence from the literatures provide a more convincing explanation of why the adapted assay did not work as expected.

**(A)****Detection of 1-MQ in 5 mM Tris HCl****(B)****Detection of 1-MQ in Assay Solution**

**Figure 52.** Detection of various concentrations of 1-MQ prepared in **(A)**. 5 mM Tris HCl Buffer. **(B)**. Assay solution contains NNMT, Buffer, SAM and Quinoline

Despite numerous attempts in validating and modifying the method, the noncoupled fluorescent-based assay was unsuccessful in replicating due to limit of detection of 1-MQ product. Although there are three more types of fluorescent-based assays, time constraint prevents the validation, optimisation and performing the inhibition studies from being implemented.

## Chapter 4      *In vivo* biological assay to assess Anticancer Properties of NNMTIs

### 4.1. General Introduction to Assessment of Cytotoxicity

As outlined in **Chapter 1**, NNMT overexpressed in several cancer cell lines. NNMT overexpression is believed to contribute to tumour progression by protecting cancer cells from oxidative damage and is therefore a potential new target for anticancer drugs. In the study of discovery new bisubstrate inhibitors of NNMT with enhanced activity, one of the synthesised NNMTIs was shown to inhibit the target enzyme at micromolar concentration and inhibited cancer cell growth with an IC of 100  $\mu\text{M}$ <sup>46</sup>. Therefore, the anticancer activity of the potential NNMTIs prepared in **Chapter 2** was explored using the MDA-MB-231 breast cancer cell line. This cell line was selected as it has been shown to express high levels of NNMT<sup>93</sup>. Eight compounds in the two synthesised analogues **FHMxx** and **FHDxx** were investigated for potential cytotoxicity using the MTS assay.

### 4.2. MTS Assay

The MTS assay is a simple colourimetric method for determination of a compound's cytotoxicity *via* establishing the number of viable cells remaining in a culture that has been treated with the tested drug candidates<sup>94</sup>. The assay was performed using the commercially available CellTiter 96® AQueous One Solution Reagent, which contains the tetrazolium salt 3-(4,5-dimethylthiazol-2-yl)-5-(3-carboxymethoxyphenyl)-2-(4-sulfophenyl)-2H-tetrazolium (MTS), and the electron coupling reagent, phenazine ethosulfate (PES). The MTS is cleaved by NADH and NADPH-dependant dehydrogenase enzymes found in the mitochondria of cells that are metabolically active<sup>95</sup>, where cell viability is defined as a cell that is metabolically active. For this reason, the MTS assay does not differentiate between the loss of viable cells resulting from apoptosis or cytostasis that is caused by the tested compounds. The cleaving of MTS forms formazan (**Figure 53**), which has a dark red colour and therefore has a measurable absorbance at 490-500 nm, where the absorbance is directly proportional to the number of viable cells in the culture.

Cultures treated with the synthesised drug candidates in 96 well plates were analysed with a spectrophotometer after addition of the MTS reagent and 3 hours of incubation.

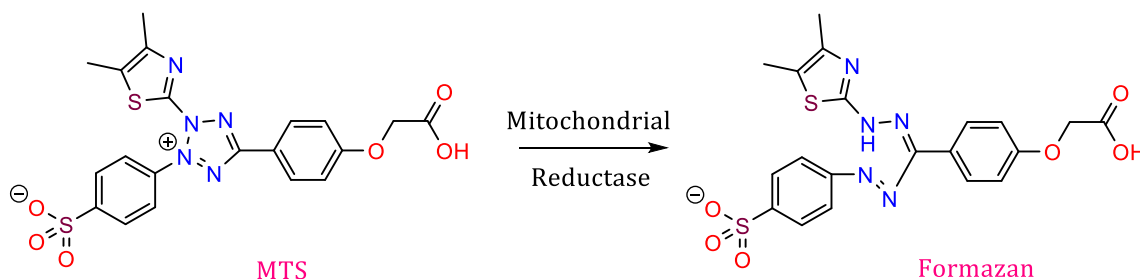


**Figure 53.** Mitochondrial cleavage of MTS to formazan

For each of the compounds tested, stock samples were prepared in DMSO and then diluted to the working concentration in media. The viability percentage was calculated by normalising the average of triplicate sample absorbance values, to the average of the triplicate control absorbance values. Control cells were treated with the highest concentration of DMSO that was present in any of the drugged cells (0.1% v/v). The results of the MTS cell proliferation assay, as described above for compounds listed in **Table 9**, are outlined in the following subsections. The initial screening data is summarised in **Figure 54** and listed in **Table 9**.

#### 4.3. Screening for Cytotoxicity

**Table 9.** displays the results obtained from the cytotoxic screening of the MTS assay for the compounds synthesised in **Chapter 2**. Each of the compounds were assessed as replicates (technical triplicate), run on different plates and different days. For each replicate, the absorbance was measured from three triplicate wells for each tested concentration (biological triplicate), the average of which was used to calculate the percentage viability. The three replicate percentage viability values obtained for each concentration were analysed with One-way ANOVA tests and Dunnett's multiple comparisons test using GraphPad Prism 9.0.0. Statistical significance was determined according to a decrease in drugged cell viability when compared to the control. The average percent viability values are listed in **Table 9**.

Based on the screening assay, four compounds showed statistically significant cytotoxic activity against MDA-MB-231 cell line, at the highest tested concentration of 50  $\mu$ M. These compounds were **FHM01**, **FHM02**, **FHM03** and **FHD01** shown in **Table 9** and **Figure 54** where statistical significance is indicated by the following: \* ( $P \leq 0.05$ ), \*\* ( $P \leq 0.01$ ), \*\*\* ( $P \leq 0.001$ ), \*\*\*\* ( $P \leq 0.0001$ ) and unlabelled values are of no significance ( $P > 0.05$ ). Of four active compounds, **FHD01** shows the most potent cytotoxicity against MDA-MB-231 as the percentage cell viability at 50  $\mu$ M and 20  $\mu$ M are 4.9% and 10.9% respectively. This gives an estimation of **FHD01**  $IC_{50}$  to be between 1  $\mu$ M and 20  $\mu$ M. Following **FHD01**, **FHM01** was deemed to be the second most active compound, with 18% cell proliferation at 50  $\mu$ M and 36.6% at 20  $\mu$ M. Although **FHM02** and **FHM03** did show activity, their cytotoxicity against MDA-MD-231 was very modest ( $> 50\%$  cell viability at 50  $\mu$ M). The remaining compounds were found to be inactive as they showed no significant decrease in cell proliferation against the MDA-MB-231 cell line at 50  $\mu$ M, as judged by the One-way ANOVA tests and Dunnett's multiple comparisons test.

### % Viability of all tested compounds at different concentrations

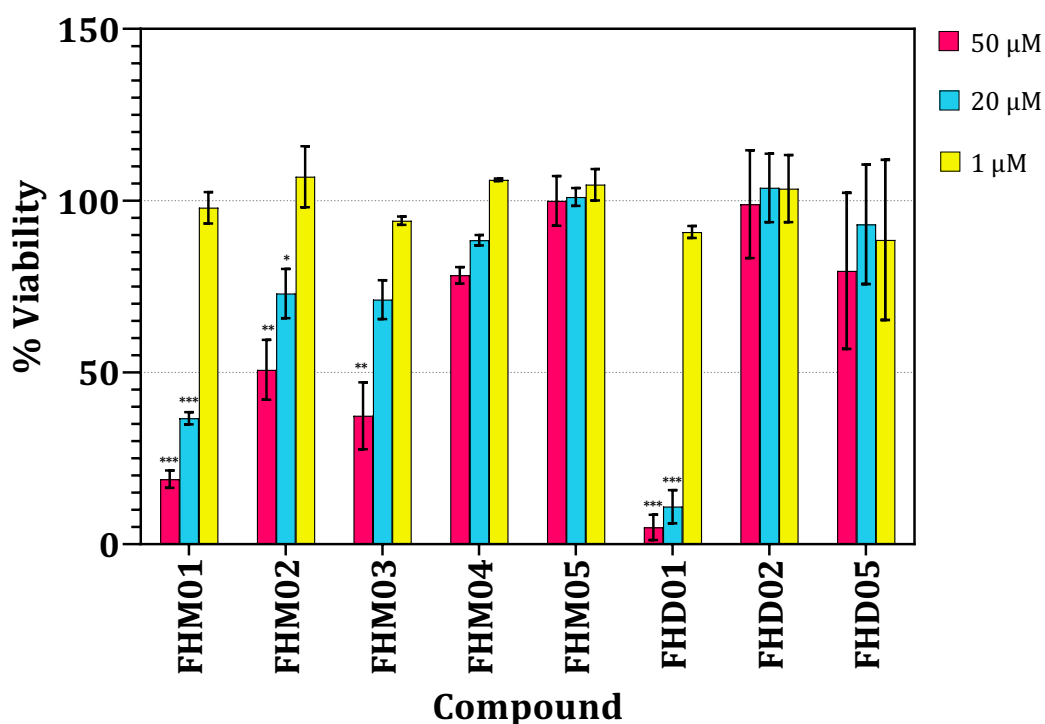


**Figure 54.** All compounds % viability at three tested concentrations (50  $\mu$ M, 20  $\mu$ M and 1  $\mu$ M). Data represented is the mean of replicate  $\pm$ SD. Statistical significance is indicated by the following: \* ( $P \leq$

0.05), \*\* ( $P \leq 0.01$ ), \*\*\* ( $P \leq 0.001$ ), \*\*\*\* ( $P \leq 0.0001$ ) and unlabelled values are of no significance ( $P > 0.05$ )

**Table 9.** MDA-MB-231 MTS screening results as % viability normalised to control.

Entry	Compound	% Viability at concentration ( $\mu\text{M}$ )		
		1	20	50
1	FHM01	98	37***	19**
2	FHM02	107	73*	51**
3	FHM03	94	71	37**
4	FHM04	106	89	78
5	FHM05	105	101	100
6	FHD01	91	11***	5***
7	FHD02	104	104	99
8	FHD05	89	93	80

Note: Statistical significance is indicated by the following: \* ( $P \leq 0.05$ ), \*\* ( $P \leq 0.01$ ), \*\*\* ( $P \leq 0.001$ ), \*\*\*\* ( $P \leq 0.0001$ ) and unlabelled values are of no significance ( $P > 0.05$ )

#### 4.4. Discussion of Cytotoxic Activity Results Against MDA-MB-231

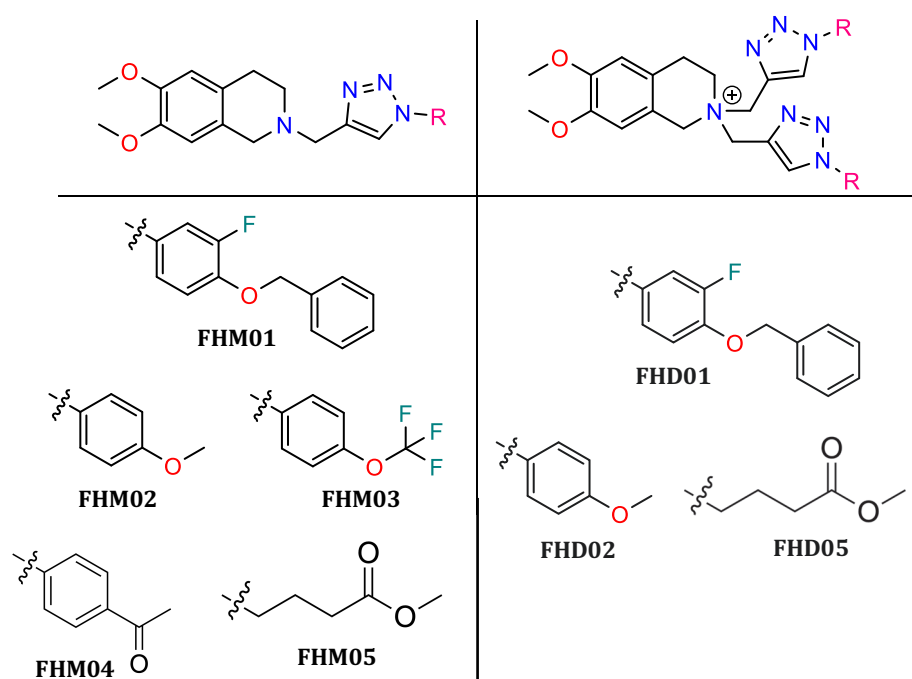


**Figure 55.** The structures of tested compounds against MDA-MB-231 for visual comparison and discussion

Although few compounds showed significant cytotoxic activity against MDA-MB-231, some information can be inferred from these results. Most notably, the presence of an aromatic ring with varieties of para-substituents that connected directly to the 1,2,3-triazole ring inferred activity, because four of the eight compounds containing this functionality displayed a significant reduction in cell viability. **FHM02** and **FHM03** showed very modest potency in cell reduction while the reverse effect is observed for the corresponding parallel compound **FHD02**, where no activity can be inferred. At 20  $\mu$ M, the cytotoxic potency of **FHM02** and **FHM03** is at 73% and 71% respectively while at 50  $\mu$ M, **FHM03** showed more significantly reduce in cell viability (37%) compared to that observed in **FHM02**. This result suggests that the trifluoromethoxy moiety assists in achieving higher potency. As shown from the % cell viability data (**Table 9**), **FHM05** and **FHD05** with an aliphatic ester moiety replaced by the aryl substituents possessed no cytotoxicity against MDA-MB-231, suggesting the alkane functionality is not necessary for potent cytotoxic activity. The activity was markedly increased when the trifluoromethoxy and methoxy functionalities were replaced with the aryl ethoxy as observed for **FHM01** (19% and 37% in cell viability at 50  $\mu$ M and 20  $\mu$ M respectively). The similar effect is observed for the corresponding parallel compound **FHD01** – is believed to be the lead compound as mentioned in **Chapter 1**. The two identical aryl ethoxy architecture gives rises to the most potent cytotoxic activity (5% and 11% in cell viability at 50  $\mu$ M and 20  $\mu$ M respectively). The structures of the discussed compounds are shown in **Figure 55**.

These obtained screening results suggest that the **FHMxx** library is generally more active than **FHDxx** library, with three compounds selectively inhibiting MDA-MB-231 cells growth. One compound in the **FHDxx** library – **FHD01**, also a lead compound, shows the strongest cytotoxic activity and is worth investigating further.



## 4.5. Experimental procedure

### 4.5.1. General reagents for cell culture

Penicillin and Streptomycin, Trypsin and fetal bovine were purchased from Thermo Fisher Scientific (Scoreby, Victoria, Australia). Dulbecco's Modified Eagle's Medium (DMEM), phosphate-buffered saline (PBS) and DMSO were purchased from Sigma-Aldrich (Castle Hill, NSW, Australia). The CellTiter 96® AQueous One Solution Reagent was purchased from Promega (Alexandria, NSW, Australia).

### 4.5.2. Cell culture

Human MDA-MB-231 breast cancer cells were obtained as a gift from Professor Michael Murray (University of Sydney) and grown at 37°C in a humidified atmosphere of 5% CO<sub>2</sub> in DMEM supplemented with 10% fetal bovine serum and 1% Penicillin/Streptomycin. Confluent cells (80 – 90%) were harvested using trypsin/EDTA after washing with PBS.

### 4.5.3. Cell Viability

For the MTS assay cells were seeded in 96-well flat-bottom plates at a density of 3500 cells/well. Serum was removed after 24 hours, after which cells were treated with various concentrations of drug candidates (1 – 50  $\mu$ M) in DMSO (final concentration 0.1%) for 72 hours; control cells received solvent alone. MTS activity was determined spectrophotometrically.



## Chapter 5      General Conclusions and Future Directions

### 5.1. General discussion and conclusions

In general, four out of five aims were achieved. The alkylation reaction of the THIQ was found to produce two products: mono-*N*-alkylated and di-*N*, *N*-dialkylated products. Various attempts were carried out to elucidate both compounds' structures to solve the chemistry's controversial problem. The proposed lead compound **23** was confirmed to be a di-alkylated click product **24**. New synthetic routes to yield exclusively the mono-*N*-alkylated **26** or di-*N*, *N*-dialkylated **27** were developed with the yield obtained for pure products are 90% and 78% respectively. Two analogue libraries of mono-*N*-alkylated and di-*N*, *N*-alkylated THIQs were synthesised and characterised. Two compounds in the **FHDxx** library were not achieved due to the solubility issues.

For the successfully synthesised compounds, purified and characterised, the broad range of biological properties was explored *via* several methods. A Noncoupled fluorescent-based NNMT inhibition assay was replicated from a literature work; however, it was unsuccessful. The assay is believed to have failed due to difficulties in detecting the reaction product 1-MQ in the plate reader. The assay forms 1-MQ to a maximum concentration of 10  $\mu\text{M}$ , however the limit of detection of 1-MQ in Tris HCl buffer was determined to be approximately 1 mM. Tris buffer could interact with the product 1-MQ to form emissive exciplexes 1-MQ $\bullet$ -RO $\bullet$ -ROH $_2^+$ , reduces in fluorescent intensity. Time constraints prevented from trying and performing other different assays.

The compounds' potential as anticancer drugs were assessed by investigating their cytotoxicity against a cancerous cell line. The breast cancer cell line MDA-MB-231 was tested, against which **FHM01**, **FHM02**, **FHM03** and **FHD01** inhibited proliferation of MDA-MB-231 breast cancer cells at concentrations below 50  $\mu\text{M}$ . The lead compound **FHD01** was the most effective in the series and reduced MDA-MB-231 cell viability to 19% and 37% of control at 50  $\mu\text{M}$  and 20  $\mu\text{M}$

respectively. The preliminary screens for cytotoxicity highlighted that the **FHMxx** analogue library is more active than the **FHDxx** analogue library.

## 5.2. Future directions

Future work should consider develop an assay technique to measure the NNMT activity. The noncoupled fluorescent-based assay, as described in **Chapter 3**, may be used with different buffer systems to examine whether potential outcomes could differ from those reported herein. NNMT inhibition of synthesised compounds needs to be measured to determine whether any correlation exists between inhibitory activity and anticancer activity.

For the compounds which showed no anticancer activity or modest anticancer activity, there is the potential to investigate for other biological properties, perform the cell growth inhibition against different cell lines, such as human epidermoid carcinoma of the oral cavity cell line (KB), the ER-positive human breast adenocarcinoma cell line MCF-7 and even with the healthy mammalian cells to assess the cytotoxicity of these synthesised drug candidates against healthy cells. By carrying out these suggested additional cell lines bioassay, each drug candidate's selectivity would be more thoroughly studied. Thus, those that show unselective cytotoxicity or possess general toxicity instead of having a cytotoxic nature would unlikely be suitable to use as a drug against any other targets.



## References

1. Szakács, G., Annereau, J. P., Lababidi, S., Shankavaram, U., Arciello, A., Bussey, K. J., Reinhold, W., Guo, Y., Kruh, G. D., Reimers, M., Weinstein, J. N., & Gottesman, M. M. Predicting drug sensitivity and resistance: Profiling ABC transporter genes in cancer cells. *Cancer Cell* **6**, 129–137 (2004).
2. Horning, B. D., Suci, R. M., Ghadiri, D. A., Ulanovskaya, O. A., Matthews, M. L., Lum, K. M., Backus, K. M., Brown, S. J., Rosen, H., & Cravatt, B. F. Chemical Proteomic Profiling of Human Methyltransferases. *J. Am. Chem. Soc.* **138**, 13335–13343 (2016).
3. Pissios, P. Nicotinamide N-Methyltransferase: More Than a Vitamin B3 Clearance Enzyme. *Trends Endocrinol. Metab.* **28**, 340–353 (2017).
4. Sternak, M., Khomich, T. I., Jakubowski, A., Szafarz, M., Szczepański, W., Białas, M., Stojak, M., Szymura-Oleksiak, J., & Chłopicki, S. Nicotinamide n-methyltransferase (nnmt) and 1-methylnicotinamide (mna) in experimental hepatitis induced by concanavalin a in the mouse. *Pharmacol. Reports* **62**, 483–493 (2010).
5. Van Haren, M. J., Sastre Toraño, J., Sartini, D., Emanuelli, M., Parsons, R. B., & Martin, N. I. A Rapid and Efficient Assay for the Characterization of Substrates and Inhibitors of Nicotinamide N-Methyltransferase. *Biochemistry* **55**, 5307–5315 (2016).
6. Kim, J., Hong, S. J., Lim, E. K., Yu, Y. S., Kim, S. W., Roh, J. H., Do, I. G., Joh, J. W., & Kim, D. S. Expression of nicotinamide N-methyltransferase in hepatocellular carcinoma is associated with poor prognosis. *J. Exp. Clin. Cancer Res.* **28**, 1–9 (2009).
7. Hong, S., Moreno-Navarrete, J. M., Wei, X., Kikukawa, Y., Tzamelis, I., Prasad, D., Lee, Y., Asara, J. M., Fernandez-Real, J. M., Maratos-Flier, E., & Pissios, P. Nicotinamide N-methyltransferase regulates hepatic nutrient metabolism through Sirt1 protein stabilization. *Nat. Med.* **21**, 887–894 (2015).
8. Belenky, P., Bogan, K. L., & Brenner, C. NAD<sup>+</sup> metabolism in health and

- disease. *Trends Biochem. Sci.* **32**, 12–19 (2007).
9. Elhassan, Y. S., Philp, A. A., & Lavery, G. G. Targeting NAD<sup>+</sup> in Metabolic Disease: New Insights Into an Old Molecule. *J. Endocr. Soc.* (2017) doi:10.1210/js.2017-00092.
  10. Komatsu, M., Kanda, T., Urai, H., Kurokochi, A., Kitahama, R., Shigaki, S., Ono, T., Yukioka, H., Hasegawa, K., Tokuyama, H., Kawabe, H., Wakino, S., & Itoh, H. NNMT activation can contribute to the development of fatty liver disease by modulating the NAD<sup>+</sup> metabolism. *Sci. Rep.* **8**, 1–16 (2018).
  11. Chang, H. C. & Guarente, L. SIRT1 and other sirtuins in metabolism. *Trends Endocrinol. Metab.* **25**, 138–145 (2014).
  12. Kannt, A., Pfenninger, A., Tönjes, A., & Blüher, M. Management of nicotinamide N-methyltransferase overexpression: inhibit the enzyme or reduce nicotinamide intake? Reply to Zhou S, Li D, Zhou Y [letter]. *Diabetologia* **58**, 2193–2194 (2015).
  13. Kannt, A., Pfenninger, A., Teichert, L., Tönjes, A., Dietrich, A., Schön, M. R., Klöting, N., & Blüher, M. Association of nicotinamide-N-methyltransferase mRNA expression in human adipose tissue and the plasma concentration of its product, 1-methylnicotinamide, with insulin resistance. *Diabetologia* **58**, 799–808 (2015).
  14. Wu, Y., Siadat, M. S., Berens, M. E., Hampton, G. M., & Theodorescu, D. Overlapping gene expression profiles of cell migration and tumor invasion in human bladder cancer identify metallothionein 1E and nicotinamide N-methyltransferase as novel regulators of cell migration. *Oncogene* **27**, 6679–6689 (2008).
  15. Tomida, M., Mikami, I., Takeuchi, S., Nishimura, H., & Akiyama, H. Serum levels of nicotinamide N-methyltransferase in patients with lung cancer. *J. Cancer Res. Clin. Oncol.* **135**, 1223–1229 (2009).
  16. Roeßler, M., Rollinger, W., Palme, S., Hagmann, M. L., Berndt, P., Engel, A. M., Schneidinger, B., Pfeffer, M., Andres, H., Karl, J., Bodenmüller, H., Rüschoff, J., Henkel, T., Rohr, G., Rossol, S., Rösch, W., Langen, H., Zolg, W., *et al.*

- Identification of nicotinamide N-methyltransferase as a novel serum tumor marker for colorectal cancer. *Clin. Cancer Res.* **11**, 6550–6557 (2005).
17. Tomida, M., Ohtake, H., Yokota, T., Kobayashi, Y., & Kurosumi, M. Stat3 up-regulates expression of nicotinamide N-methyltransferase in human cancer cells. *J. Cancer Res. Clin. Oncol.* **134**, 551–559 (2008).
  18. Lim, B. H., Cho, B. I., Yu, N. K., Jae, W. K., Park, S. T., & Lee, C. W. Overexpression of nicotinamide N-methyltransferase in gastric cancer tissues and its potential post-translational modification. *Exp. Mol. Med.* **38**, 455–465 (2006).
  19. Jang, J. S. J., Cho, H. Y., Lee, Y. J., Ha, W. S., & Kim, H. W. The Differential Proteome Profile of Stomach Cancer: Identification of the Biomarker Candidates. *Oncol. Res. Featur. Preclin. Clin. Cancer Ther.* **14**, 491–499 (2017).
  20. Song, M., Li, Y., Miao, M., Zhang, F., Yuan, H., Cao, F., Chang, W., Shi, H., & Song, C. High stromal nicotinamide N-methyltransferase (NNMT) indicates poor prognosis in colorectal cancer. *Cancer Med.* (2020) doi:10.1002/cam4.2890.
  21. Wang, Y., Zeng, J., Wu, W., Xie, S., Yu, H., Li, G., Zhu, T., Li, F., Lu, J., Wang, G. Y., Xie, X., & Zhang, J. Nicotinamide N-methyltransferase enhances chemoresistance in breast cancer through SIRT1 protein stabilization. *Breast Cancer Res.* (2019) doi:10.1186/s13058-019-1150-z.
  22. Wu, M., Hu, W., Wang, G., Yao, Y., & Tian, W. NNMT Regulates Cancer Immunity and Is a Potential Prognostic Biomarker in Gastric and Colorectal Cancers. *SSRN Electron. J.* (2020) doi:10.2139/ssrn.3408041.
  23. Ulanovskaya, O. A., Zuhl, A. M., & Cravatt, B. F. NNMT promotes epigenetic remodeling in cancer by creating a metabolic methylation sink. *Nat. Chem. Biol.* **9**, 300–306 (2013).
  24. Parsons, R. B. Nicotinamide N-methyltransferase and metastasis: a new player in cancer therapeutics. *Biotarget* (2019) doi:10.21037/biotarget.2019.11.01.
  25. Zhou, S. S., Li, D., Zhou, Y. M., Sun, W. P., & Liu, Q. G. B-vitamin consumption



- and the prevalence of diabetes and obesity among the US adults: Population based ecological study. *BMC Public Health* **10**, (2010).
26. Li, J. H., Wang, Y. H., Zhu, X. J., Zhou, Q., Xie, Z. H., & Yao, T. F. Metabolomics study on the association between nicotinamide N-methyltransferase gene polymorphisms and type 2 diabetes. *Int. J. Diabetes Dev. Ctries.* **38**, 409–416 (2018).
  27. Kraus, D., Yang, Q., Kong, D., Banks, A. S., Zhang, L., Rodgers, J. T., Pirinen, E., Pulinilkunnil, T. C., Gong, F., Wang, Y. C., Cen, Y., Sauve, A. A., Asara, J. M., Peroni, O. D., Monia, B. P., Bhanot, S., Alhonen, L., Puigserver, P., *et al.* Nicotinamide N-methyltransferase knockdown protects against diet-induced obesity. *Nature* **508**, 258–262 (2014).
  28. Watała, C., Kaźmierczak, P., Dobaczewski, M., Przygodzki, T., Bartuś, M., Łomnicka, M., Słomińska, E. M., Duračková, Z., & Chłopicki, S. Anti-diabetic effects of 1-methylnicotinamide (MNA) in streptozocin-induced diabetes in rats. *Pharmacol. Reports* **61**, 86–98 (2009).
  29. Bromberg, A., Lerer, E., Udawela, M., Scarr, E., Dean, B., Belmaker, R. H., Ebstein, R., & Agam, G. Nicotinamide-N-methyltransferase (NNMT) in schizophrenia: Genetic association and decreased frontal cortex mRNA levels. *Int. J. Neuropsychopharmacol.* **15**, 727–737 (2012).
  30. Jongkees, B. J., Hommel, B., Kühn, S., & Colzato, L. S. Effect of tyrosine supplementation on clinical and healthy populations under stress or cognitive demands-A review. *J. Psychiatr. Res.* **70**, 50–57 (2015).
  31. Parsons, R. B., Aravindan, S., Kadampeswaran, A., Evans, E. A., Sandhu, K. K., Levy, E. R., Thomas, M. G., Austen, B. M., & Ramsden, D. B. The expression of nicotinamide N-methyltransferase increases ATP synthesis and protects SH-SY5Y neuroblastoma cells against the toxicity of Complex i inhibitors. *Biochem. J.* **436**, 145–155 (2011).
  32. Schmeisser, K. & Parker, J. A. *Nicotinamide-N-methyltransferase controls behavior, neurodegeneration and lifespan by regulating neuronal autophagy.* *PLoS Genetics* vol. 14 (2018).

33. Parsons, R. B., Williams, A. C., Waring, R. H., Ramsden, D. B., & Smith, M.-L. Expression of Nicotinamide N-Methyltransferase (E.C. 2.1.1.1) in the Parkinsonian Brain. *J. Neuropathol. Exp. Neurol.* **61**, 111–124 (2016).
34. Williams, A. C. & Ramsden, D. B. Autotoxicity, methylation and a road to the prevention of Parkinson's disease. *J. Clin. Neurosci.* **12**, 6–11 (2005).
35. Palanichamy, K., Kanji, S., Gordon, N., Thirumoorthy, K., Jacob, J. R., Litzenberg, K. T., Patel, Di., & Chakravarti, A. NNMT silencing activates tumor suppressor PP2A, inactivates oncogenic STKs, and inhibits tumor forming ability. *Clin. Cancer Res.* **23**, 2325–2334 (2017).
36. Sazci, A., Ozel, M. D., Ergul, E., & Onder, M. E. Association of nicotinamide-N-methyltransferase (NNMT) gene rs694539 variant with bipolar disorder. *Gene* **532**, 272–275 (2013).
37. Aksoy, S., Brandriff, B. F., Ward, A., Little, P. F. R., & Weinshilboum, R. M. Human nicotinamide N-methyltransferase gene: Molecular cloning, structural characterization and chromosomal localization. *Genomics* **29**, 555–561 (1995).
38. Aksoy, S., Szumlanski, C. L., & Weinshilboum, R. M. Human liver nicotinamide N-methyltransferase. cDNA cloning, expression, and biochemical characterization. *J. Biol. Chem.* **269**, 14835–14840 (1994).
39. Ramsden, D. B., Waring, R. H., Barlow, D. J., & Parsons, R. B. Nicotinamide N-methyltransferase in health and cancer. *Int. J. Tryptophan Res.* **10**, (2017).
40. Van Haren, M. J., Taig, R., Kuppens, J., Sastre Toraño, J., Moret, E. E., Parsons, R. B., Sartini, D., Emanuelli, M., & Martin, N. I. Inhibitors of nicotinamide: N -methyltransferase designed to mimic the methylation reaction transition state. *Org. Biomol. Chem.* **15**, 6656–6667 (2017).
41. Neelakantan, H., Wang, H. Y., Vance, V., Hommel, J. D., McHardy, S. F., & Watowich, S. J. Structure-Activity Relationship for Small Molecule Inhibitors of Nicotinamide N-Methyltransferase. *J. Med. Chem.* **60**, 5015–5028 (2017).
42. van Haren, M. J., Thomas, M. G., Sartini, D., Barlow, D. J., Ramsden, D. B.,

- Emanuelli, M., Klamt, F., Martin, N. I., & Parsons, R. B. The kinetic analysis of the N-methylation of 4-phenylpyridine by nicotinamide N-methyltransferase: Evidence for a novel mechanism of substrate inhibition. *Int. J. Biochem. Cell Biol.* **98**, 127–136 (2018).
43. Ruf, S., Hallur, M. S., Anchan, N. K., Swamy, I. N., Murugesan, K. R., Sarkar, S., Narasimhulu, L. K., Putta, V. P. R. K., Shaik, S., Chandrasekar, D. V., Mane, V. S., Kadnur, S. V., Suresh, J., Bhamidipati, R. K., Singh, M., Burri, R. R., Kristam, R., Schreuder, H., *et al.* Novel nicotinamide analog as inhibitor of nicotinamide N-methyltransferase. *Bioorganic Med. Chem. Lett.* **28**, 922–925 (2018).
44. Peng, Y., Sartini, D., Pozzi, V., Wilk, D., Emanuelli, M., & Yee, V. C. Structural basis of substrate recognition in human nicotinamide N-methyltransferase. *Biochemistry* **50**, 7800–7808 (2011).
45. Babault, N., Allali-Hassani, A., Li, F., Fan, J., Yue, A., Ju, K., Liu, F., Vedadi, M., Liu, J., & Jin, J. Discovery of Bisubstrate Inhibitors of Nicotinamide N-Methyltransferase (NNMT). *J. Med. Chem.* **61**, 1541–1551 (2018).
46. Gao, Y., Van Haren, M. J., Moret, E. E., Rood, J. J. M., Sartini, D., Salvucci, A., Emanuelli, M., Craveur, P., Babault, N., Jin, J., & Martin, N. I. Bisubstrate inhibitors of nicotinamide N-methyltransferase (NNMT) with enhanced activity. *J. Med. Chem.* **62**, 6597–6614 (2019).
47. Chen, D., Li, L., Diaz, K., Iyamu, I. D., Yadav, R., Noinaj, N., & Huang, R. Novel Propargyl-Linked Bisubstrate Analogues as Tight-Binding Inhibitors for Nicotinamide N-Methyltransferase. *J. Med. Chem.* **62**, 10783–10797 (2019).
48. Policarpo, R. L., Decultot, L., May, E., Kuzmič, P., Carlson, S., Huang, D., Chu, V., Wright, B. A., Dhakshinamoorthy, S., Kannt, A., Rani, S., Dittakavi, S., Panarese, J. D., Gaudet, R., & Shair, M. D. High-Affinity Alkynyl Bisubstrate Inhibitors of Nicotinamide N-Methyltransferase (NNMT). *J. Med. Chem.* **62**, 9837–9873 (2019).
49. Sen, S., Mondal, S., Zheng, L., Salinger, A. J., Fast, W., Weerapana, E., & Thompson, P. R. Development of a Suicide Inhibition-Based Protein Labeling Strategy for Nicotinamide N-Methyltransferase. *ACS Chem. Biol.* **14**, 613–618

- (2019).
50. Tuley, A. & Fast, W. The Taxonomy of Covalent Inhibitors. *Biochemistry* (2018) doi:10.1021/acs.biochem.8b00315.
  51. Johnson, C. M., Linsky, T. W., Yoon, D. W., Person, M. D., & Fast, W. Discovery of halopyridines as quiescent affinity labels: Inactivation of dimethylarginine dimethylaminohydrolase. *J. Am. Chem. Soc.* (2011) doi:10.1021/ja109207m.
  52. Schardon, C. L., Tuley, A., Er, J. A. V., Swartzel, J. C., & Fast, W. Selective Covalent Protein Modification by 4-Halopyridines through Catalysis. *ChemBioChem* (2017) doi:10.1002/cbic.201700104.
  53. Johnson, C. M., Monzingo, A. F., Ke, Z., Yoon, D. W., Linsky, T. W., Guo, H., Robertus, J. D., & Fast, W. On the mechanism of dimethylarginine dimethylaminohydrolase inactivation by 4-halopyridines. *J. Am. Chem. Soc.* (2011) doi:10.1021/ja2033684.
  54. Larghi, E. L., Amongero, M., Bracca, A. B. J., & Kaufman, T. S. The intermolecular Pictet-Spengler condensation with chiral carbonyl derivatives in the stereoselective syntheses of optically-active isoquinoline and indole alkaloids. *Arkivoc* **2005**, 98–153 (2005).
  55. Okano, K., Tokuyama, H., & Fukuyama, T. Total synthesis of (. *J. Am. Chem. Soc.* **128**, 7136–7137 (2006).
  56. Thanh, N. D., Hai, D. S., Bich, V. T. N., Hien, P. T. T., Duyen, N. T. K., Mai, N. T., Dung, T. T., Van, H. T. K., Toan, V. N., Toan, D. N., & Dang, L. H. Using Sodium Hydride and Potassium Carbonate as Bases in Synthesis of Substituted 2-Amino-4-aryl-7-propargyloxy-4H-chromene-3-carbonitriles. *Curr. Org. Synth.* (2019) doi:10.2174/1570179416666190104124652.
  57. Keskin, S. & Balci, M. Intramolecular heterocyclization of o -propargylated aromatic hydroxyaldehydes as an expedient route to substituted chromenopyridines under metal-free conditions. *Org. Lett.* (2015) doi:10.1021/acs.orglett.5b00067.
  58. Batool, T., Rasool, N., Gull, Y., Noreen, M., Nasim, F. U. H., Yaqoob, A., Zubair,

- M., Rana, U. A., Ud-Din Khan, S., Zia-Ul-Haq, M., & Jaafar, H. Z. E. A convenient method for the synthesis of (prop-2-ynoxy)benzene derivatives via reaction with propargyl bromide, their optimization, scope and biological evaluation. *PLoS One* (2014) doi:10.1371/journal.pone.0115457.
59. Shi, M. & Shen, Y. M. Synthesis of mixed carbonates via a three-component coupling of alcohols, CO<sub>2</sub>, and alkyl halides in the presence of K<sub>2</sub>CO<sub>3</sub> and tetrabutylammonium iodide. *Molecules* (2002) doi:10.3390/70400386.
60. Ohkawa, K., Tenmaru, K., Hayashi, M., & Hirata, Y. Mechanism of Alkylation Using Potassium Carbonate in Synthesis of the Anti-psychotic Drug Zotepine. *Kagaku Kogaku Ronbunshu* (2003) doi:10.1252/kakoronbunshu.29.727.
61. Pájaro, Y., Sathicq, Á., Puello-Polo, E., Pérez, A., Romanelli, G., & Trilleras, J. An Efficient K<sub>2</sub>CO<sub>3</sub>-Promoted Synthesis of 1-Bromo-2-aryloxyethane Derivatives and Evaluation of Larval Mortality against *Aedes aegypti*. *J. Chem.* (2017) doi:10.1155/2017/6175315.
62. Khachatryan, D. S. & Matevosyan, K. R. Potassium carbonate as a base for generation of carbanions from CH-acids in organic synthesis. *Russian Chemical Bulletin* (2016) doi:10.1007/s11172-016-1260-z.
63. Shmidt, M. S., Reverdito, A. M., Kremenichuzky, L., Perillo, I. A., & Blanco, M. M. Simple and efficient microwave assisted N-alkylation of isatin. *Molecules* (2008) doi:10.3390/molecules13040831.
64. Subramanyam, S. & Blumstein, A. Conjugated Ionic Polyacetylenes. 3. Polymerization of Ethynylpyridinium Salts. *Macromolecules* (1991) doi:10.1021/ma00010a004.
65. Colabufo, N. A., Berardi, F., Cantore, M., Perrone, M. G., Contino, M., Inglese, C., Niso, M., Perrone, R., Azzariti, A., Simone, G. M., Porcelli, L., & Paradiso, A. Small P-gp modulating molecules: SAR studies on tetrahydroisoquinoline derivatives. *Bioorganic Med. Chem.* (2008) doi:10.1016/j.bmc.2007.09.039.
66. Sommer, H. Z., Lipp, H. I., & Jackson, L. L. Alkylation of Amines. A General Exhaustive Alkylation Method for the Synthesis of Quaternary Ammonium Compounds. *J. Org. Chem.* (1971) doi:10.1021/jo00805a021.

67. Ma, D. & Jiang, Y. Cu ( I ) / Amino Acid Catalyzed Coupling Reactions of Aryl Halides and Nucleophiles : Applications in Large-scale Production. **65**, 914–918 (2011).
68. Cai, Q., Zhang, H., Zou, B., Xie, X., Zhu, W., He, G., Wang, J., Pan, X., Chen, Y., Yuan, Q., Liu, F., Lu, B., & Ma, D. Amino acid-promoted Ullmann-type coupling reactions and their applications in organic synthesis. *Pure Appl. Chem.* **81**, 227–234 (2009).
69. Taylor, P., Zhang, H., & Cao, W. Synthetic Communications : An International Journal for Rapid Communication of Synthetic Organic Chemistry L - Proline - Promoted CuI - Catalyzed C - S Bond Formation between Aryl Iodides and Thiols CuI-Catalyzed C-S Bond Formation between Aryl. *Synth. Commun. An Int. J. Rapid Commun. Synth. Org. Chem.* **37**, 25–35 (2007).
70. Zhu, W. & Ma, D. Synthesis of aryl azides and vinyl azides via proline-promoted CuI-catalyzed coupling reactions †. 888–889 (2004).
71. Grimes, D., Gupte, A., & Aldrich, C. C. Copper ( II ) -Catalyzed Conversion of Aryl / Heteroaryl Boronic Acids , Boronates , and Trifluoroborates into the Corresponding Azides : (2010) doi:10.1055/s-0029-1218683.
72. Intermediate, C. Direct Evidence of a Dinuclear. **340**, 457–461 (2010).
73. Intermediate, C. Direct Evidence of a Dinuclear. **340**, 457–461 (2013).
74. Hein, C. D., Liu, X., & Wang, D. Expert Review Click Chemistry , A Powerful Tool for Pharmaceutical Sciences. **25**, 2216–2230 (2008).
75. Engineering, F. Y. & Pune, W. CLICK REACTION : A NEW APPORACH. **4**, 821–823 (2015).
76. Liu, X. M., Thakur, A., & Wang, D. Efficient synthesis of linear multifunctional poly(ethylene glycol) by copper(I)-catalyzed Huisgen 1,3-dipolar cycloaddition. *Biomacromolecules* (2007) doi:10.1021/bm070430i.
77. Vural Gürsel, I., Aldiansyah, F., Wang, Q., Noël, T., & Hessel, V. Continuous metal scavenging and coupling to one-pot copper-catalyzed azide-alkyne cycloaddition click reaction in flow. *Chem. Eng. J.* (2015)

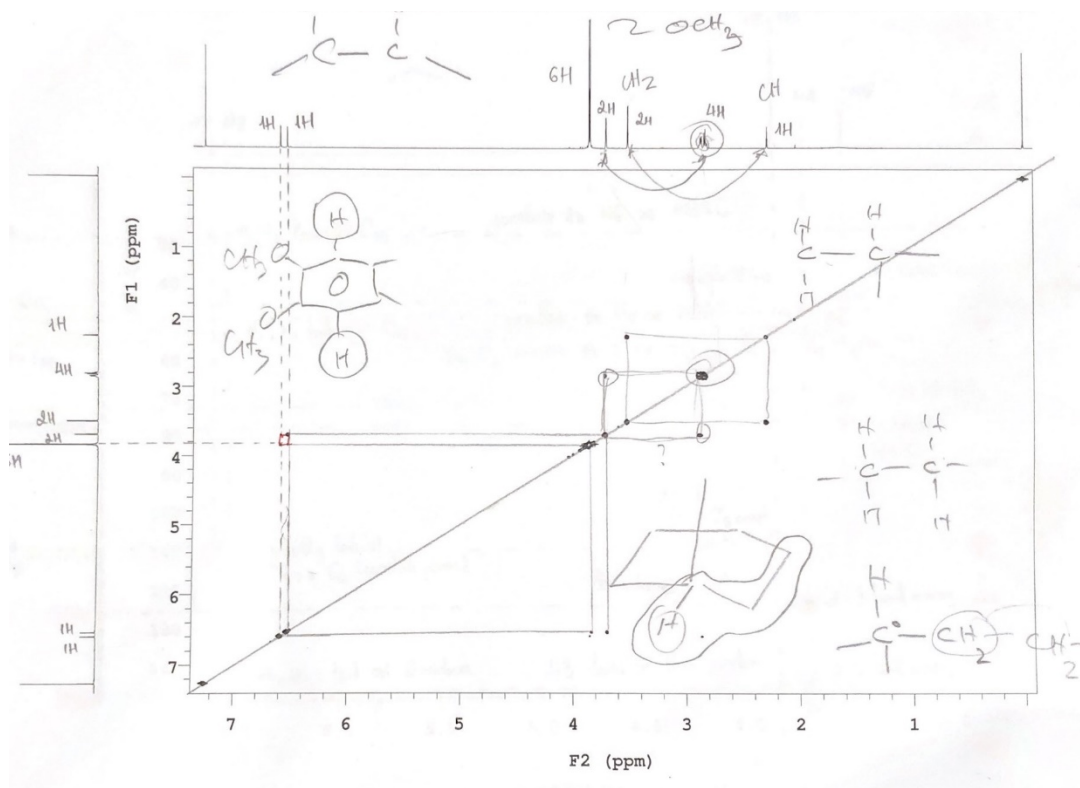
doi:10.1016/j.cej.2015.02.035.

78. Yu, J. & Klarup, D. Extraction kinetics of copper, zinc, iron, and manganese from contaminated sediment using Disodium Ethylenediaminetetraacetate. *Water, Air, Soil Pollut.* (1994) doi:10.1007/BF00482938.
79. Pasini, D. The click reaction as an efficient tool for the construction of macrocyclic structures. *Molecules* (2013) doi:10.3390/molecules18089512.
80. Pickens, C. J., Johnson, S. N., Pressnall, M. M., Leon, M. A., & Berkland, C. J. Practical Considerations, Challenges, and Limitations of Bioconjugation via Azide-Alkyne Cycloaddition. *Bioconjugate Chemistry* (2018) doi:10.1021/acs.bioconjchem.7b00633.
81. Presolski, S. I., Hong, V. P., & Finn, M. G. Copper-Catalyzed Azide–Alkyne Click Chemistry for Bioconjugation. *Curr. Protoc. Chem. Biol.* (2011) doi:10.1002/9780470559277.ch110148.
82. Wu, H., Li, H., Kwok, R. T. K., Zhao, E., Sun, J. Z., Qin, A., & Tang, B. Z. A recyclable and reusable supported Cu(I) catalyzed azide-alkyne click polymerization. *Sci. Rep.* (2014) doi:10.1038/srep05107.
83. Maketon, W., Zenner, C. Z., & Ogden, K. L. Removal efficiency and binding mechanisms of copper and copper - EDTA complexes using polyethyleneimine. *Environ. Sci. Technol.* (2008) doi:10.1021/es702420h.
84. Sallustrau, A., Bregant, S., Chollet, C., Audisio, D., & Taran, F. Scalable and practical synthesis of clickable Cu-chelating azides. *Chem. Commun.* **53**, 7890–7893 (2017).
85. Neelakantan, H., Vance, V., Wang, H. Y. L., McHardy, S. F., & Watowich, S. J. Noncoupled Fluorescent Assay for Direct Real-Time Monitoring of Nicotinamide N-Methyltransferase Activity. *Biochemistry* **56**, 824–832 (2017).
86. Hendricks, C. L., Ross, J. R., Pichersky, E., Noel, J. P., & Zhou, Z. S. An enzyme-coupled colorimetric assay for S-adenosylmethionine-dependent methyltransferases. *Anal. Biochem.* **326**, 100–105 (2004).

87. Lakowski, T. M., Zurita-Lopez, C., Clarke, S. G., & Frankel, A. Approaches to measuring the activities of protein arginine N-methyltransferases. *Analytical Biochemistry* (2010) doi:10.1016/j.ab.2009.09.021.
88. Luo, M. Current chemical biology approaches to interrogate protein methyltransferases. *ACS Chemical Biology* (2012) doi:10.1021/cb200519y.
89. Brown, P. E. R. United States Patent ( 19 ). (1978).
90. Matos, J. R. & Wong, C. H. S-adenosylmethionine: Stability and stabilization. *Bioorg. Chem.* **15**, 71–80 (1987).
91. Iyamu, I. D. & Huang, R. Development of fluorescence polarization-based competition assay for nicotinamide N-methyltransferase. *Anal. Biochem.* (2020) doi:10.1016/j.ab.2020.113833.
92. Rodríguez-Prieto, F., Corbelle, C. C., Fernández, B., Pedro, J. A., Ríos Rodríguez, M. C., & Mosquera, M. Fluorescence quenching of the: N - methylquinolinium cation by pairs of water or alcohol molecules. *Phys. Chem. Chem. Phys.* (2017) doi:10.1039/c7cp07057h.
93. Yu, H., Zhou, X., Wang, Y., Huang, X., Yang, J., Zeng, J., Li, G., Xie, X., & Zhang, J. Nicotinamide N-methyltransferase inhibits autophagy induced by oxidative stress through suppressing the AMPK pathway in breast cancer cells. *Cancer Cell Int.* (2020) doi:10.1186/s12935-020-01279-8.
94. Mosmann, T. Rapid colorimetric assay for cellular growth and survival: Application to proliferation and cytotoxicity assays. *J. Immunol. Methods* (1983) doi:10.1016/0022-1759(83)90303-4.
95. Santini, V., Bernabei, P. A., Silvestro, L., Pozzo, O. D., Bezzini, R., Viano, I., Gattei, V., Saccardi, R., & Ferrini, P. R. *In vitro* chemosensitivity testing of leukemic cells: Prediction of response to chemotherapy in patients with acute non-lymphocytic leukemia. *Hematol. Oncol.* (1989) doi:10.1002/hon.2900070405.

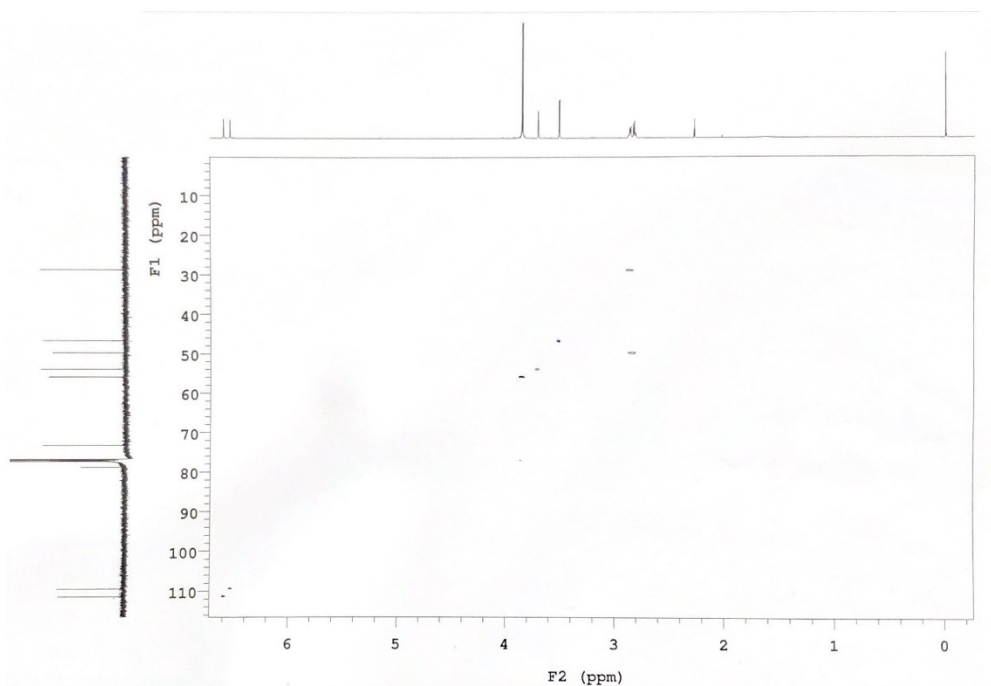
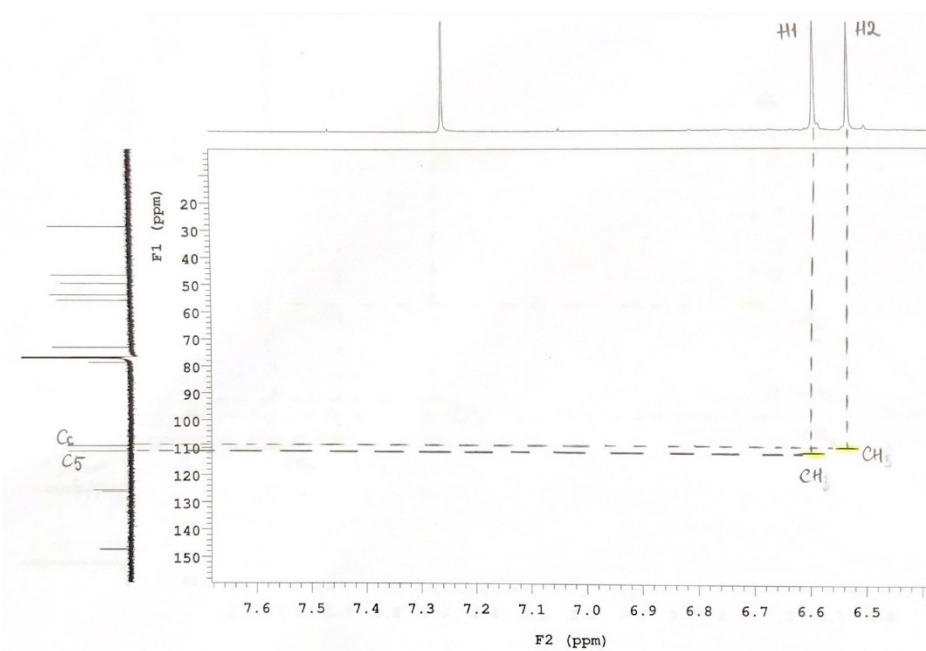


## Appendix

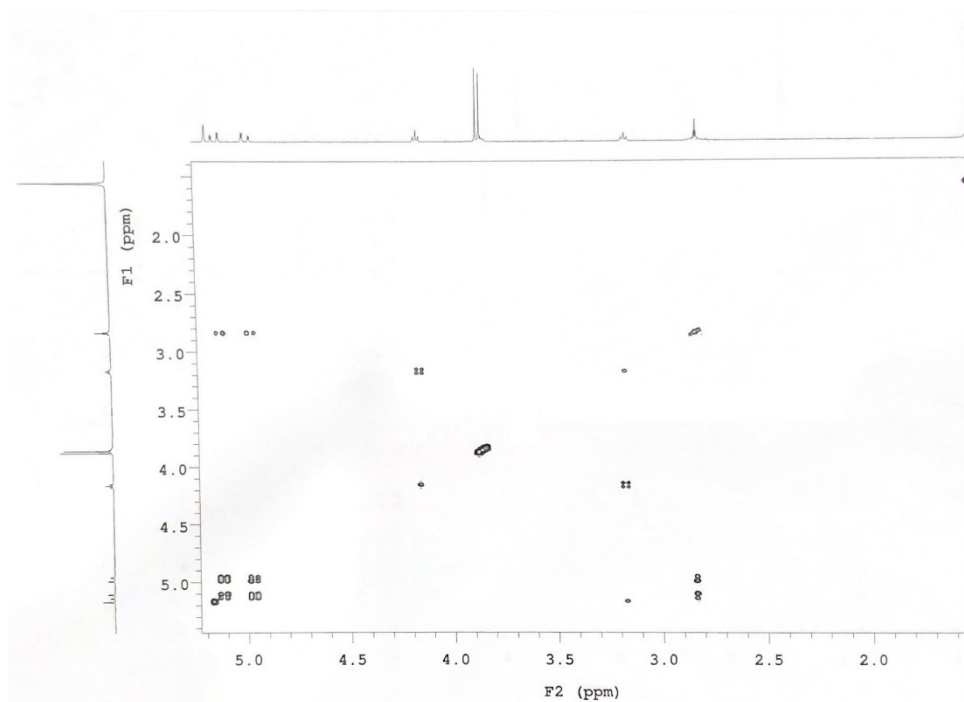
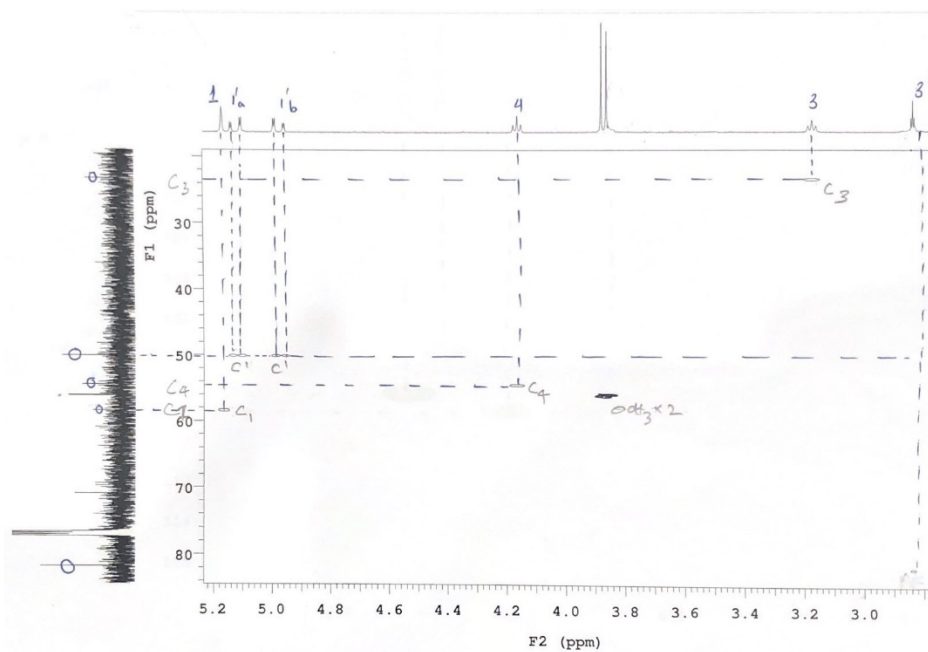


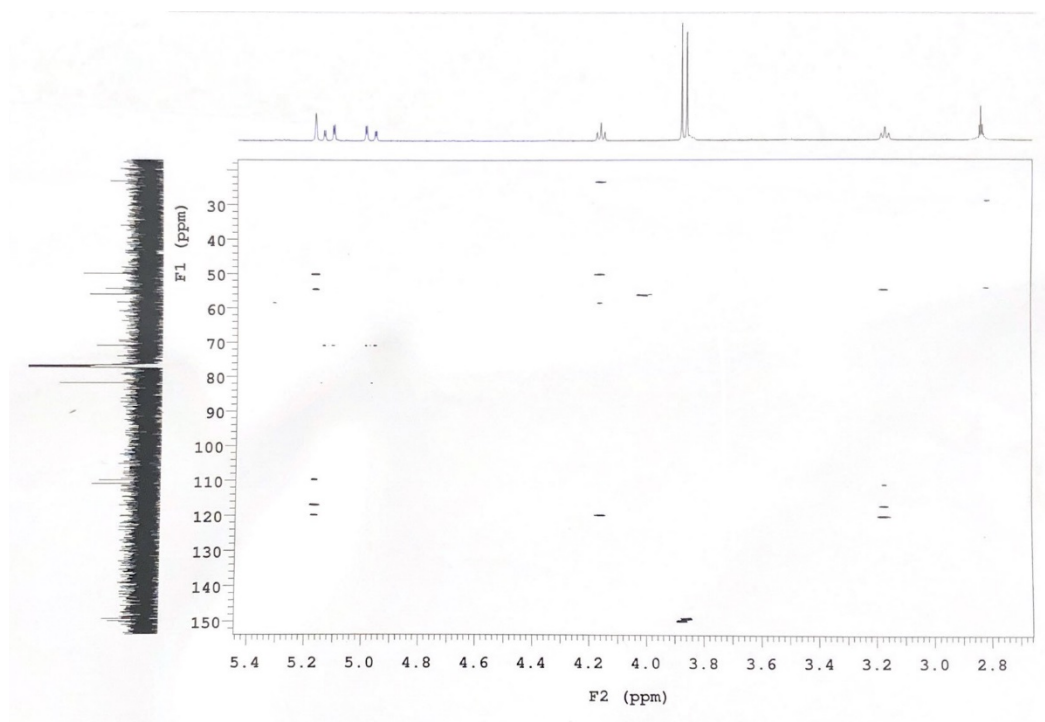
COSY NMR OF COMPOUND 26

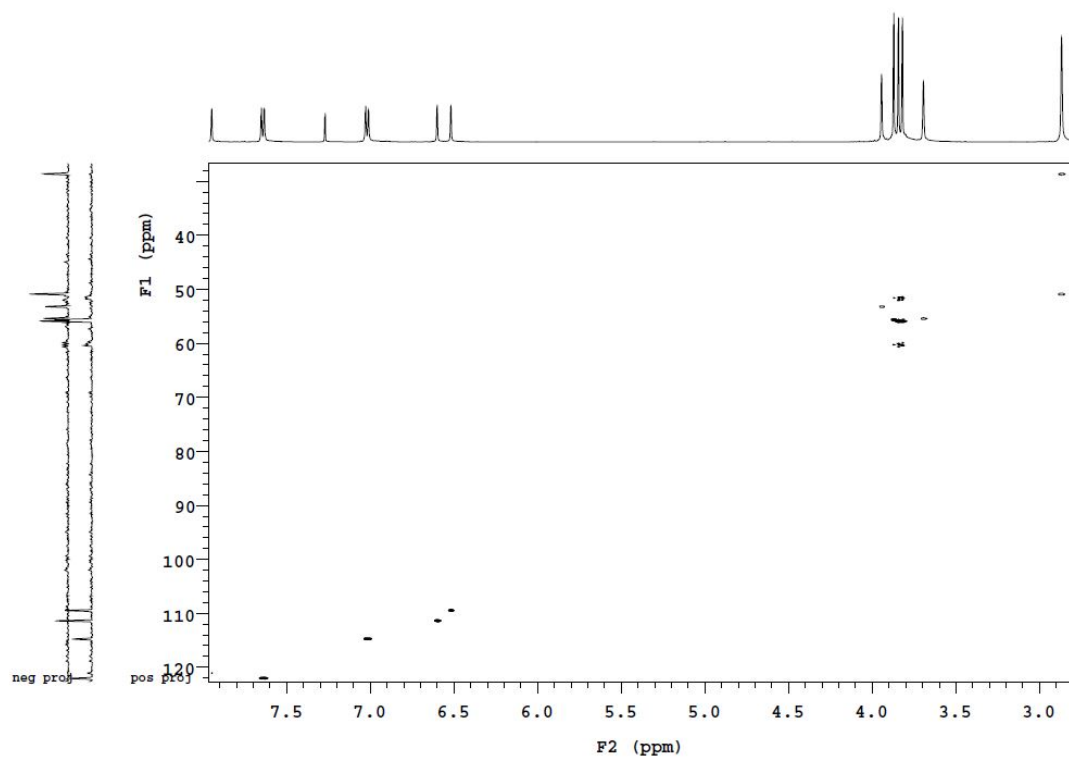


**HSQC SPECTRA OF COMPOUND 26****HSQC SPECTRA OF COMPOUND 26**

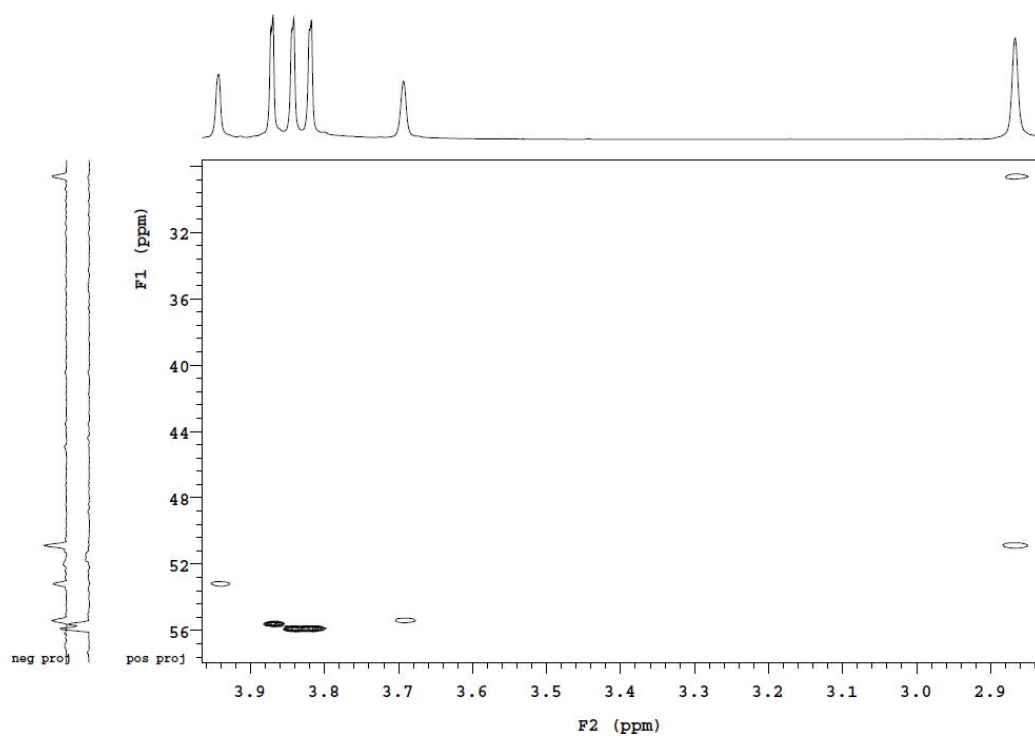


**COSY NMR OF COMPOUND 27****HSQC SPECTRA OF COMPOUND 27**

**HMBC SPECTRA OF COMPOUND 27**



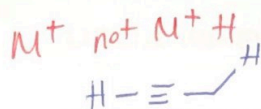
### HSQC SPECTRA OF FHM02



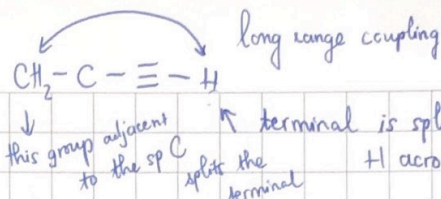
### HSQC SPECTRA OF FHM02 (ZOOM IN)



## STRUCTURAL ELUCIDATION OF COMPOUND 26



$J = 2$  to  $4$  Hz



④  $^1H$  NMR:

	ppm	type	n	number of proton	J-coupling
1/	6.596	s	0	1H	-
2/	6.535	s	0	1H	-
3/	<del>3.844</del> - 3.845	d	0	6H	0.5 Hz
4/	3.694	s	0	2H	-
5/	<del>3.504</del> - 3.499	d	1	2H	2.5 Hz
6/	<del>2.589</del> - 2.816	dd	2	4H	5 Hz, 16 Hz
7/	<del>2.276</del> - 2.266	t	2	1H	5 Hz, 16 Hz
	2.27				2.5 Hz

$\therefore$  No of proton = 17H

✓ 2 singlets @ 3.844 - 3.845 ppm indicate  $O-CH_3$  proton

$\therefore$  2 Oxygen atoms in the structure

④  $^{13}C$  NMR Showing 14 peaks ranging from 20 ppm - 150 ppm

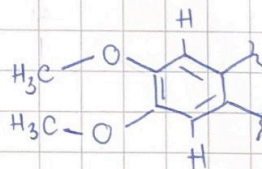
$\therefore$  14 Carbons in the structure

$\Rightarrow$  Formula:  $C_{14}H_{17}O_2N$

$$\text{DoU} = \frac{2C + N + 2 - X - H}{2} = \frac{2 \times 14 + 1 + 2 - 0 - 17}{2} = 7$$

✓ From ① to ④ unchanged structure based on starting material

$\therefore$  Structure should be

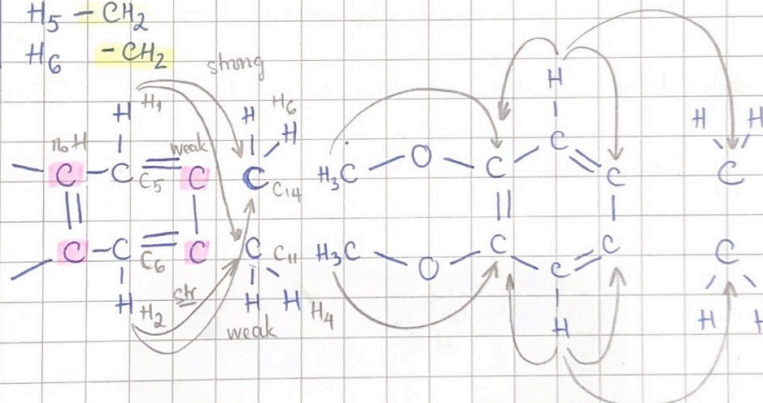


$\therefore$  DoU =  $7 - 4 = 3$  since an Ar has DoU = 4.




	$^{13}\text{C}$ ppm	assignment	From HSQC
1/	147.8	Ar - C connect to -OMe	✓ H1 peak - C5 (6.596) (111.328)
2/	147.6	Ar - C connect to -OMe	✓ H2 peak - C6 (6.535) (109.397)
3/	125.4	Ar - C no H	
4/	125.7	Ar - C no H	
5/	111.328	H1 (Ar-) -CH	✓ H3 peak (d) - C9 + C10 (3.844-3.845) (55.908-55.878)
6/	109.397	H2 (Ar-) -CH	
7/	79.00	C before terminal $\equiv\text{C}$	
8/	73.197	H7	✓ H4 peak - C11
9/	55.908	H3 (OMe) -CH <sub>3</sub>	✓ H5 peak - C13
10/	55.878	H3 (OMe) -CH <sub>3</sub>	✓ H6 peaks - C12 + C14
11/	53.932	H4 -CH <sub>2</sub>	✓ H7 peak - C8
12/	49.755	H6 various -CH <sub>2</sub> + CH/CH <sub>3</sub> ???	
13/	46.712	H5 -CH <sub>2</sub>	
14/	28.802	H6 -CH <sub>2</sub>	

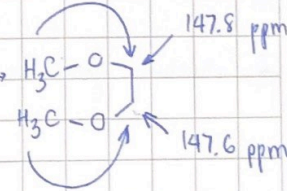
⊕ HMBC



✓ C H<sub>1</sub> & H<sub>2</sub> look at 4 Carbons with no H- correlation

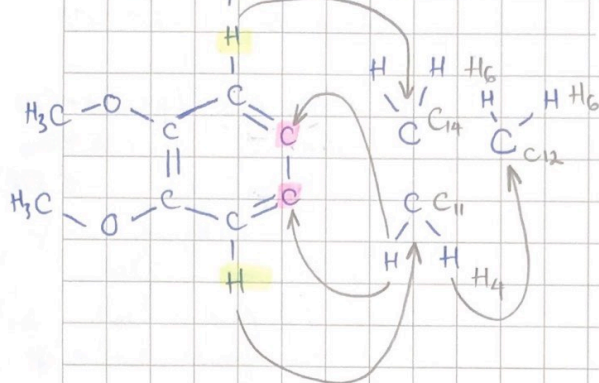
→ 4 C should sit beside C<sub>5</sub> & C<sub>6</sub>

✓ 4 C do not carry any protons. → 

✓ 2C no proton looked at by the proton H3 → 

⑧ HMBC : Look @ H4

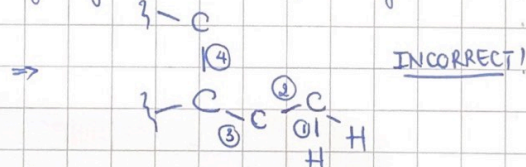
From previous elucidation.



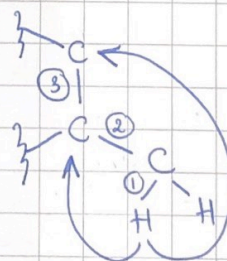
✓ The highlight (H) looks @ C<sub>11</sub> connect H<sub>4</sub>  
 @ C<sub>14</sub> connect H<sub>6</sub>

✓ H<sub>4</sub> looks @ 2C on Aromatic (Pink) ←

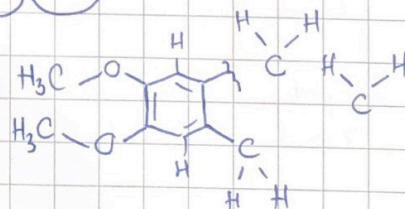
✓ If from C<sub>11</sub> couple only 2-3 bonds away & see



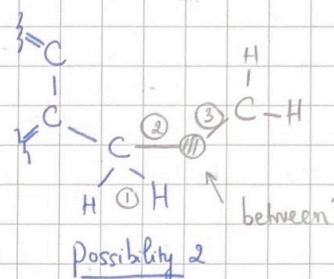
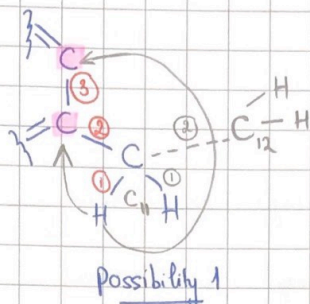
∴ Should be:



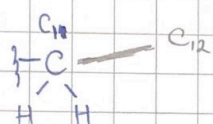
⊕ Structure after look @ H4 :



⊕  $H_4$  sees  $C_{12}$  &  $C_{12}$  is correlated to  $H_6$  (w various  $CH_2$ )  
 $\rightarrow H_4 - C_{12}$  is 2/3 bonds away

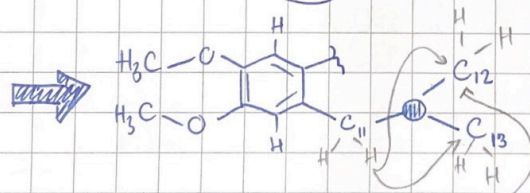
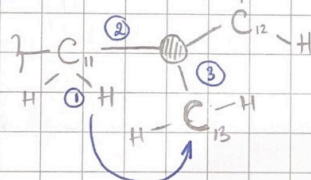


✓  $H_4$  sees  $C_{13}$  connected to  $H_5$ . [(2 protons) on  $C_{13}$ ]  
 $\rightarrow H_4 - C_{13}$  is 2/3 bonds away

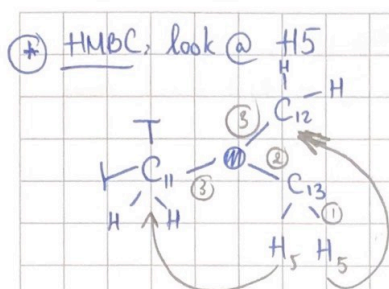


✓ As determine in HSQC  $C_{11}$  carry 2H &  $C_{12}$  carry 2H  
 $\rightarrow C_{13}$  cannot attached to  $C_{11}$  &  $C_{12}$ .

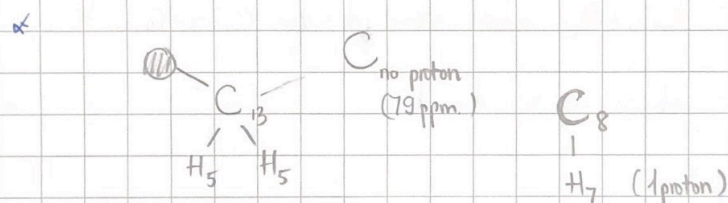
$\rightarrow$  Possibility 2 above is considered!





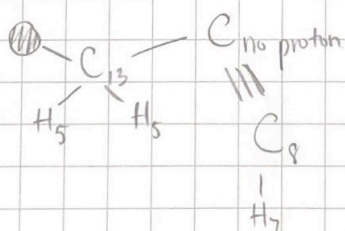


- ✓ H5 looks @ C<sub>12</sub> (3 bonds away) ✓ CONFIRM
- ✓ H5 looks @ C<sub>11</sub> (3 bonds away) ✓ CONFIRM
- ✓ H5 looks @ C (79 ppm) and this Carbon has no protm. attached to it.
- ✓ H5 looks @ C<sub>8</sub> - C<sub>8</sub> correlated to H<sub>7</sub>.

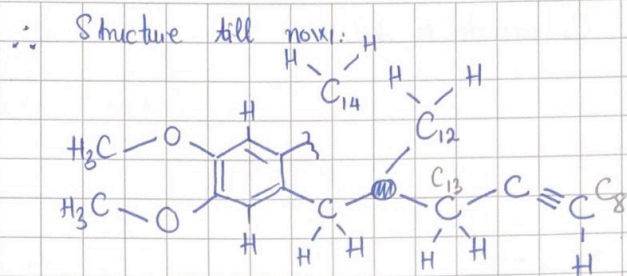


- ✓ Since we have ruled out 12 Carbon. (including  $C_{13}$  &  $C_{14}$ )  
 $\Rightarrow C_{no. proton} + C_8$  is the last 2 Carbon.

$\Rightarrow$   $p_{\text{orb}}$   $\Rightarrow$  from  $C_{13}$  to  $C_{10}$  proton should not go thru any atom in the middle (2-3 bonds away only)



$\checkmark$  to be a C w no H  $\rightarrow$   $\equiv$  attached  
 $\checkmark$  C<sub>g</sub> w 1H  $\rightarrow$



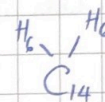
\* 1 Aromatic ring take up 4 DoU.

\* 1 triple bond take up 2 DoU

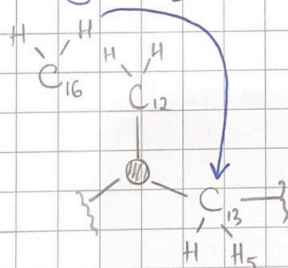
⇒ 1 DoU left.

⊛ HMBC: look @ H6

✓ H6 correlated to C14 and has 2 protons.

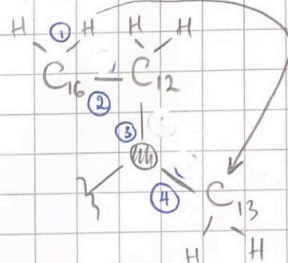


✓ H6 looks @ C13 connected to H5.



✓ If 2 bonds away C16 has to connect directly to C13 ⇒ **INCORRECT!**

✓ ⇒ CONNECT THRU C12



✓ 4 bonds away!

✓ However ⑩ is undefined yet!

✓ No of C is enough ⇒ Not quaternary C.

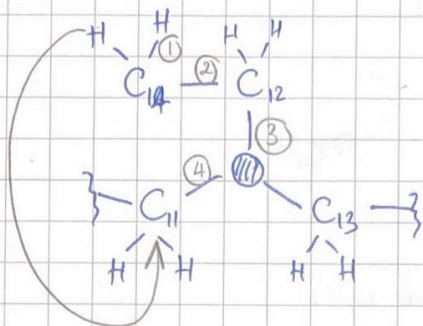
✓ ⇒ Must be O, S or N

✓ 3 bonds around ⑩ ⇒ **(N)**

⇒ H on C16 can see thru **(N)** to detect C13.

10% HCl + bit MeOH + vacu.  $\rightarrow$  high vac.

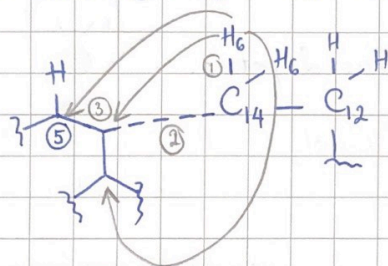
✓ H6 looks @ C<sub>11</sub>. C<sub>11</sub> connects to 2H.



⊕ Similar explanation to H6 looks @ C<sub>13</sub>.

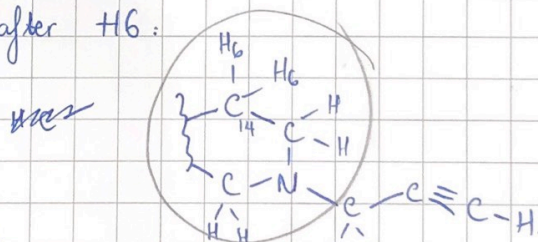
Ⓢ atom is a N  $\Rightarrow$  H on C<sub>14</sub> can see thru to detect C<sub>11</sub>.

✓ H6 looks @ C<sub>5</sub>. C<sub>5</sub> has 1 proton



✓ H6 looks @ 2C on Ar- with no proton!

$\therefore$  Structure after H6:



⊕ 1 ring structure

$\rightarrow$  has equiv to 1 DoU:  $\Rightarrow$  0 DoU left:

**CONFIRM STRUCTURE**

